

March 2022

## Origin and Epigenetic Regulation of Cutaneous T Cell Lymphoma

Carly M. Harro  
*University of South Florida*

Follow this and additional works at: <https://digitalcommons.usf.edu/etd>



Part of the [Biology Commons](#), [Genetics Commons](#), and the [Oncology Commons](#)

---

### Scholar Commons Citation

Harro, Carly M., "Origin and Epigenetic Regulation of Cutaneous T Cell Lymphoma" (2022). *USF Tampa Graduate Theses and Dissertations*.  
<https://digitalcommons.usf.edu/etd/10296>

This Dissertation is brought to you for free and open access by the USF Graduate Theses and Dissertations at Digital Commons @ University of South Florida. It has been accepted for inclusion in USF Tampa Graduate Theses and Dissertations by an authorized administrator of Digital Commons @ University of South Florida. For more information, please contact [digitalcommons@usf.edu](mailto:digitalcommons@usf.edu).

Origin and Epigenetic Regulation of Cutaneous T Cell Lymphoma

by

Carly M. Harro

A dissertation submitted in partial fulfillment  
of the requirements for the degree of  
Doctor of Philosophy  
Department of Cell Biology, Microbiology and Molecular Biology  
College of Arts and Sciences  
University of South Florida

Major Professor: José Conejo-Garcia, M.D. Ph.D.  
John Cleveland, Ph.D.  
Kenneth Wright Ph.D.  
Javier Pinilla-Ibarz, M.D., Ph.D.  
Lubomir Sokol, M.D., Ph.D.  
Owen O' Connor, M.D., Ph.D.

Date of Approval:  
February 28, 2022

Keywords: Cancer, SATB1, Sézary syndrome, Mycosis Fungoides, TCR

Copyright © 2022, Carly M. Harro

## DEDICATION

I dedicate this dissertation to my late mother, Karen Harro, who lost her battle to pancreatic cancer during my time in the Cancer Biology graduate program. Despite having metastatic cancer, she tried to take care of everyone up until her passing. I am thankful to have had a mother with such a beautiful soul. I have often been told that I am her Doppelgänger, and my parents would often joke that they were the first scientists to ever clone a human being. Anytime someone needed help, she never considered anyone undeserving of it. She truly believed that if you poured your love and care into someone that they would eventually heal.

She thought the same way about animals, and that was evident by the number rescues we had when I was growing up. My mom loved horses, and she rescued a thoroughbred named Max, an ex-racehorse who injured himself and walked with a limp. When my mom bought him, people asked her why she wanted a lame horse. She replied that she had not given up on him and started physical therapy. Eventually, Max became strong enough to ride again. My mother never minded what other people thought if she knew she was doing the right thing. She was my moral compass, and when she passed, I thought “I am going to feel so lost without her direction.”

She raised a good family and taught us to stay together through tough times. When my mom became ill, everybody sprang into action taking shifts at the hospitals. My mom had had incredible bravery; the kind that would have helped her fight tigers for the people she loved if necessary. I love my mom, and I will miss her so much. I hope that in my future career I can contribute to the treatment and early detection for many rare and deadly cancers.

## ACKNOWLEDGEMENTS

I would like to thank my mentor Dr. José Conejo-Garcia his guidance throughout my doctoral studies. I am grateful to have worked with such an esteemed and innovative scientist who constantly pushes the field forward. I had the unique opportunity to tackle challenging and interdisciplinary projects which melded my two passions: Immunology and Epigenetics. The experience has helped me grow tremendously both as a scientist and as a person. It is difficult to find someone who matches Dr. Conejo-Garcia's work ethic and dedication to science, which certainly left a lasting impression on myself as well as the rest of the lab.

I would also like to sincerely thank my lab mates for their support. I would like to give a special thank you to Tära Lee Costich, Kyle Payne, Kim Sprenger, Ricardo Chaurio, Subir Biswas, Gunjan Mandal, Pat Innamarato, Jairo Perez, and Carmen Anadon. I really cannot thank them enough for their extraordinary contributions to my projects as well as their valued personal support. We all spent many long hours experimenting together and encouraging each other during difficult times both personally and professionally. It is incredible how such unique blend of personalities were able to build such a strong team. It is not often a lab fosters that level of comradery.

I am also extremely grateful for the mentorship of my committee members. Thank you, Dr. John Cleveland, for being a tremendous student advocate and mentor throughout the years. He is an exemplary scientist and leader at H. Lee Moffitt Cancer Center, who I hope to emulate in my future career. I would like to thank Dr. Lubomir Sokol and Dr. Javier Pinilla for their support in my professional development in leukemia and lymphoma research. It is a privilege to

have experts in the field play a role in my development. I would like to thank Dr. Kenneth Wright for his support through the Cancer Biology program and his excellent guidance throughout my academic career. I would also like to thank Dr. Owen O' Connor for acting as my external chair. It is an honor to have someone who has contributed such seminal work in T cell lymphoma to oversee my defense.

I would also like to thank the many talented graduate and post-doctoral students that have contributed to my growth as a scientist and for their remarkable friendship in the Cell and Molecular Biology Program and the Cancer Biology Program. From the Cell and Molecular Biology program I would like to thank Christina Moss, Stephanie Rockfield, and Wade Borchers. From the Cancer Biology Program, I would like to thank Christopher Letson, Alycia Gardner, Daniel Lester, Kamira Maharaj, and Natalia Sumi. There are many memories which I shall cherish of potlucks, breweries, pumpkin carving contests, festivals, game nights, escape rooms, farmer's markets, trivia nights, ugly sweater holiday parties, and more. I would also like to thank Paulo Cilas Morias Lyra Jr. for keeping my spirits up throughout graduate school and for being a good friend.

I would also like to thank the many other scientists and clinicians I had the pleasure of collaborating with at H. Lee Moffitt Cancer Center. The Molecular Genomics Core, Flow Cytometry Core, Microscopy Core, Bioinformatics Core, Tissue Core, and the Vivarium staff have been tremendously helpful during my graduate studies. I would like to thank the clinical collaborators that have helped me understand the disease and assisted in sample collections for my projects Dr. Yumeng Zhang, Dr. Pei-Ling Chen, Dr. Dasom Lee and Dr. Ning Dong. I would also like to thank our scientific collaborators in the Pinilla lab, Rodriguez lab, and Tsai lab for their amazing contributions to a variety of projects.

Lastly, I would like to thank my loved ones as they have supported and inspired me throughout this entire process. To my father David Harro, who helped shaped me into the scientist I am today. As a geophysicist and inventor, he is constantly seeking innovative ways to tackle unique problems and is one of the hardest working people I have ever known. As the daughter of geologists, both my parents fostered an appreciation and curiosity for natural world. Many family vacations were spent visiting volcanos, digging for ancient fossils, exploring deep caves, and admiring erosion-carved canyons. It taught me to think beyond myself and to ask more questions about the world. To my sister Dawn Nies, who has been my second mother, eldest sister, and best friend. Being an officer in the Navy Reserves, I have always admired her ability to make intelligent decisions. My sister has always been someone I could confide in and ask for counsel regardless of the circumstances. To my grandfather Thomas Nies, who has always been a role model for perseverance and indomitable spirit. His dream was always to become a pilot. He joined the U.S. Army as his vision did not qualify him to be a pilot in the U.S. Airforce during the Korean War. However, after years of studying to become an electrical engineer and running his own business, he now flies his own plane named Rudolf, a Piper Cherokee PA-151 with a red nose. He has taught me to never give up on dreams and to never accept the first “no” you are given as defeat. To my beloved husband AJ Bizub, who has been the light of my life and has stuck with me through these tumultuous years. You have made me happier than I could ever imagine. I could not do this without you, and I cannot wait to see what the future unfolds.

## TABLE OF CONTENTS

Table of Contents .....	i
List of Tables .....	iv
List of Figures .....	v
Abstract .....	vii
Chapter One: Introduction .....	1
Overview of Leukemia and Lymphomas.....	1
Staging and Survival of Cutaneous T cell Lymphoma .....	2
Phenotypic Characteristic of Cutaneous T cell Lymphoma .....	3
Epigenetic Gene Regulation and Histone Modification of Cutaneous T cell Lymphoma .....	6
Current Treatments of Cutaneous T cell Lymphoma .....	9
Cell lines for Cutaneous T cell Lymphoma .....	11
Current Murine Models for Cutaneous T cell Lymphoma .....	11
Chapter Two: Methyltransferase inhibitors restore SATB1 protective activity against Cutaneous T Cell Lymphoma .....	20
Introduction.....	20
Results.....	21
Ablation of Satb1 cooperates with Notch1 overexpression to cause T cell lymphoma .....	21
Ablation of Satb1 induces malignant lymphocytic expansion by promoting phosphorylation of Notch-induced Stat5 .....	23
Ablation of Satb1 in mature CD4+ T cells causes fatal lymphomas with massive T cell skin infiltrates .....	24
SATB1 silencing differentiates cutaneous T cell lymphomas from other peripheral T cell malignancies .....	25
Reversing H3K9 trimethylation, but not targeting H3K27 trimethylation, rescues protective SATB1 activity in Sézary T cells.....	26
SUV39H1/2 inhibition de-represses SATB1 and arrests primary Sézary cell expansion more effectively than romidepsin .....	29
Discussion .....	30
Materials and Methods.....	32
Animals and human samples .....	32
Retroviral Transduction .....	33
Cell lines and MTT assays.....	33

Antibodies and Flow Cytometry .....	34
Cell Trace Violet Assays and Annexin V staining .....	35
Immunohistochemistry, Giemsa, and Western blot.....	36
Q-PCR and ChIP PCR .....	37
RNA-sequencing.....	38
ChIP-sequencing.....	39
Statistics .....	40
Study approval .....	40
Chapter Three: Pathogenic Mechanisms Driving Cutaneous T cell Lymphoma .....	59
Introduction.....	59
Results.....	61
Different stem-like/tumor-initiating cells and differentiation trajectories in Sézary syndrome versus Mycosis fungoides .....	61
Sézary syndrome and Mycosis fungoides are also different in terms of clonality and transcription factors driving malignant phenotypes.....	62
Heavily mutated hematopoietic progenitors share mutations in key oncogenes with malignant Sézary cells in all patients analyzed, but not their normal T cell counterparts in some patients.....	63
Sézary cells show hallmarks of recent thymic egression, but not response to skin antigens .....	65
Discussion.....	65
Materials and Methods.....	68
Human Samples .....	68
Antibodies and Flow Cytometry.....	68
Cell Trace Violet Assays .....	69
Antigen Presentation.....	69
10x RNA, VDJ, and ATAC sequencing.....	70
Single-cell RNA-seq data processing, filtering, batch effect correction, and clustering.....	71
Differential gene expression analysis, cluster annotation, and trajectory analysis.....	72
Trajectory analysis.....	72
Single-cell 10X VDJ analysis.....	72
Single-cell ATAC-seq data processing, filtering, batch effect correction and clustering.....	73
Gene activity scores and cluster annotation.....	74
Identification of group-specific peaks and TF motifsene activity scores and cluster annotation .....	74
Whole Exome Sequencing.....	75
Identification of somatic mutations .....	75
Molecular Cloning .....	76
Q-PCR.....	77
Study approval .....	77
Chapter Four: Conclusions and Future Perspectives .....	88

References .....92

Appendix A: Table of Mutations in CTCL Patients .....105

Appendix B: Copyright Permission .....129

Appendix C: Institutional Animal Care and Use Committee Approval .....130

Appendix D: IRB Approval .....131

## LIST OF TABLES

Table 1. ISCL/EORTC revision to the staging of MF and SS.....	13
Table 2. Mycosis Fungoids and Sézary Syndrome Survival by Clinical Stages .....	14
Table 3. Summary of Histone Deacetylase (HDAC) Classes.....	15
Table 4. Summary of Murine models for CTCL. ....	16
Table 5. RT-qPCR primers for SATB1 gene expression.....	41
Table 6. ChIP-PCR Primers .....	42
Table 7. Summary of repeated overlapping mutations across SS patients .....	78
Table 8. Primers for cloning of Human sjTREC and TRAC sequences .....	79
Table 9. RT-qPCR primers for amplification of sjTRAC and TRCAC sequences .....	80
Table A1. Summary of overlapping mutations in samples of SS patients.....	105

## LIST OF FIGURES

Figure 1:	Overview of tumor microenvironment in CTCL skin. ....	17
Figure 2:	Cell surface markers of MF/SS cells. ....	18
Figure 3:	Overview of Extra-Corporeal Photoimmunotherapy.....	19
Figure 4:	Schematic of triple transgenic murine model. ....	43
Figure 5:	Concurrent ablation of <i>Satb1</i> and increased expression of <i>Notch1</i> in mature T cells results in lethal adenopathy. ....	44
Figure 6:	<i>Satb1</i> ablation transforms the <i>Notch</i> -dependent expansion of CD8 <sup>+</sup> T cells into a full-blown CD4 <sup>+</sup> CD8 <sup>+</sup> T cell lymphoma.....	45
Figure 7:	<i>Satb1</i> ablation and <i>Notch</i> activation cooperate to transform post-thymic CD8 <sup>+</sup> T lymphocytes into skin-homing lymphoma cells with phosphorylated <i>Stat5</i> and cytokine increase.....	46
Figure 8:	Immunohistochemistry staining for CD3 <sup>+</sup> T cell infiltration in mouse skin for CD11cCre model. ....	47
Figure 9:	<i>Satb1</i> ablation and <i>Notch</i> activation cooperate to transform post-thymic CD4 <sup>+</sup> T lymphocytes into skin-homing lymphoma cells.....	48
Figure 10:	Organ weight and immunohistochemistry staining for CD3 <sup>+</sup> T cell infiltration in mouse skin for CD4CreERT2 model.....	49
Figure 11:	Sézary cells, but not other malignant lymphocytes, consistently exhibit <i>SATB1</i> down-regulation.....	50
Figure 12:	Peaks adjacent to <i>SATB1</i> promoter in HuT78, Jurkat, K562 cell lines for ChIP pulled down for H3K27ac, H3K27me3, and H3K9me3 antibodies. ....	51
Figure 13:	H3K27me3 and H3K9me3 occlude the <i>SATB1</i> promoter in a Sézary cell line.....	52
Figure 14:	H3K27me3 and H3K9me3 occlude the <i>SATB1</i> promoter in a Sézary cell line.....	53
Figure 15:	Categorized Pre-ranked GSEA on HuT78 cell line treated with F5446 and Chaetocin. ....	54

Figure 16: Screening epigenetic inhibitors in primary Sézary cells.....	55
Figure 17: H3K9me3 repression of SATB1 in malignant Sézary patient cells.....	56
Figure 18: H3K9me3 repression of SATB1 in CD4+ T cells of Sézary patients.....	57
Figure 19: Summary of epigenetic mechanism silencing SATB1 expression in Sézary cells .....	58
Figure 20: Gene expression patterns in Sézary syndrome and Mycosis fungoides .....	81
Figure 21: Gene expression and open chromatin patterns in Sézary syndrome and Mycosis fungoides .....	82
Figure 22: Chromatin conformation patterns in Sézary syndrome and Mycosis fungoides .....	83
Figure 23: TCR clonality patterns in Sézary syndrome and Mycosis fungoides .....	84
Figure 24: Clonality distributed across distinct SS and MF groups.....	85
Figure 25: Somatic mutations overlapping in hematopoietic stem cells and other cell compartments in Sézary syndrome .....	86
Figure 26: Thymic egression of Sézary syndrome and Antigen presentation capacity in Sézary syndrome and Mycosis fungoides.....	87

## ABSTRACT

The pathogenesis of Cutaneous T cell lymphoma (CTCL) remains unclear. Using conditional knockout mice, we found that ablation of the genomic organizer Special AT-rich sequence-binding protein-1 (Satb1) caused malignant transformation of mature, skin-homing, Notch-activated CD4<sup>+</sup> and CD8<sup>+</sup> T cells into progressively fatal lymphoma. Mechanistically, Satb1 restrained Stat5 phosphorylation and the expression of skin-homing chemokine receptors in mature T cells. H3K27 and H3K9 trimethylation occluded the SATB1 promoter in Sézary cells, while inhibition of SUV39H1/2 methyltransferases (unlike EZH2 inhibition), restored protective SATB1 expression and selectively abrogated the growth of primary Sézary cells more effectively than romidepsin. Additionally, using single-cell RNA/TCR sequencing of 106,130 CD3<sup>+</sup>CD4<sup>+</sup>, CD26<sup>-</sup>/CD7<sup>-</sup> malignant lymphocytes from the peripheral blood of 7 patients with CTCL, coupled to single-cell ATAC-seq of 35,857 CTCL cells, we show that tumor-initiating cells in Sézary syndrome and Mycosis fungoides (MF) exhibit different trajectories of differentiation. Sézary cells exhibit narrower repertoires of TCRs, compared to MF, which are maintained throughout malignant cell expansion, while differentiated MF cells exhibit clonal enrichment. Surprisingly, we identified  $\geq 200$  mutations in hematopoietic stem cells from Sézary syndrome patients. Mutations in key oncogenes were also present in peripheral Sézary cells, which showed the hallmarks of recent thymic egression. However, Sézary cells expand independently of antigen recognition, while mutations in non-malignant cells suggest that they complete their malignant transformation in the periphery. Therefore, CTCL arises from mutated lymphocyte progenitors that acquire TCRs in the thymus.

## CHAPTER ONE: INTRODUCTION

### Overview of Leukemia and Lymphomas

The estimated number of new cases per year for Leukemia and Lymphoma are 60,530 and 85,720, and the number of cancer related deaths per year in the United States are 23,100 and 20,910, respectively presenting as one of the leading lethal cancers for both men and women (1). The two main forms of lymphoma are Hodgkin's Lymphoma (approximately 10%) and non-Hodgkin lymphoma (NHL) (approximately 90%) (2). Hodgkin's Lymphoma is defined by the presence of multi-nucleated B lymphocytes known as Reed-Sternberg cells (CD45<sup>-</sup>CD20<sup>-</sup>CD30<sup>+</sup>CD15<sup>+</sup>) (3, 4) with a favorable prognosis depending on the stage (SEER 88.3% 5 year relative survival rate) compared to NHL (SEER 72.7% 5 year relative survival rate) (4, 5). Symptoms and complications shared by most forms of lymphoma consist of swelling of the lymph nodes (lymphadenopathy), enlarged spleen (splenomegaly), night sweats, weight loss, fever, fatigue, and impaired immunity (6, 7). Peripheral T cell Lymphoma (PTCL) are a heterogeneous group of aggressive lymphomas consisting of mature T cells that is presented in 29 forms as recognized by the World Health Organization and comprises 10-15% of NHL in western countries (6). Clinical subgroup of PTCL include extranodal involvement such as the skin which are known as Cutaneous T cell Lymphomas (CTCL) (7).

## Staging and Survival of Cutaneous T cell Lymphoma

CTCL is comprised of many diseases, with the most prevalent being mycosis fungoides (MF) and Sézary syndrome (SS) accounting for approximately 50% of cases with an increase incidence rate in males, individuals over 70, and African descent (8). In the United States, the incidence rate per 100,000 person-years is approximately 0.55 mycosis fungoides (MF) and 0.01 for Sézary syndrome (SS) (9). Mycosis fungoides and Sézary syndrome are typically CD4<sup>+</sup> T cells diseases (10) and rarely does mycosis fungoides presents as CD8<sup>+</sup> T cells (5%) (11, 12). Reports have also described the presence of CTCL cases being double positive for CD4 and CD8 surface markers (13, 14). The International Society for Cutaneous Lymphomas (ISCL) classifies MF and SS using the tumor-node-metastasis-blood (TNMB) classification system. This system defines staging based on peripheral blood (B), lymph node (N), involvement in the skin (T) and visceral organs (M) (Table 1) (15, 16).

Sézary syndrome is often described as the leukemic variant of mycosis fungoides; however, Sézary syndrome is a distinct form of CTCL which can occur *de novo* without prior history of mycosis fungoides (17). Clinical presentation of mycosis fungoides patients are skin lesions typically defined as patches (T<sub>1,2</sub>), plaques (T<sub>1,2</sub>), or tumors (T<sub>3</sub>) whereas Sézary syndrome presents with erythroderma (T<sub>4</sub>), or erythema (reddening of the skin) that covers at least 80% body surface area (BSA) of the skin (15, 18). There are cases in which mycosis fungoides will present with erythroderma known as erythrodermic MF usually without systemic involvement (19, 20). Blood involvement is characterized by percentage and absolute count of CD4<sup>+</sup>CD26<sup>-</sup> or CD7<sup>-</sup> cells with stage B<sub>0</sub> as <5% of lymphocytes are MF/SS cells (<250 cells/ul), B<sub>1</sub> as >5% MF/SS cells (≥250-1,000 cells/ul), and B<sub>2</sub> (≥1000cells/ul) (21). Sézary syndrome is defined at B<sub>2</sub> whereas mycosis fungoides typically lacks robust peripheral blood involvement

(15, 22). The prognosis for Sézary syndrome is dismal with 5-year survival rate around 15-30% once the patient has been diagnosed. Mycosis fungoides is fairly indolent disease with a high survival rate at early stages (16) (Table 2). Considering the aggressive and heterogenous nature of Sézary syndrome as well as the low survival rate of patients at advanced stages, a variety of treatments have emerged with varying clinical success.

### **Phenotypic Characteristic of Cutaneous T cell Lymphoma**

Flow cytometry immunophenotyping (FCI) of Sézary syndrome and mycosis fungoides has shown to be an important component of staging both diseases. CTCL is most often characterized by CD2<sup>+</sup>, CD3<sup>+</sup>, CD4<sup>+</sup>, CD5<sup>+/-</sup>, CD8<sup>-</sup>, CD7<sup>-</sup>, and CD26<sup>-</sup> surface markers. CD7 is cell surface homodimer that is part of the immunoglobulin superfamily and is one of the first markers in T cell maturation. It is expressed on all thymocytes, most mature peripheral T cells and natural killer (NK) cells (23). The precise function of CD7 remains unclear; however, it is speculated to be involved in signal transduction, T cell proliferation, T cell activation, and intercellular adhesion (24). Its loss has been reported in both benign and malignant inflammatory skin conditions as well as hematological malignancies. The expression of CD7 is potentially regulated by epigenetic factors such as mutations in CCAAT/enhancer-binding protein- $\alpha$  (CEBPA), a leucine zipper transcription factor needed for granulocytes, or DNA promoter methylation as shown in AML and CML (25-27). CD26 is a glycoprotein with dipeptidyl peptidase IV (DPP-IV) activity located in the extracellular domain responsible for cleavage of polypeptides with L-proline or L-alanine (28). Expression of this marker appears in late thymic differentiation, typically on CD4<sup>+</sup> Th1 helper cells, and responds to ligands such as caveolin-1 on monocytes and adenosine deaminase (29, 30). CD26 acts as co-stimulatory molecule associated with T cell activation and IL-2 production in response to antigens in humans (30), unlike their

murine counterparts (31). The difference in function between human and murine homologs for CD26 and CD7 has made *in vivo* studies of their role in CTCL pathology and other associated conditions challenging.

The majority of CD4<sup>+</sup> cells lack the presence of CD26 (>90%) compared to CD7 (approximately 50%) in Sézary patients (32). However, it should be mentioned that a multiparameter approach to FCI has shown that there is a percentage of non-malignant T cells in normal donors which share the CD3<sup>+</sup>CD4<sup>+</sup>CD26<sup>-</sup> (range 4.0-34.6%, mean absolute cell count 159/ul) and CD3<sup>+</sup>CD4<sup>+</sup>CD7<sup>-</sup> (range 1.6-23.5%, mean absolute cell count 78.1/ul) phenotype (33). Additionally, CD26 positivity was shown for 56-86% of CD4<sup>+</sup> T cells and CD7 positivity for 73%-97% of CD4<sup>+</sup> T cells from peripheral blood of normal control samples demonstrating there are CD26 negative and CD7 negative populations in non-malignant cells. Therefore, quantification of CD4<sup>+</sup>CD26<sup>-</sup> or CD4<sup>+</sup>CD7<sup>-</sup> T cells exclusively does not provide an accurate absolute count of malignant cells (34). Despite these limitations, the loss of CD26 and CD7 expression is well correlated with MF and SS cells and quantified for staging of patients.

The expression of C-C chemokine receptor type 4 (CCR4) has been reported in CTCL (35) and high expression is associated with poor prognosis (36, 37). CCR4 is a member of G protein-coupled seven transmembrane receptors responsible for the trafficking of leukocytes in inflammatory diseases such as atopic asthma and atopic dermatitis (38, 39). CCR4 ligands are CCL17 and CCL22, which are secreted by dendritic cells, and is expressed on Th2 cells which produce pro-inflammatory cytokines IL-4, IL-5 and IL-13 (38). Furthermore, CCR4 has shown to play an important role in tissue homeostasis and maintenance of Th2 inflammation. Its regulation is ligand-induced as well as subject to constitutive endocytosis based on the C-

terminus amino acid sequence (40). The usage of anti-CCR4 antibody, mogamulizumab, in CTCL is discussed in later sections.

The complete etiology of CTCL is unknown; however, the accumulation of these cells in the skin is suspected to be antigen driven. Mycosis fungoides is typically described as having an effector T cell phenotype by expressing E-selectin ligand, cutaneous lymphocytes antigen (CLA), CCR4, CCR8, and CCR10 which facilitate trafficking to the skin. These cells eventually become tissue resident memory T cells ( $T_{RM}$ ) (41, 42). Mechanistically, as the plaques and patches form there is an accumulation of malignant cells which home to the skin via interactions through CCR4 and CLA (ligand is E-selectin). The cells begin to produce Th2 cytokines (IL-4, IL-5, and IL-10) which inhibits the immune response by decreasing the number of  $CD8^+$  T cells, NK cells, and dendritic cells. As the lesions transform into tumors, there is an increase in the number of eosinophils and malignant T cells. Overtime, it is hypothesized these cells gain the ability to escape the tumor microenvironment as Sézary cells by adopting a T cell central memory phenotype ( $T_{CM}$ ) (L-selectin and CCR7) which allows homing to the peripheral blood and lymph nodes (Figure 1). Additionally, both MF and SS cells evade the immune system by upregulation of exhaustion markers PD-1 and CTLA-4 (Figure 2) (43, 44).

The morphology of Sézary and MF cells have been described as small to medium sized cells with a cerebriform or “brain-like” nuclei. These cells have a high nucleus to cytoplasm ratio as well as condensed chromatin. The presence of cerebriform nuclei have also been found in less than 10% of lymphoid cells in circulating normal cord and peripheral blood (45). Cerebriform nuclei have been described in T cell prolymphocytic leukemia (46), and in rare cases B-cell lymphoma (47). The purpose and stage at which Sézary and MF cells develop this morphology in the malignant transformation is currently unclear.

There is a subset of CTCL patients which undergo Large Cell Transformation (LCT), adopting a large blast-like T cell morphology. This aggressive form of the disease has poor outcomes for patients with a median survival of 2-3 years after transformation (48). LCT occurs in 20-55% of advanced MF cases (48), with expression of the marker CD30 in 30-40% of LCT-MF cases (49, 50) and 50% of LCT-SS cases (50). LCT is defined when more than 25% of lymphoid or tumor cells are large cells infiltrating the skin (50). CD30, also known as Ki-1 or TNFRSF8, is a trans-membrane glycoprotein that is part of the tumor necrosis factor receptor superfamily and is activated via the NF- $\kappa$ B pathway (51, 52). CD30 is expressed on other primary cutaneous T cell lymphoma such as cutaneous anaplastic large cell lymphoma and lymphomatoid papulosis (6). Direct targeting has been achieved using Brentuximab vedotin which is a CD30 specific monoclonal antibody conjugated with monomethylauristatin E, a microtubule targeting agent, in CTCL (53) as well as other CD30<sup>+</sup> PTCL (54) and Hodgkin Lymphoma (55-57).

### **Epigenetic Gene Regulation and Histone Modification of Cutaneous T cell Lymphoma**

In many cancers, the conformation of DNA is abrogated with global effects on the transcriptional programming of cells. Gene regulation has been attributed to several mechanisms, most notably post-translational modification (PTM) of the lysine tails of histones. Modification of lysine residue occurs in a variety of sites involved in either gene activating or repressing functions. Acetylation of these lysine tails by Histone acetyltransferases (HATs) modifies chromatin accessibility and allows for an “open” conformation for transcriptional machinery to bind to enhancer and promoter regions. Conversely, histone deacetylases (HDACs) remove the acetyl group and result in changing of DNA from an “open” to a “closed” conformation, preventing transcription factors and other co-factors from mediating transcription of tumor

suppressor genes. The HDAC superfamily is divided into 18 members and grouped into four main classes consisting of two protein families based on their yeast homologs (Table 3) (58). Classes I, II, and IV are zinc-dependent HDACs while Class III (sirtuins) are NAD<sup>+</sup>-dependent HDACs (59). Inhibitors have been developed to prevent the acetylation of histones, resulting in changes in the chromatin conformation landscape. Subsequently, the expression of tumor suppressors in cancer cells are potentially restored. Inhibitors of HDACs (iHDAC) target only zinc-dependent HDAC proteins and prevent the removal of acetyl groups from histone lysine tails to maintain transcriptional activity.

HDACs which have been shown to be relevant to CTCL pathology have been HDAC1, 2, and 6. Increased expression of HDAC2 has been previously associated with aggressive disease whereas increased expression of HDAC6 is associated with favorable outcomes regardless of subtype (60, 61). Mechanistically, the overexpression of IL-15 has contributed to the initiation and progression of CTCL. Downstream signaling molecules of IL-15, HDAC1 and HDAC6, have therefore been targeted in preclinical studies (58). Conversely, inhibition of HDAC6 alongside the PI3K pathway has abrogated cell proliferation (62). The efficacy of HDAC inhibitors in pre-clinical studies opens the possibility of other methods of epigenetic modification in CTCL via inhibitors of other histone modifying compounds.

Repressing tumor suppressive genes can be regulated via other epigenetic modifiers containing Su(var)3-9-Enhancer of zeste-Trithorax (SET) domains which act as histone methyltransferases (HMTases). The mono- and dimethylation of lysine 9 of histone 3 (H3K9) and lysine 27 (H3K27) is mainly mediated by SET containing epigenetic modifiers, G9 and G9 like protein (GLP), to produce heterochromatin (63). Furthermore, Suppressor of variegation 3-9 homolog (SUV39H1) is responsible for the trimethylation of H3K9 (64). Several

naturally and synthetically derived inhibitors for HMTases have been developed. Firstly, an inhibitor for SUV39H1/2 was developed by Greiner et al. known as Chaetocin which was an isolated fungal toxin from *Chaetomium minutum* (65). The role of SUV39H1 and its inhibition using Chaetocin have been previously reported in acute myeloid leukemia (AML) preclinical studies. Interaction of factors relating to self-renewal of hematopoietic stem cells such as RUNX1 (AML1) with SUV39H1 and G9a as transcriptional repressors allow for bone marrow immortalization in AML. Combination of chaetocin with HDAC inhibitor (vorinostat) or bromodomain extra terminal protein (BET) inhibitor (JQ-1) demonstrated a synergistic effect in AML cells (66, 67). Another study demonstrated that treatment with chaetocin on AML cell lines and *ex vivo* patient samples increased reactive oxygen species (ROS) and death-receptor dependent apoptosis (68).

Another fungal toxin was screened by the Lui lab to identify an inhibitor for SUV39H1/2 and G9a/GLP known as Verticillin A. Treatment with Verticillin A inhibited H3K9me3 deposition near the promoter of *FAS* gene to mediate apoptosis via cytotoxic T lymphocytes (CTLs) in 5-Fluorouracil resistant colorectal carcinoma (CRC) (69). However, both chaetocin and Verticillin A are non-specific inhibitors for SUV39H1 and interact with other HMTases (69, 70). This group has also developed a second generation of a specific SUV39H1 inhibitor, F5446, which recovered *FAS* expression and induced cell cycle arrest and apoptosis in CRC (71). Additionally, expression levels of *SUV39H1* were found to be elevated in CD8<sup>+</sup> CTLs in which inhibition via F5446 restored expression of *GZMB*, *PRF1*, *FASLG*, and *IFNG* (72). Although HMTases have not been previously tested in CTCL, there is precedence for their use in leukemia as well as altering expression patterns in T cells.

## **Current Treatments of Cutaneous T cell Lymphoma**

The National Cancer Center Network (NCCN) and European Organization for Research and Treatment of Cancer (EORTC) have guidelines available for treatment of this rare and heterogenous disease (50, 73). Unfortunately, patients rarely achieve long-term remission and treatment often follows a stage-adapted approach depending on treatment goals (73). Typically, patients at earlier stages of disease receive skin directed therapies such as ultraviolet B light (UVB) phototherapy for patch and thin plaques (74), psoralen plus ultraviolet A light (PUVA) for thicker plaques (74) and topical corticosteroids (75). Patients at more advanced stages are treated with systemic therapies such as retinoids (bexarotene) (76, 77), Interferon-alpha (78, 79), and Histone De-acetylase (HDACs) inhibitors such as vorinostat (80-82) and romidepsin (83). However, standard chemotherapies are rarely curative for Sézary syndrome patients. The following section will focus on first- and second-line therapies used for stage III or SS patients (stage III or IVA).

Regarding first line therapy, the Food and Drug Administration (FDA) approved the use of extra-corporeal photoimmunotherapy (ECP) for Sézary syndrome and erythrodermic mycosis fungoides with high blood involvement in 1988 and was initially pioneered by Edelson and colleagues (84). The whole peripheral blood is collected and separates out leukocytes to be exposed extracorporeally to photosensitizing agent 8-Methoxypsoralen (8MOP), which belongs to a group of compounds known as psoralen, and subsequently UVA irradiated (Figure 3). The precise mechanism of action is still unknown; however, it is plausible that monocytes differentiate into immature dendritic cells (iDCs) and the induction of apoptosis in T cells provides patient specific antigens (85). This process has been compared to having a vaccine like effect in patients and can be used as a monotherapy as well as in combination with other agents

(86). The response rate across all stages is 56% OR (18% CR), but 43% OR (10% CR) in SS. Similarly, PUVA is a photosensitizing agent taken orally with direct skin exposure to UVA radiation and is typically used on stages IA and IIB, but is less effective in erythrodermic patients or thicker plaques (54-65% OR) (87).

Second line therapies include HDAC inhibitors, which as previously discussed have a prominent role in the disease pathology of CTCL. Vorinostat and romidepsin were the first HDAC inhibitors to be approved by the FDA for treatment CTCL. Vorinostat was approved in 2006 by the FDA with an overall response rate (ORR) of 24-30% and inhibits class I and class II HDACs (81, 88). Patient OR to romidepsin as a monotherapy; however, are still approximately 34% in the clinic (6% CR and 28% PR) (83). Treatment with romidepsin in combination with other agents may improve outcomes for relapse and refractory PTCL (89).

In 2018, the first FDA approved drug specifically for Sézary syndrome was the defucosylated monoclonal antibody against CC chemokine receptor 4 (CCR4 or CD194), known as mogamulizumab (90). In a randomized controlled phase 3 trial of CTCL patients treated with mogamulizumab showed superior progression free survival (7.7 months) compared to vorinostat (3.1 months) (90). However, treatment with mogamulizumab can result in autoimmune conditions such as Stevens-Johnson syndrome in adult T cell leukemia/lymphoma (91, 92) and potentially Graft-vs-host-disease (GVHD) in CTCL (93) as CCR4 is also expressed on Tregs. Despite the numerous clinic approaches in treating Sézary syndrome, patients often relapse and rarely are cured of this aggressive disease. This warrants additional treatments and understanding of the pathogenesis of the CTCL.

## **Cell lines for Cutaneous T cell Lymphoma**

There are 11 main cell lines for CTCL which are composed of HTLV-1<sup>+</sup> or HTLV-1<sup>-</sup> cells. However, HTLV-1<sup>+</sup> cell lines are more reflective of Adult T cell Leukemia/Lymphoma (ATLL) than MF/SS as previously investigated (94). Generally, MJ and HuT102 are HTLV-1<sup>+</sup> while My-La, HUT78, HH, H9, SZ4, Sez4, Mac2a, SeAx, and PB2B are HTLV-1<sup>-</sup>. These cell lines are further characterized by whether they are considered MF (My-La) (95), Leukemic MF (HH) (96), SS (HUT78 (97), H9 (98), SZ4, Sez4 (99), and SeAx(100)), or CD30<sup>+</sup> lymphoma (Mac2a and PB2B) (94). HTLV-1<sup>-</sup> cell lines for MF and SS have been shown to have more sensitivity to HDAC inhibitors, more aneuploidy, heterogenous mutations in *TP53* gene, and more heterogeneity in karyotyping and gene expression compared to HTLV-1<sup>+</sup> cell lines (94). However, none of these MF or SS cell lines represents early-stage MF or LCT transformation, which currently limits *in vitro* studies.

## **Current Murine Models for Cutaneous T cell Lymphoma**

Ideally, murine models replicate clinical presentation as well as the genetics of the tumor. The peripheral blood of mice are predominantly lymphocytes rather than neutrophils like in humans (101). Xenograft models are relatively simple, inexpensive, high yielding, and typically give more rapid results compared to other murine models which are useful systems for initial studies. However, the microenvironment often greatly differs compared to patients and lacks the coordination of other essential immune players. Cell line-derived xenografts can be challenging as cell lines are prone to acquire chromatin mutations which do not faithfully recapitulate the primary tumor. Patient-derived xenografts recapitulate the genetics of the primary tumor, but also are immunodeficient and are unable to precisely test specific combinations of initiating

mutations. Conditional transgenic mice have the advantage of specific cell targeting and temporal control in an immunocompetent model (102). Previous strategies for CTCL murine models have utilized several strategies to recapitulate the diseases patient derived xenografts, cell line-derived xenografts, spontaneous, adoptive transfer, germline and conditional transgenic models.

Early CTCL murine models used xenografts from patient derived CD4<sup>+</sup> lymphocytes or blood or skin derived CTCL cell lines in immunodeficient mice models. However, these models were either unable to disseminate outside of the graft (103) or displayed perivascular locations and circulating cells but were unable to develop large secondary tumors (104, 105). Several cell line xenograft models for CTCL have been developed studying therapeutic efficacy such as HDAC inhibitors (106) and Methotrexate (107). Previous transgenic models overexpressing human IL-15 showed a 30% developed aggressive large granular lymphocyte (LGL) leukemia or 70% developed cutaneous lesions and atypical hyperchromatic nuclei similar to cerebriform structure in CTCL patients. However, this model displayed only moderate increases in total peripheral leukocytes compared to wild type mice and has been typically described as having expansion and activation of NK cells and CD8<sup>+</sup> T cells (108, 109).

In a bone marrow transplantation model, a retroviral transduction for constitutively active form of JAK3, JAK3A572V, produced effector CD8<sup>+</sup>TCRαβ<sup>+</sup>CD44<sup>+</sup>CD122<sup>+</sup>Ly-6C<sup>+</sup> T cells which acted as an aggressive lymphoproliferative disorder which infiltrated the skin with cerebriform nuclei. When the procedure was repeated in an MHC-I deficient model, there was an accumulation of CD4<sup>+</sup> T cells (110) (Table 4). Few murine models have been developed to assess the pathogenesis of the disease which should be addressed with additional transgenic murine models.

**Table 1. ISCL/EORTC revision to the staging of MF and SS**

<b>Stage</b>	<b>T</b>	<b>N</b>	<b>M</b>	<b>B</b>
<b>IA</b>	1	0	0	0,1
<b>IB</b>	2	0	0	0,1
<b>IIA</b>	1,2	1,2	0	0,1
<b>IIB*</b>	3	0-2	0	0,1
<b>III*</b>	4	0-2	0	0,1
<b>IIIA*</b>	4	0-2	0	0
<b>IIIB*</b>	4	0-2	0	1
<b>IVA<sub>1</sub>*</b>	1-4	0-2	0	2
<b>IVA<sub>2</sub>*</b>	1-4	3	0	0-2
<b>IVB*</b>	1-4	0-3	1	0-2

Abbreviations: B, blood; M, metastasis; N, node; T, tumor. \*Considered “advanced-stage” disease. (Sean Whittaker, Richard Hoppe, H. Miles Prince, *Blood*, 2016).

**Table 2. Mycosis Fungoids and Sézary Syndrome Survival by Clinical Stages**

5 year Overall Survival			
Stage	Percentage	Symptoms	Disease
IA	94-100%	Plaques cover <10% of the skin surface	MF
IB	73-86%	Plaques cover >10% of the skin surface	MF
IIA	78%	Lymph nodes are abnormal, but not cancerous	MF
IIB	40-65%	Tumors 1cm or larger, lymph nodes are abnormal	MF
III	40-60%	>80% of the skin surface has patches, lymph nodes are abnormal	MF
IVA1	37-48%	High number of Sézary cells in the blood	SS
IVA2	18-33%	Cancer forms in lymph nodes, high number of Sézary cells in the blood	SS
IVB	18-39%	Cancer spreads to spleen or liver	SS

(Sean Whittaker, Richard Hoppe, H. Miles Prince, *Blood*, 2016)

**Table 3. Summary of Histone Deacetylase (HDAC) Classes**

<b>Class</b>	<b>HDACs</b>	<b>Mechanism</b>
<b>I</b>	HDACs 1,2,3 & 8	zinc-dependent
<b>IIa</b>	HDAC 4,5,7 & 9	zinc-dependent
<b>IIb</b>	HDAC 6 & 10	zinc-dependent
<b>III</b>	SIRT1-7	NAD <sup>+</sup> -dependent
<b>IV</b>	HDAC 11	zinc-dependent

**Table 4. Summary of Murine models for CTCL**

<b>Disease</b>	<b>Model Description</b>	<b>Mouse strain</b>	<b>Reference</b>
CTCL	Patient skin xenograft; CD4 <sup>+</sup> lymphocytes	C.B.-17 SCID	(103)
MF	Cell line xenograft; MyLa	Athymic nude mice (nu/nu)	(104)
CTCL	Cell line xenograft; MyLa2059	NOD/SCID-B2m <sup>-/-</sup> (NOD.Cg-Prkdc <sup>scid</sup> B2 <sup>mtm1Unc</sup> /J)	(106)
SS	Cell line xenograft; intrahepatic injection; HUT78 and SeAx	RAG2 <sup>-/-</sup> $\gamma$ c <sup>-/-</sup>	(105)
CTCL	Cell line xenograft; intrahepatic injection; My-La, HUT78, HH, MAC2A, MAC2B, FE-PD and MAC1	NOD.Cg- Prkdc <sup>scid</sup> Il2rg <sup>tm1Wjl</sup> /SzJ	(107)
CTCL/T-NK	Transgenic; overexpression human IL-15 CD4 <sup>+</sup> and CD8 <sup>+</sup> T cells	C57BL/6	(108, 109)
CTCL	Activated JAK3 CD8 <sup>+</sup> or CD4 <sup>+</sup> T cells	Retroviral transduction/BMT model; C57BL/6, C57BL/6-2Kb <sup>tm1</sup> H-2D <sup>btm1</sup> and Balb/c	(110)

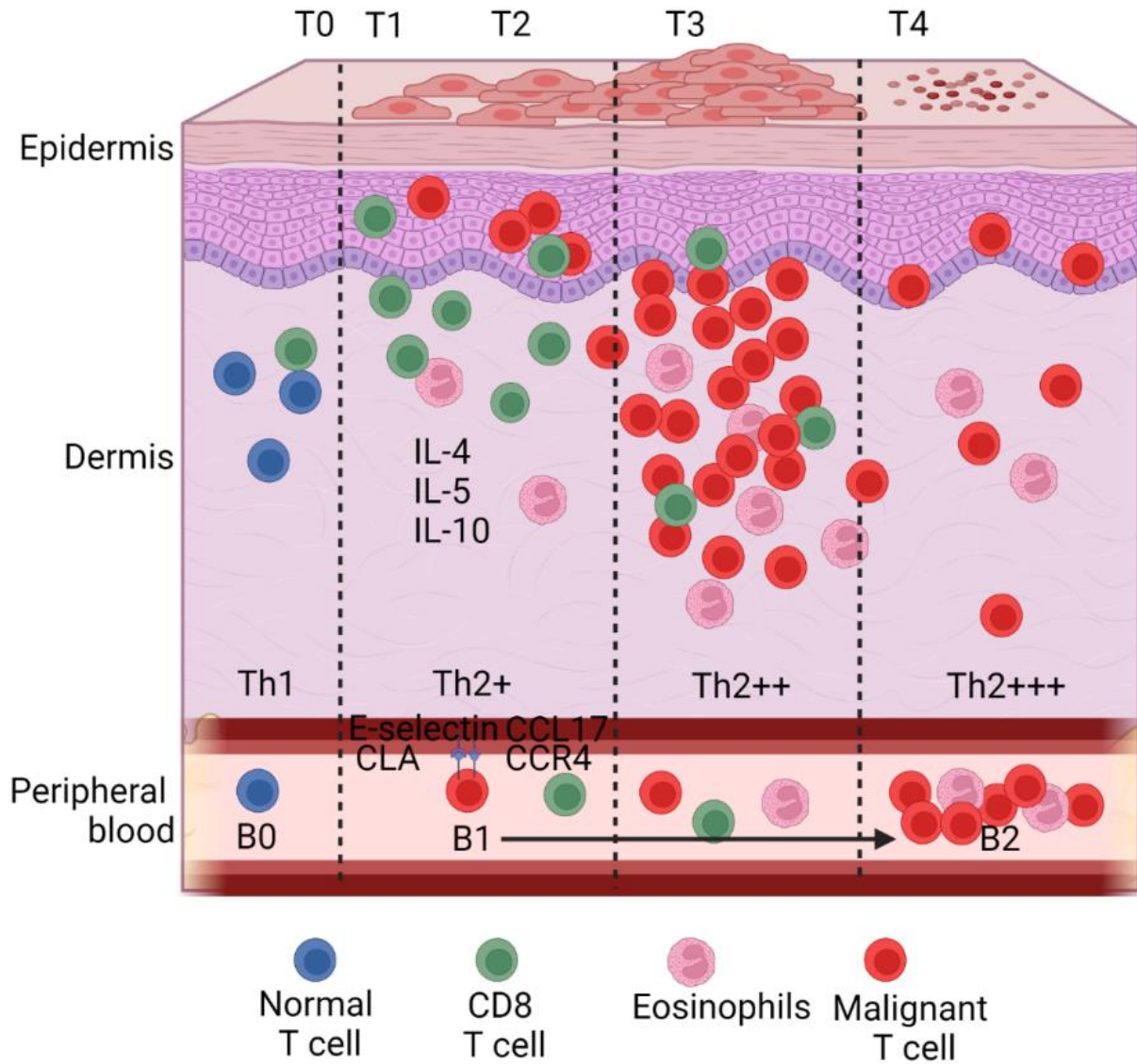


**Figure 1. Overview of tumor microenvironment in CTCL skin.**

Malignant T cells begin to home to the skin via cell surface receptors CLA and CCR4 to their ligands E-selectin and CCL17. Accumulation of malignant cells in the epidermis begin to produce Th2 cytokines IL-4, IL-5, and IL-10 and impacting CD8 T cells, NK cells, and DCs in the microenvironment as patches and plaques form. Eventually the number of CD8 T cells, NK cells, and DC cells declines with the rapid increase of malignant cells as tumor lesions form. Finally, erythroderma appears, and malignant cells migrate from the skin to the peripheral blood causing Sézary syndrome. (Kim et al., *Journal of Clinical Investigation*, 2005)

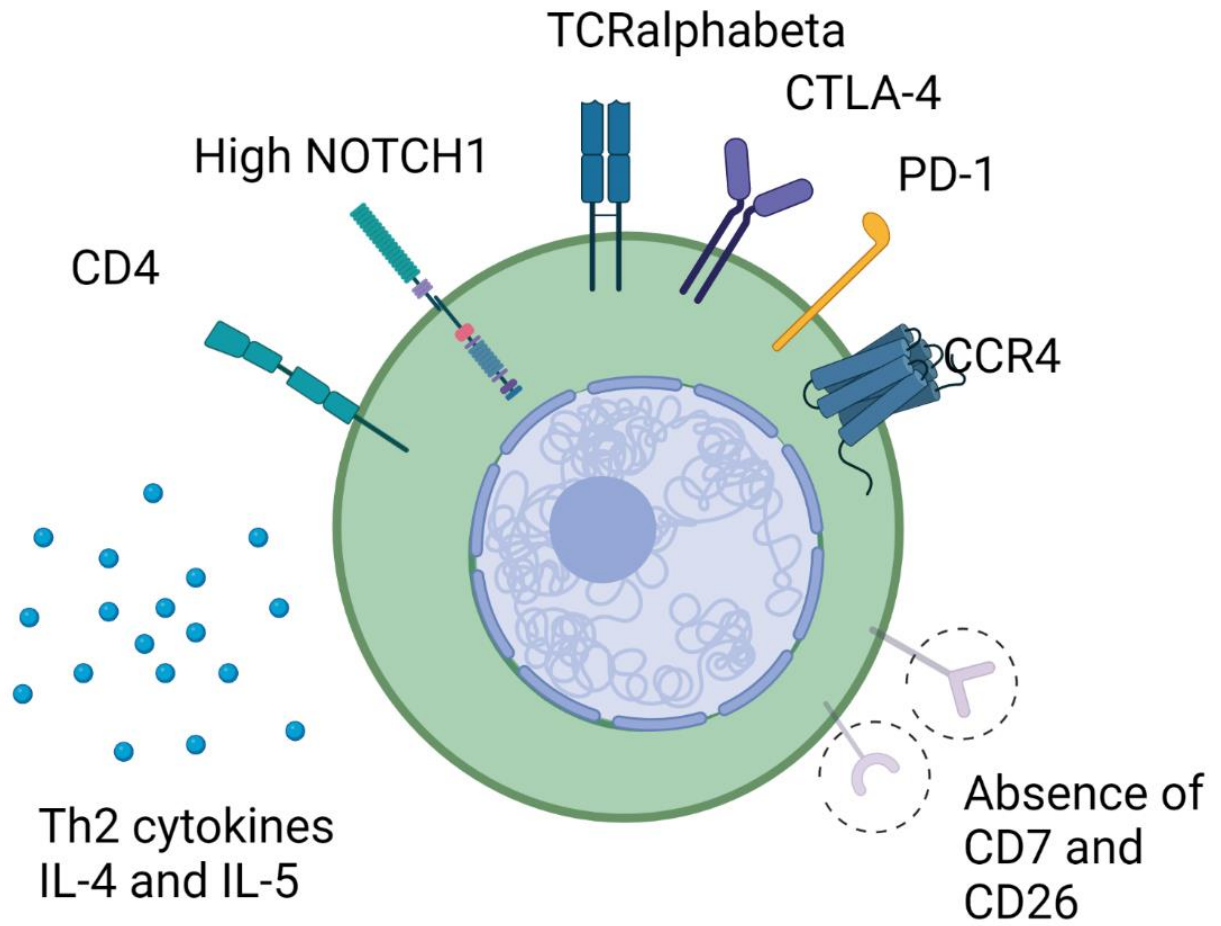


**Figure 2. Cell surface markers of MF/SS cells.**

Cutaneous T cell lymphoma is characterized by presence of CD4, CCR4, high expression of NOTCH1, expression of Th2 cytokines, absence of CD7 and CD26, and exhaustion markers PD-1 and CTLA.

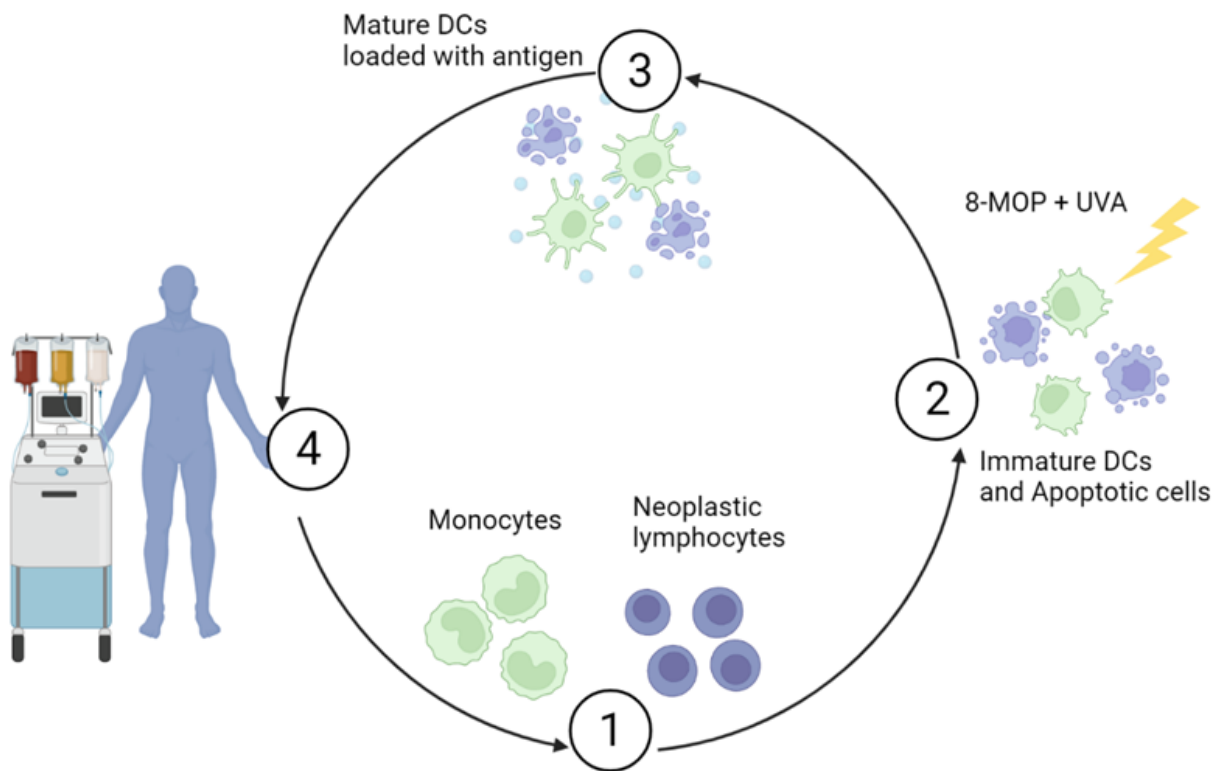


**Figure 3. Overview of Extra-Corporeal Photoimmunotherapy.**

Circulating leukocytes including monocytes and neoplastic cells are concentrated outside of the patient and exposed to 8-MOP and UVA radiation. The neoplastic cells undergo apoptosis in the presence of immature DCs to eventually form mature DCs loaded with tumor antigen before being reinfused into the patient.

## **CHAPTER TWO: METHYLTRANSFERASE INHIBITORS RESTORE SATB1 PROTECTIVE ACTIVITY AGAINST CUTANEOUS T CELL LYMPHOMA**

**A note to the reader: the majority of this chapter has been published in a research article in *Journal of Clinical Investigation*, Harro et. al., 2020**

### **Introduction**

Peripheral T cell lymphomas (PTCL) represent a collection of aggressive disorders with unfavorable outcome that account for about 12% of lymphoid tumors worldwide (111). Cutaneous T cell lymphoma (CTCL) belongs to a heterogeneous group of T cell lymphomas characterized by a cutaneous infiltration of malignant T cells. No curative therapies are currently available for advanced Mycosis fungoides and its leukemic variant, Sézary syndrome, which are the most common forms of CTCL with an annual incidence of about 0.5 per 100,000 (112). NOTCH1 is overexpressed in CTCL in a stage-dependent manner (113), and recent studies have suggested a role for other potential oncogenic drivers, including TP53, RB1, PTEN and DNMT3A (114). The similarities and differences in the molecular underpinnings of these heterogeneous diseases remain poorly understood, and seminal genomic analyses are restricted to a handful of patients in the pathogenesis of Mycosis fungoides/Sézary syndrome (114). Informative animal models that reflect multi-step oncogenesis and cover a broader spectrum of CTCL are therefore needed to test more effective treatments and identify potentially novel therapeutic targets. Lack of mechanistic understanding and the subsequent absence of curative

interventions have led to a poor prognosis and serious deterioration in the quality of life for patients with advanced CTCL disease. A better understanding of the pathogenesis of this disease is urgently needed to design new treatments that improve both quality of life and survival outcome.

The chromatin organizer Special AT-rich sequence-binding protein-1 (SATB1) plays essential roles in the process of apoptosis, cell invasion, metastasis and proliferation of cancer cells (115). In addition, a dynamic SATB1 expression pattern controls the phenotype of tumor-associated dendritic cells (116) and cytotoxic T cells (117), which in coordination determine malignant progression. In addition to cancer, SATB1 modulates the phenotype of regulatory T cells (118) as well as the epigenetic and transcriptional pathways required for hematopoietic stem cell division and self-renewal (119). Interestingly, recent reports suggest that SATB1 could be down-regulated in Mycosis fungoides (120), although epigenetic silencing mechanisms via histone modification and the consequences of *SATB1* downregulation remain uninvestigated. Using a triple transgenic mouse for concurrent ablation of *Satb1* and activation of Notch1 signaling specifically in mature T cells, we generated a reproducible model of progressive fatal T cell lymphoma/leukemia. This system provides possible insight into the role of *SATB1* as a suppressor gene in CTCL and allowed us to identify potential interventions to restore SATB1 function in primary malignant T cells.

## Results

### *Ablation of Satb1 cooperates with Notch1 overexpression to cause T cell lymphoma*

We generated a triple (*CD11c<sup>Cre</sup>Satb1<sup>flx/flx</sup>Rosa26<sup>NI-ICD</sup>*) transgenic mouse model to bypass the requirement of *Satb1* for Notch1 expression in Bone Marrow Dendritic Cells

(BMDCs). In this system, cre expression triggers *Satb1* ablation while simultaneously driving the expression of Notch1 intracellular domain (N1<sup>ICD</sup>) (Figure 4) (121). Mice developed normally as neonates but exhibited a progressive increase in T cell numbers in peripheral blood.

Unexpectedly, all triple transgenic mice, but never *CD11c<sup>Cre</sup>Satb1<sup>flx/flx</sup>* or *CD11c<sup>Cre</sup>Rosa26<sup>N1-ICD</sup>* littermates, developed a decrease in activity and ruffled fur after ~10 weeks, followed by tensional ascites and difficulty breathing within the next 2 weeks, when the mice became moribund. Compared to littermates, 8-10 week-old triple transgenic mice showed prominent splenomegaly and hepatomegaly, along with pronounced adenopathy and effacement of normal architecture in the kidneys (Figure 5 A, C and D). Triple transgenic mice demonstrated significantly decreased survival compared to *CD11c<sup>Cre</sup>Satb1<sup>flx/flx</sup>* and *CD11c<sup>Cre</sup>Rosa26<sup>N1-ICD</sup>* littermates (Figure 5B).

T cell accumulation of tumor-bearing *CD11c<sup>Cre</sup>* mice presented no detectable expansion of NK or  $\gamma\delta$  T cells in the peripheral blood (Figure 6A). Although the phenotype was driven by a *CD11c<sup>Cre</sup>* transgene, flow cytometric analyses of *Satb1* excised cells (based on green fluorescence linked to Notch1 expression) revealed progressive accumulation of GFP<sup>+</sup>CD8<sup>+</sup>CD3<sup>+</sup> T cells in peripheral blood, which is consistent with the expression of *CD11c* in a subset of CD8<sup>+</sup> T cells (122, 123) (Figure 6B). Accordingly, the disease evolved from the accumulation of a population of CD8<sup>+</sup> T cells in peripheral blood, which progressively turned into CD4<sup>+</sup>CD8<sup>+</sup> double positive T lymphocytes and became the most abundant T cell subset after ~8 weeks (Figure 6C). In contrast, although *Satb1<sup>+</sup>CD11c<sup>Cre</sup>Rosa26<sup>N1-ICD</sup>* littermates also showed some progressive expansion of Notch<sup>Knock-in</sup> (GFP<sup>+</sup>) CD8<sup>+</sup> T cells (Figure 6D), no mice in this group exhibited accumulation of CD4<sup>+</sup>CD8<sup>+</sup> lymphocytes at identical temporal points or signs of disease at any time (Figure 6E). Together, these results indicate that Notch1

overexpression in a subset of mature CD11c<sup>+</sup>CD8<sup>+</sup> T cells alone is not sufficient to drive malignant progression. However, additional ablation of *Satb1* results in progressive and lethal accumulation of T cells that become CD4<sup>+</sup>CD8<sup>+</sup> double positive lymphocytes at terminal disease stages.

*Ablation of Satb1 induces malignant lymphocytic expansion by promoting phosphorylation of Notch-induced Stat5*

Microscopic examination of skin harvested from *CD11c<sup>Cre</sup>Satb1<sup>flx/flx</sup>Rosa26<sup>NI-ICD</sup>* showed CD3<sup>+</sup> T cell infiltrates which were stained as described previously (124). CD3<sup>+</sup> T cell infiltrates densely cluster within the dermis with individual lymphocytic cells present within the epidermis in the majority of *CD11c<sup>Cre</sup>Satb1<sup>flx/flx</sup>Rosa26<sup>NI-ICD</sup>* mice examined (Figure 7A and Figure 8A-D). Quantification via Positive Pixel Count (PPC) of CD3<sup>+</sup> T cells showed significant infiltration in *CD11c<sup>Cre</sup>Satb1<sup>flx/flx</sup>Rosa26<sup>NI-ICD</sup>*, compared to single genotype littermates (Figure 7B). Examination of peripheral blood smears at ~8 weeks confirmed the expansion of immature lymphocytic cells with larger nuclei and prominent nucleoli (Figure 7C), matching the morphology of malignant lymphocytes.

To understand how ablating *Satb1* transforms the mild expansion of CD8<sup>+</sup> T cells observed in *CD11c<sup>Cre</sup>Rosa26<sup>NI-ICD</sup>* mice into a fatal lymphocytic expansion, we focused on differences in Stat signaling. As shown in Figure 7D, knocking-in Notch1 in CD11c<sup>+</sup>CD8<sup>+</sup> T cells resulted in the up-regulation of total Stat5a, while *Satb1* ablation alone had no effect on Stat5 expression. However, we only observed high levels of Stat5 phosphorylation upon combined *Satb1* ablation and Notch1 (N1<sup>ICD</sup>) overexpression.

To elucidate what the mechanism driving Stat5 phosphorylation upon Satb1 deletion, we focused on cytokine secretion by transgenic T cells. We found that  $CD11c^{Cre}Satb1^{flx/flx}Rosa26^{NI-ICD}$  T cells produce an approximately 7-fold increase of IL-2, compared to their counterparts from Cre<sup>-</sup> littermates (Figure 7E). These data indicate that *Satb1* ablation de-represses IL-2 production by T cells. Therefore, Notch1 signaling results in Stat5 overexpression. When *Satb1* deletion de-represses IL-2 production in the same lymphocytes, up-regulated Stat5 is more actively phosphorylated in an autocrine manner, driving malignant progression.

*Ablation of Satb1 in mature CD4<sup>+</sup> T cells causes fatal lymphomas with massive T cell skin infiltrates*

Our results so far suggested that SATB1 could act as a tumor suppressor in T cells with deregulated NOTCH1 activity. To confirm that *Satb1* expression prevents the malignant transformation of truly mature (post-thymic) CD4<sup>+</sup> T cells upon deregulated Notch1 expression, we next generated  $CD4^{Cre}ER^{T2}Satb1^{flx/flx}Rosa26^{NI-ICD}$  mice and  $CD4^{Cre}ER^{T2}Rosa26^{NI-ICD}$  littermates. In this system, Cre is selectively activated in mature CD4<sup>+</sup> T cells in adult mice (125). Administration of tamoxifen at 6-8 weeks-old triple transgenic mice again led to adenopathy and splenomegaly (Figure 9A) while tamoxifen-injected  $CD4^{Cre}ER^{T2}Rosa26^{NI-ICD}$  or vehicle and untreated  $CD4^{Cre}ER^{T2}Satb1^{flx/flx}Rosa26^{NI-ICD}$  mice did not show signs of disease. Examination of the skin of mice with advanced disease showed dermal damage, with obvious CD3<sup>+</sup> lymphocytic infiltrates in the dermis and, to a lesser extent, in the epidermis (Figure 9B) as well as a trend to enlarged spleen and liver (Figure 10), albeit less pronounced than in the CD11c-driven model. In CTCL, a disease in which NOTCH1 is overexpressed in a stage-dependent manner (113), homing of T cells to the skin is associated with the up-regulation of the

chemokine receptors CCR4, CCR6 and CCR10 (126, 127). Supporting a role for SATB1 as a CTCL suppressor, tamoxifen-driven ablation of *Satb1* in CD4<sup>+</sup> T cells (unlike their CD8<sup>+</sup> counterparts) resulted in the overexpression of CCR4 in *CD4<sup>Cre</sup>ER<sup>T2</sup>Rosa26<sup>NI-ICD</sup>* mice compared to vehicle controls (Figure 9C).

Tamoxifen-induced *Satb1* silencing associated with Notch1 overexpression in mature CD4<sup>+</sup> T lymphocytes produced peripheral cells with convoluted cerebriform nuclei, characteristic of Sézary cells, with the presence of malignant CD3<sup>+</sup>CD4<sup>+</sup> lymphocytes (Figure 9D). Interestingly, the majority of these malignant T cells co-express CD8 at terminal stages, along with the myeloid marker CD11b, a determinant also found in CD4<sup>+</sup> T cells in experimental autoimmune encephalomyelitis (EAE) mouse model (128) (Figure 9E). Mice without the *CD4ER<sup>T2</sup>Cre* gene do not present with splenomegaly unlike their *CD4ER<sup>T2</sup>Cre* positive counterparts. Together, these data indicate that *Satb1* prevents the expression of the chemokine receptors of Notch-activated CD4<sup>+</sup> mature lymphocytes that promote the homing of malignant T cells to the skin.

#### *SATB1 silencing differentiates cutaneous T cell lymphomas from other peripheral T cell malignancies*

To determine whether *SATB1* repression plays a role in the pathogenesis of human lymphoproliferative disorders derived from CD4<sup>+</sup> and CD8<sup>+</sup> T cells, we first analyzed the expression of SATB1 in malignant T cells in the bone marrow from a group of 16 patients with a confirmed diagnosis of T cell large granular lymphocyte (T-LGL) leukemia (n=7); T cell prolymphocytic leukemia (T-PLL; n=6); and Sézary syndrome (SS; n=3).

In malignant T cells from 7 patients with T-LGL leukemia specifically driven by malignant CD3<sup>+</sup>CD8<sup>+</sup> lymphocytes (Figure 11A), we found that SATB1 was expressed at

reproducibly higher levels than in activated CD8<sup>+</sup> T cells from healthy subjects by intracellular flow cytometry analysis (Figure 11D).

In 4 out of 5 patients with T-PLL driven by malignant CD4<sup>+</sup> T cells, SATB1 expression was even higher than in activated CD4<sup>+</sup> T cells from healthy donors (Figure 11, A and D, center). Similarly, SATB1 was overexpressed in malignant CD3<sup>+</sup>CD4<sup>-</sup>CD8<sup>-</sup> cells in one of these patients, as well as in malignant cells from a different T-PLL patients driven by CD3<sup>+</sup>CD4<sup>+</sup>CD8<sup>+</sup> cells (Figure 11, A and D, right). In contrast, we found a significant reduction in the levels of SATB1 in malignant T cells in the bone marrow of 3 different SS patients (Figure 11, B and D). Further supporting that *SATB1* repression is a common event in cutaneous T cell lymphoma, low levels of SATB1 were found in CD3<sup>+</sup>CD4<sup>+</sup>CD7<sup>-</sup> T cells sorted from the peripheral blood of 11 additional patients compared to CD4<sup>+</sup> T cells from healthy donors (Figure 11, C and D). Therefore, SATB1 silencing appears to be also a pathogenic factor in Mycosis fungoides, although it is not universally found in malignant cells, as in Sézary syndrome. These data validate the relevance of the phenotype identified in our tumor model, and indicate that *SATB1* repression is a common pathogenic driver in cutaneous T cell malignancies (but not other peripheral T cell malignancies) and acts by dysregulating the expression of chemokine receptors that promote skin homing.

*Reversing H3K9 trimethylation, but not targeting H3K27 trimethylation, rescues protective SATB1 activity in Sézary T cells*

As supported by emerging genomic analysis and recent publications (114), *SATB1* downregulation in Sézary cells is not the result of deletions or point mutations. To determine how *SATB1* is silenced in peripheral T cell malignancies, we focused on the activity of polycomb

repressive complex 2 (PRC2) and histone-lysine N-methyltransferase Suppressor Of Variegation 3-9 Homolog 1 and 2 (SUV39H1/2) in HuT78 Sézary cells, which have been reported to be *SATB1* deficient (129). Epigenetic repression often requires coordinated gain of H3K9 trimethylation and H3K27 trimethylation (130) to effectively occlude DNA (131, 132). To test this proposition, we quantified occupancy of H3K9me<sup>3</sup> at the *SATB1* promoter. We performed Chromatin Immuno-precipitation (ChIP) sequencing on several leukemia cell lines with various level of *SATB1* expression; HuT78 (low expression), Jurkat (high expression), and RAJI (no detectable expression) to ascertain the regulatory landscape near the *SATB1* Transcription Start Site (TSS) (GSE 159962). Immunoprecipitations were performed on all cell lines for H3K27me<sup>3</sup>, H3K9me<sup>3</sup>, H3K27ac to reveal several sites of enrichment as shown in Figure 12. There were no sites in RAJI for any markers, H3K27me<sup>3</sup> for Jurkat, or H3K27ac for K562 near the TSS of *SATB1* gene. Ensembl regulatory regions at ~4.8kb and ~5.6kb were also found for repressive histone markers H3K27me<sup>3</sup> and H3K9me<sup>3</sup> from the TSS of *SATB1*, respectively. We found several regions in the H3K9me<sup>3</sup> pulldown of ChIP-seq from which we designed primers to validate by ChIP-PCR using specific antibodies or an irrelevant IgG isotype in control immunoprecipitations as shown in Figure 13A. Enrichment of H3K27me<sup>3</sup> and H3K9me<sup>3</sup> appeared in HuT78 cells in the ~4.8kb and ~5.6kb regions, but no significant enrichment was found for a control adjacent sequence (Figure 13B). Out of the 3 regions identified via ChIP-seq for H3K9me<sup>3</sup>, Region 1 was shown to be enriched in HuT78 cells and RAJI cells in which *SATB1* is repressed, but not in Jurkat cells in which *SATB1* is highly expressed (Figure 13C).

To define the requirement of PRC2-dependent *SATB1* repression for the expansion of Sézary T cells, we next treated HuT78 cells with increasing concentrations of the EZH2 inhibitor GSK126. As shown in Figure 13D, inhibition of EZH2 decreased the number of viable Sézary

cells and increased *SATB1* mRNA expression (Figure 14E). Treatment with 10 $\mu$ M of GSK126 decreased the occupancy of H3K27me<sup>3</sup> in the ~4.8kb site of the *SATB1* promoter compared to the vehicle control (DMSO) (Figure 14A).

SUV39H1/2 enzymes are primarily responsible for eliciting and maintaining H3K9 trimethylation at constitutive heterochromatin regions (64, 133). Accordingly, the histone lysine methyltransferase inhibitor Chaetocin reduced the number of viable Sézary cells (Figure 13E). These effects were not the result of the nonselective activity of Chaetocin as F5446, a recently reported SUV39H1/2-specific inhibitor (72), also blocked Sézary cell expansion at inhibitory concentrations 50% (IC<sub>50</sub>) values in the nanomolar range (Figure 13F), which are 4-fold lower than those needed to restore effector gene expression in tumor-reactive T cells (72). In contrast, the IC<sub>50</sub> of romidepsin (Figure 13G) was 44-fold higher, than the IC<sub>50</sub> of Chaetocin (Figure 13E). Interestingly, combinations of HDAC inhibitor romidepsin and SUV39H1/1 inhibitor Chaetocin abrogated the protective effect of either individual treatment. Treatment on HuT78 cells at 72 hours resulted in significantly increased *SATB1* mRNA expression (Figure 14F). Treatment of HuT78 cells with Chaetocin, F5446, or romidepsin versus the DMSO control showed that F5446 and romidepsin produce a cytostatic effect compared to Chaetocin (Figure 14G). RNA-seq of HuT78 cells collected after 72 hours treatment with Chaetocin and F5446 revealed pathways associated with negative regulation of  $\alpha\beta$  T cell activation, methyltransferase activity, and chemokine binding pathways, while having positive regulation of cellular senescence, nucleosome binding, and histone modification (GSE 159963) (Figure 15). Together, these data suggest that H3K9 trimethylation, H3K27 deacetylation, and H3K27 trimethylation are potential targetable mechanism to rescue *SATB1* expression and abrogate malignant cell growth.

*SUV39H1/2 inhibition de-represses SATB1 and arrests primary Sézary cell expansion more effectively than romidepsin*

To compare the effects of methyltransferase, histone deacetylase, and EZH2 inhibitors against CTCL, we next treated purified malignant primary CD3<sup>+</sup>CD4<sup>+</sup>CD26<sup>-</sup> cells from the aphaeresis of four Sézary patients with high blood tumor burden (>1,000 malignant cells/ $\mu$ L) (Figure 16A and Figure 17A) as well as four additional Sézary patients with CD3<sup>+</sup>CD4<sup>+</sup> cells from peripheral blood (Figure 18A). Notably, both methyltransferase inhibitors Chaetocin and F5446 were effective at abrogating the expansion of Sézary cells from all patients, at IC<sub>50</sub> values in the nanomolar range. In contrast, the class I HDAC inhibitor romidepsin, FDA-approved for the treatment of relapsed/refractory CTCL, only decreased the number of viable Sézary cells from the same patients at doses >8-fold higher than F5446, under identical conditions, while treatment with EZH2 inhibitor GSK126 was not effective under any condition (Figure 16A and Figure 17A). Primary Sézary cells treated with F5446, as opposed to Chaetocin, significantly increased the expression of *SATB1* mRNA (Figure 17B). Accordingly, ChIP-PCR analysis on purified primary Sézary cells showed negligible H3K27me<sup>3</sup> occupancy, compared to H3K9me<sup>3</sup> in their respective regions of occupancy in the *SATB1* promoter (Figure 17C and D) (Figure 18B and C). In order to determine the effects of *SATB1* recovery in primary Sézary samples, malignant CD4<sup>+</sup>CD26<sup>-</sup> cells were retrovirally transduced to ectopically express *SATB1*. Levels of pSTAT5 was assessed in positively transduced *SATB1* high cells and compared to cells expressing endogenous levels of *SATB1* from the same donor where an increase in pSTAT5 upon *SATB1* recovery was observed (Figure 17E). The recovery of *SATB1* resulted in an impairment of proliferative potential (Figure 17F) and is congruent with our observation with HuT78 cells where *SATB1* recovery from epigenetic inhibitors does not induce significant apoptosis.

Therefore, SUV39H1/2-mediated repression of SATB1 emerges as a major potential therapeutic target to restore tumor-suppressor *SATB1* expression in Sézary patients in a manner that preserves healthy cells.

## **Discussion**

Here we show that *SATB1* silencing in peripheral T cell lymphoma cells cooperates with NOTCH1 activation to drive mature T cell expansion through STAT5 activation and CCR4 expression. Correspondingly, we found that *SATB1* is epigenetically repressed in human Sézary syndrome through H3K27me<sup>3</sup>- and H3K9me<sup>3</sup>-mediated chromatin occlusion, and SUV39H1/2 inhibition has significant anti-proliferative effects in malignant cells from multiple Sézary syndrome patients (Figure 19).

CTCL is a disease with no curative therapies that is accompanied by painful and pruritic skin lesions causing both disfigurement and significant deterioration in quality of life. At advanced stages, the disease progresses rapidly with short survival. With the exception of palliative anti-CCR4 antibodies to reduce circulating cells in the blood and skin homing (134), no new treatments have been FDA-approved for advanced refractory CTCL since romidepsin in 2009. This is due, in part, to a poor understanding of its pathophysiology. We find that expression levels of the master epigenetic organizer *SATB1* are significantly reduced in CTCL CD4<sup>+</sup> T cells in the bone marrow and the periphery of multiple Sézary syndrome patients, compared to CD4<sup>+</sup> lymphocytes from healthy donors or other peripheral T cell malignancies. *SATB1* is a key regulator of T cell development and maturation, but also governs the function of other mature immune cells (116, 117, 135, 136). Although recent reports suggested that SATB1 could be universally down-regulated in CTCL (120), the causes and the effects of *SATB1*

silencing remain elusive. Using a transgenic model, we found that ablation of *Satb1* in mature T cells promotes the malignant and skin homing properties of mature Notch-activated lymphocytes through a mechanism that involves de-repression of CCR4 and constitutive activation of Stat5 signaling. Importantly, NOTCH and STAT5 signaling are activated in a stage-dependent manner in CTCL (113, 137), while the homing of malignant T cells to the skin is driven by the up-regulation of chemokine receptors such as CCR4 (126, 127). Interestingly, phosphorylation of Stat5 requires cooperation between *Satb1* ablation and Notch signaling, because the individual events were insufficient to activate Stat5 signaling. Future studies will determine whether this is the result of enhanced secretion of IL-2 in malignant cells; or the effect of deregulation in JAK activity.

*SATB1* silencing does not appear to be restricted to Sézary syndrome because a recent study identified that among 57 Mycosis fungoides patients, 35% were deficient in *SATB1* or presented low expression specifically in the skin, which was associated with worse outcome (138). Importantly, seminal publications support that *SATB1* silencing in Sézary cells is not the result of mutations (114), indicating epigenetic repression. We found that the *SATB1* promoter in primary Sézary cells is marked by trimethylated H3K27 and H3K9 and acetylated H3K27. Histone deacetylase inhibitors and SUV39H1/2 partially restored *SATB1* and had significant anti-proliferative effects on malignant cells. Although H3K27me<sup>3</sup> occupancy is consistently associated with gene repression, transcription factors can still access H3K27me<sup>3</sup>-marked promoters, unlike H3K9me<sup>3</sup>-marked chromatin, which remains completely occluded (131). Hence, inhibition of the enzymes primarily responsible for causing and maintaining H3K9 trimethylation at constitutive heterochromatin (64, 133) (namely, SUV39H1/2) emerges as novel intervention for urgent testing against refractory CTCL. Our results therefore offer potentially

new insight into the pathophysiology of CTCL as well as a mechanistic rationale for targeting histone methyltransferases to abrogate malignant expansion and skin homing in advanced CTCL patients.

## **Materials and Methods**

### *Animals and human samples*

Genetically-deficient *Satb1* mice were generated in the Wistar Institute's transgenic facility on a C57BL/6 background (116, 117). *Rosa26*<sup>N1-ICD</sup> mice were kindly provided by Ben Stanger (University of Pennsylvania) and backcrossed for at least 10 generations to a C57BL/6 background. These transgenic mice have a floxed version of *Notch1* interrupted by a STOP codon at the permissive locus *Rosa26*. *Satb1*<sup>flx/flx</sup> mice were crossed with *CD11c*<sup>Cre</sup> mice (Taconic, 4196M) and *Rosa26*<sup>N1-ICD</sup> mice to generate triple transgenic (116) and control mice. *Satb1*<sup>flx/flx</sup> mice were also bred with *Cre-ERT2*<sup>+</sup> (Jackson Labs, Jax 022356) and *Rosa26*<sup>N1-ICD</sup> mice to generate *CD4*<sup>Cre</sup>*ERT2**Satb1*<sup>flx/flx</sup>*Rosa26*<sup>N1-ICD</sup> mice. *CD4*<sup>Cre</sup>*ERT2**Satb1*<sup>flx/flx</sup>*Rosa26*<sup>N1-ICD</sup> mice were male and injected at 6-8 weeks of age with 75mg/kg Tamoxifen (Sigma, T5648) in corn oil (Sigma, C8267). All animals were maintained in pathogen free barrier facilities.

De-identified human bone marrow aspirates were procured under a protocol approved by Moffitt's Scientific Review Committee. Sorted bone marrow was maintained in RPMI media with 10% human serum (Sigma, H5667), Penicillin/Streptomycin (Lonza, 17-602E) and 100U/ml IL-2 (Peprotech, 200-02) and 5ng/ml IL-7 (Peprotech, 200-07). *CD4*<sup>+</sup>*CD7*<sup>+</sup>/*CD26*<sup>+</sup> and *CD4*<sup>+</sup>*CD7*<sup>-</sup>/*CD26*<sup>-</sup> cells were isolated with Human *CD4*<sup>+</sup> T cell Isolation Kit (STEM CELL, 17952) and Release Human PE Positive Selection Kit (STEM CELL, 17654) from peripheral blood of patients with Sézary syndrome and cultured in complete RPMI (10% heat-inactivated

Fetal Bovine Serum, 0.5 mM Sodium Pyruvate (Gibco, 11360070), 2 mM L-glutamine (Sigma, G7513), 100 I.U./mL Penicillin, 100 ug/mL Streptomycin (Lonza, 17-602E) with 100U/ml IL-2 (Peprotech, 200-02)) in an incubator (37°C, 5% CO<sub>2</sub>). Memory CD4<sup>+</sup> T cells from peripheral blood of normal donors were isolated using Human Memory CD4<sup>+</sup> T Cell Enrichment Kit (STEM CELL, 19157) and cultured exactly as peripheral blood Sézary cells.

### *Retroviral Transduction*

Primary Sézary CD4<sup>+</sup>CD26<sup>-</sup> cells were transduced activated with human CD3/CD28 Dynabeads (Gibco, 1132D) with retrovirus produced using Phoenix-AMPHO (ATCC, CRL-321) cells following transfection using Lipofectamine<sup>™</sup> 3000 Transfection Reagent (ThermoFisher, L3000001) following manufacture's recommendations with pBMN-I-GFP vector containing human *SATB1* ORF (GenScript Biotech) cloned using the EcoRI and BamHI restriction sites. Virus was collected in complete medium at 48 and 72hrs and filtered through a 40uM filter. 50ug/ml of Retronectin in sterile PBS was used to coat non-tissue treated 24-well plates overnight at 4°C. Wells were blocked with 2% BSA in PBS solution for 15 minutes at RT and washed twice in sterile PBS. Plates were spin with 3mL viral supernatant for 1.5hrs at 32°C at 2,000g). Supernatant was removed except ~500ul and cells were added and spun for 10 minutes at 1500rpm 32°C and cultured at 37°C at 5% CO<sub>2</sub> until GFP expression was detected at ~96hrs.

### *Cell lines and MTT assays*

The HuT78 Sézary cell line was purchased from the American Tissue Culture Collection, ATCC. (ATCC TIB-161) and cultured with Iscove's Modified Dulbecco's Medium (IMDM) with 20% of FBS (and Penicillin/Streptomycin (Lonza, 17-602E). For viability analysis, HuT78 cells were seeded at 40,000 cell/well in triplicates in 96-well plates in the presence of vehicle control

ethanol or DMSO the EZH2 inhibitor GSK126 (Cayman Chemical Co, 15415), Chaetocin (Abcam, ab144534), romidepsin (FK228, Depsipeptide) (Selleck, S3020-5mg), F5446 (acquired from Dr. Liu Lab) and placed at 37C, 5% CO<sub>2</sub> for 48hrs or 72hrs. 10ul of 5mg/ml MTT reagent (Sigma, M2128-1G) was added for 3hrs, followed by 100ul of Lysis Buffer (44% DMF, 2.2% Acetic Acid, 1.8% 1N HCL, 17.7%w/v SDS, add NaOH as needed) overnight at 37C, 5% CO<sub>2</sub>. Result measured at 560nm on microplate spectrophotometer (Biorad, Benchmark Plus). Jurkat (ATCC TIB-152) grown in RPMI 10% FBS with Penicillin/Streptomycin, K562 (ATCC CCL-243) grown in IMDM 10% FBS and Penicillin/Streptomycin, and RAJI (ATCC CCL-86) grown in RPMI 10% FBS with Penicillin/Streptomycin.

#### *Antibodies and Flow Cytometry*

We used the following anti-human antibodies: CD45 (Clone HI30), CD45RO (UCHL1), CD26 (BA5b), CD3 (Clone OKT3), CD2 (Clone RPA-2.10), CD5 (Clone UCHT2), CD7 (Clone CD7-6B7), TCR $\beta$  (Clone IP26), CD52 (Clone HI186), CD56(Clone 5.1H11), CD57 (Clone HCD57), and CCR4/CD194 (Clone L291H4); all from Biolegend; and CD4 (Clone SK3), CD8 (Clone RPA-T8), SATB1 (Clone 14/satb1) and TCR $\gamma\delta$  (Clone B1), from BD Bioscience. Human  $\gamma$ -globulin (Sigma, G4386) was used for Fc Receptor blockade.

Mouse antibodies were as follows: CD45 (Clone 30-F11), CD5 (Clone 53-7.3), CD11b (Clone M1/70), CD11c (Clone N418), Ly6G (Clone 1A8), Ly6C (Clone HK1.4), TCR $\beta$  (Clone H57-597), TCR $\gamma\delta$  (Clone GL3), NK1.1 (Clone PK136), NKG2D (Clone CX5), CD96 (Clone 6A6), CD25(Clone PC61), CD34 (Clone MEC14.7), CCR4 (Clone 2G12), CCR7 (Clone 4B12), CCR6 (Clone 29-2L17), CD19 (Clone 6D5), CD62L (Clone MEL-14); all from Biolegend. MHCII (Clone M5/114), CD2 (Clone RM2-5), CD3e (Clone 145-2C11), CD4 (Clone GK1.5),

CD8 (Clone 53-6.7) and CD69 (Clone H1.2F3), from BD Bioscience. CD44 (Clone IM7), from Tonbo and CCR10 (Clone 248918), from R&D systems. Zombie yellow (Biolegend) was used as viability probe for all samples. Anti-CD16/32 mAb (Clone 2.4G2) was used for Fc Receptor blockade.

For Flow Cytometry, all Samples were run on a LSRII (BD) and sorted using a FACSAria SORP. Data were analyzed using FlowJo software. Intracellular staining was performed with Transcription Factor Staining Buffer Set (ThermoFisher).

The following antibodies were used for immunoblot analysis: anti-pSTAT5 (Tyr694; rabbit clone#D47E7; Cell Signaling), STAT5 (rabbit clone#D2O6Y; Cell Signaling), anti-mouse/human  $\beta$ -actin (BA3R; ThermoScientific) and anti-Satb1 (BDBiosciences, clone#14).

When indicated, CD3<sup>+</sup> T cells were isolated from mouse spleens using Dynabeads™ Untouched Mouse T Cells Kit (Invitrogen, 11413D) from 5x10<sup>6</sup> total splenocytes following manufacturer's recommendations.

#### *Cell Trace Violet Assays and Annexin V staining*

Cell Trace Assays were performed using CellTrace™ Violet (Invitrogen, C34571) following manufacture's recommendations with 5uM stock concentration resuspended in DMSO starting with 10<sup>6</sup>cell/mL cell concentration in sterile PBS. Cells were incubated at 37°C for 20 minutes protected from light. Reaction was quenched using complete cell culture medium 5 times the reaction volume and incubated for 5 minutes, spun for 5 minutes 4°C at 1500rpm, and resuspended at cell concentration of 10<sup>6</sup> cells/ml in fresh warm media and cultured for 5 days prior to FACs analysis. Cells were stained with DAPI (Invitrogen, D1306), to remove dead cells from analysis.

Annexin V staining was performed with APC Annexin V Apoptosis Detection Kit (Biolegend, 640932) and Propidium Iodide (PI) (Biolegend, 421301) for the identification of apoptotic and necrotic cells following manufactures recommendations. Cells were washed twice with cold Cell Staining Buffer (Biolegend, 420201) and then resuspend cells in Annexin V Binding Buffer (Biolegend, 422201) at a concentration between 0.25-1.0 x 10<sup>7</sup> cells/mL. Cells were then stained with APC Annexin and PI. Cells were then incubated for 15 minutes at RT in dark prior to resuspension in Annexin V Binding Buffer and FACS analysis. For Flow Cytometry, all Samples were run on a LSRII (BD) and data were analyzed using FlowJo software.

#### *Immunohistochemistry, Giemsa, and Western blot*

Formalin-Fixed, Paraffin-Embedded ventral and dorsal skin sections on charged slides (APEX-SAS, 3800080E) were stained using Ready-to-use IHC/ICC kit (Bio Vision, 501119739), following manufacturer's instructions, following antigen retrieval (10 min boiling in citrate buffer) and deparaffination. Anti-CD3 was from Abcam (rabbit monoclonal SP7). Slides were counterstained with Hematoxilin (RICCA, 3530-32), dehydrated and mounted with Permount (Fisher, SP15-100). For Giemsa staining, 5µl of non-coagulated blood smears were left to air dry and fixed in methanol 10 min at room temperature. Slides were then incubated in Giemsa (Sigma 48900) 1:20, in PBS for 1 hour, washed in ddH<sub>2</sub>O and mounted with Permount (Fisher, SP15-100). Histology slides were scanned using the Aperio™ ScanScope AT2 (Leica Biosystems, Vista, CA) with a 200x/0.8NA objective lens with a doubler to image at 400X. Image analysis for mouse slides were performed using an Aperio Positive Pixel Count® v9.0 algorithm with the following thresholds: [Hue Value =.1; Hue Width =.5; Color Saturation

Threshold =0.04; IWP(High) = 220; Iwp(Low)=Ip(High) = 175; Ip(low) =Isp(High) =100  
Isp(Low) =0] to segment positive staining of various intensities.

For Western blot analysis, cells were lysed in RIPA buffer (Pierce) supplemented with protease inhibitors (Roche). Equal amounts of protein were quantified using the BCA protein Assay kit (Pierce) and resolved by SDS-PAGE, blotted onto PVDF membranes (Millipore) and probed with the aforementioned antibodies.

### *Q-PCR and ChIP PCR*

Real Time PCR amplification was carried out using Sybr Green on a 7500 Fast Real-Time PCR system (Applied Biosystem). Human *SATB1* mRNA expression was quantified using the following primers, common to all human splicing variants, and mRNA expression was normalized by GAPDH levels or TATA-binding protein (TBP) levels with primers listed in Table 5. The average of three independent analyses for gene and sample was calculated using the  $\Delta\Delta$  threshold cycle (Ct) method and was normalized to the endogenous reference control gene *GAPDH* or *TBP*.

For ChIP experiments, the HuT78 cell line was seeded at  $1.5 \times 10^6$  cells/well in 6 well-plates. ChIP assays were performed as we previously reported (117). Input and immunoprecipitated DNA were analyzed using the SYBR Green in a real-time PCR machine (Applied Biosystem). Results shown for each ChIP condition were analyzed using the percent input method; namely, the amount of DNA recovered from the ChIP were divided by signals obtained from the input sample (signals calculated with 2.5% of the amount of chromatin used in the ChIP). Anti-H3K27me<sup>3</sup> (Cell Signaling; rabbit clone# C36B11), H3K9me<sup>3</sup> (Abcam; rabbit clone# ab8898), H3K27ac (Abcam; rabbit clone# ab4729), and control IgG (Cell Signaling,

rabbit IgG) antibodies were used for chromatin immunoprecipitation. The primers used for quantification of human SATB1 promoter for H3K27me<sup>3</sup>, H3K9me<sup>3</sup>, control regions, and validating the ChIP-seq experiment are listed in Table 6. All sequences designed to give amplicons <200 bp. Amplification of target gene is shown as fold enrichment compared to that of irrelevant antibody controls.

### *RNA-sequencing*

Total RNA was collected from HuT78 cells at 72hrs using a Qiagen RNAeasy Mini Kit and treated with RNase-Free DNase, Qiagen, Cat#79254 for removal of genomic DNA. Sequencing libraries were prepared by using NuGEN Universal RNA-Seq kit and run on NextSeq v2 300 cycles (75x2). Read depth was approximately ~35M reads per sample, and raw sequencing reads were trimmed and aligned to human genome assembly GRCh37 using STAR (139) (version 2.5.3a). Uniquely mapped reads were counted by htseq-count (140) (version 0.6.1) using Gencode v30 annotation. Differential expression analysis was performed using DESeq2 taking into account of RNA composition bias (141) and genes were ranked based on  $-\log_{10}(\text{p-value}) * (\text{sign of } \log_2(\text{fold-change}))$ . The ranked gene list was used to perform pre-ranked gene set enrichment analysis (GSEA version 4.0.2) (142) to assess enrichment of hallmarks, Reactome, and Gene Ontology (143) terms in MSigDB (143). The resulting normalized enrichment score (NES) and FDR controlled p-values were used to assess the transcriptome changes induced by F5446 and Chaetocin.

### *ChIP-sequencing*

Samples were prepared in a similar method to the aforementioned ChIP section. Chromatin immunoprecipitation sequencing (ChIP-seq) was performed by the Molecular Genomics Core Facility at the Moffitt Cancer Center. Ten nanograms of immunoprecipitated DNA was fragmented to 300 base pairs using a Covaris M220 Focused-ultrasonicator (Covaris, Inc., Woburn, MA) and then used to generate sequencing libraries using the Kapa HyperPrep Kit (Roche Sequencing and Life Science, Wilmington, MA). The size and quality of the library was evaluated using the Agilent BioAnalyzer, and the library was quantitated with the Kapa Library Quantification Kit. Each enriched DNA library was then sequenced on an Illumina NextSeq 500 sequencer to generate 50 million 75-base paired-end reads (Illumina, Inc., San Diego, CA) (144). Sequencing adaptors and low-quality bases were trimmed off from the raw sequencing reads using cutadapt (145). Processed reads were aligned to human reference genome GRCh37 using Bowtie2 (144) and further filtered to remove discordant read pairs and reads with low alignment scores. Strand cross-correlation (SCC) analysis and calculation of NSC (normalized strand coefficient) and RSC (relative strand coefficient) values were performed using phantompeakqualtools. Narrow peaks were called by MACS2 (146) for histone marker H3K27ac with a minimal cutoff at narrow peak q-value (nq)  $<0.05$ . Broad peaks were called by MACAS2 for histone markers H3K27m3 and H2K9m3 with a minimal cutoff at nq $<0.05$  and broad peak q-value (bp)  $<0.05$ . The enriched reads and peaks were further annotated and analyzed using Chipseeker (147), deeptools (148), and ngsplot (149). Peak regions were lifted over to GRCh38 for primer design purpose using UCSC lift-over online tool (<https://genome.ucsc.edu/cgi-bin/hgLiftOver>).

### *Statistics*

All statistical assays were performed using GraphPad Prism 5.0 software. Student's t test was used for calculating differences between means of experimental groups and two-tailed P-values less than 0.05 were considered significant. One-way ANOVA was used for calculating differences between means using multiple comparisons between groups with P-values (Tukey's test) less than 0.05 were considered significant. Log-rank (Mantel-Cox) was used to for survival curve analysis. P-values less than 0.05 were considered significant. Mean  $\pm$  SEM for each group or measurement is shown.

### *Study approval*

Study conformed to approvals granted by Moffitt's research regulatory committees, including IRB approvals MCC 50175 (TCPL), MCC 50218 (T-LGL), and MCC 50229 (Sézary). Further, MCC 20032 for Sézary syndrome peripheral blood samples were acquired with informed written consent protocol MCC 14690. All experimental procedures involving vertebrate animals were conducted in accordance with The Institutional Animal Care and Use Committee (IACUC) approvals IS00006598, IS00006654, and IS00002583.

**Table 5. RT-qPCR primers for SATB1 gene expression**

<b>Primer ID</b>	<b>Sequence</b>
<b>SATB1 Forward</b>	5'- AGTGGGTACGCGATGAACTGAA-3'
<b>SATB1 Reverse</b>	5'-ATGCAGTCTTGGGGTCCTCTTC-3
<b>GAPDH Forward</b>	5'-CCTGCACCACCAACTGCTTA-3'
<b>GAPDH Reverse</b>	5'-GTGATGGCATGGACTGTGGT-3'
<b>TBP Forward</b>	5'-CACGAACCACGGCACTGATT-3'
<b>TBP Reverse</b>	5'- TTTTCTTGCTGCCAGTCTGGAC-3'

**Table 6. ChIP-PCR Primers**

<b>Primer ID</b>	<b>Sequence</b>
<b>SATB1 promoter H3K27me3 Forward</b>	5'- TTTCCCCTGTTGGTCTTCTGAGG-3'
<b>SATB1 promoter H3K27me3 Reverse</b>	5'- TGGCCTTTTCCTATTGCTCCAGT-3'
<b>SATB1 promoter H3K9me3 Forward</b>	5'-TCTATTGGGCAGGTGTGGTGG-3'
<b>SATB1 promoter H3K9me3 Reverse</b>	5'- GCAGGGCTTCAACGGTCTTC-3'.
<b>SATB1 promoter Control Forward</b>	5'-GAGGAGGAGGAAGATCAGAAGGC-3'
<b>SATB1 promoter Control Reverse</b>	5'-GTTTTGTCTGGGGTTTCTGGGTTT-3'
<b>ChIP H3K9me3 Region 1 Forward</b>	5'-TTGCTTTTTTCCTCCCATAG-3'
<b>ChIP H3K9me3 Region 1 Reverse</b>	5'-GAAATTTGTGGCCAACACTACA-3'
<b>ChIP H3K9me3 Region 2 Forward 1</b>	5'-AACCTGCCAGCTAAACAGTC-3'
<b>ChIP H3K9me3 Region 2 Reverse 1</b>	5'- GCCGACACTTAGGGAAAATA-3'
<b>ChIP H3K9me3 Region 2 Forward 2</b>	5'- AAGAAGGTCGGATAGTGCAG-3'
<b>ChIP H3K9me3 Region 2 Reverse 2</b>	5'- AGACTTGGGCCATAAAGCTA-3'
<b>ChIP H3K9me3 Region 2 Forward 3</b>	5'- AACAGGACCAGAGCAAAATC-3'
<b>ChIP H3K9me3 Region 2 Reverse 3</b>	5'- ACTAGGATTGGGAAACACCA-3'
<b>ChIP H3K9me3 Region 3 Forward</b>	5'- TTTCTACTGAAGGTCAAAGTGTTT-3'
<b>ChIP H3K9me3 Region 3 Reverse</b>	5'- CAGGTATGCATGTATAGGACAAA-3'

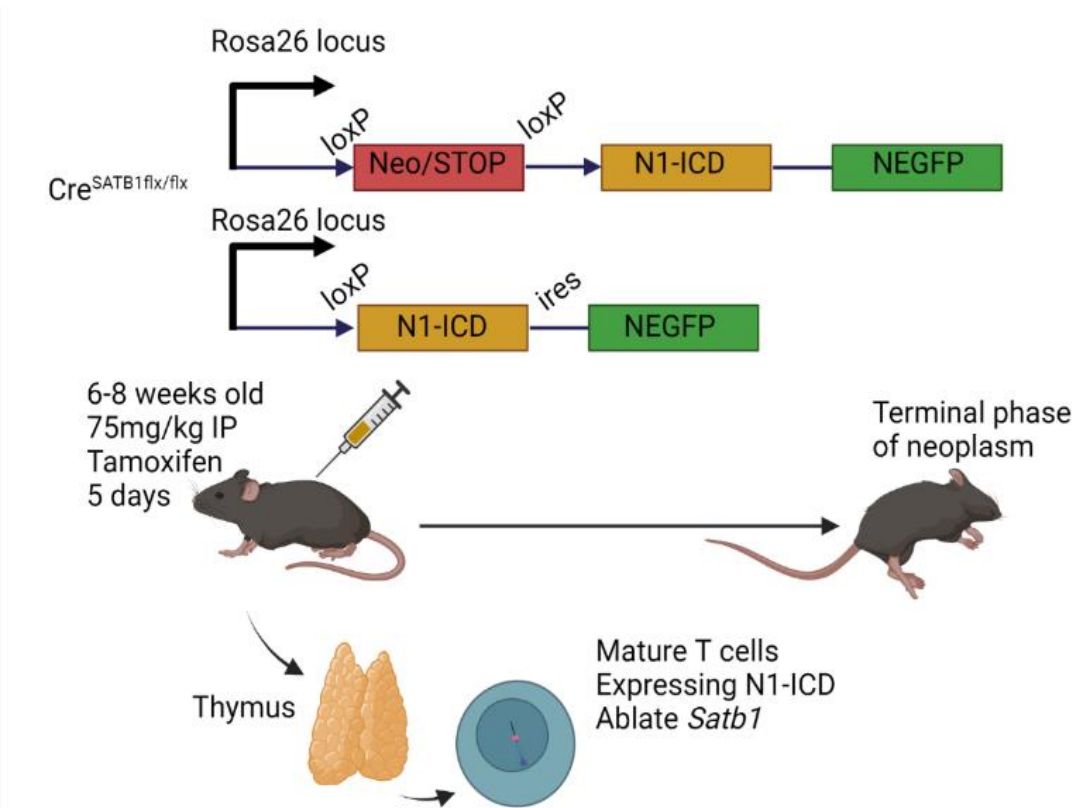


**Figure 4. Schematic of triple transgenic murine model.**

Overview of the removal of stop codon via Cre at loxP sites upstream of N1-ICD region conjugated with report gene GFP. Mice are injected with 75mg/kg of tamoxifen for 5 days at 6 to 8 weeks old resulting in terminal neoplasm.

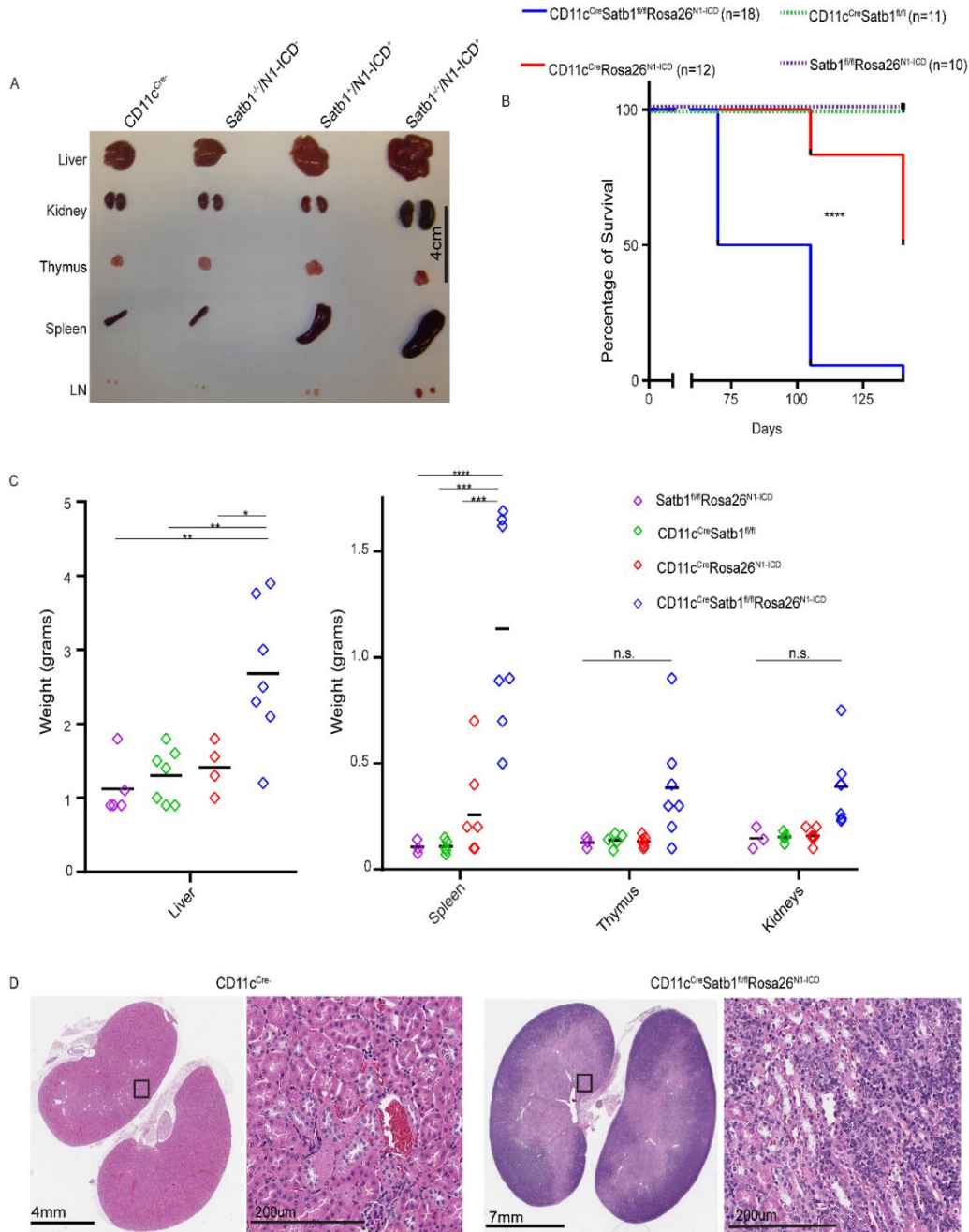


**Figure 5. Concurrent ablation of Satb1 and increased expression of Notch1 in mature T cells results in lethal adenopathy.** (A) Representative size of different organs in *CD11c<sup>Cre</sup>Satb1<sup>flx/flx</sup>Rosa26<sup>N1-ICD</sup>* mice; mice with *CD11c<sup>Cre</sup>*-dependent Notch1 (N1-ICD) overexpression alone (*CD11c<sup>Cre</sup>Rosa26<sup>N1-ICD</sup>*); and mice with *CD11c<sup>Cre</sup>*-induced ablation of Satb1 alone (*CD11c<sup>Cre</sup>Satb1<sup>flx/flx</sup>*); LN, Axillary Lymph Nodes. (B) Survival curve of *CD11c<sup>Cre</sup>Satb1<sup>flx/flx</sup>Rosa26<sup>N1-ICD</sup>* mice (n=18); mice with *CD11c<sup>Cre</sup>*-dependent Notch1 overexpression alone (*CD11c<sup>Cre</sup>Rosa26<sup>N1-ICD</sup>*) (n=12), mice with *CD11c<sup>Cre</sup>*-dependent Satb1 ablation alone (*CD11c<sup>Cre</sup>Satb1<sup>flx/flx</sup>*) (n=10), mice without *CD11c<sup>Cre</sup>* (n=11). Log-rank (Mantel-Cox) test  $p < 0.0001$ . (C) Weight of different organs in *CD11c<sup>Cre</sup>Satb1<sup>flx/flx</sup>Rosa26<sup>N1-ICD</sup>* mice (n=5-3); *CD11c<sup>Cre</sup>Rosa26<sup>N1-ICD</sup>* mice (n=5-7); *CD11c<sup>Cre</sup>Satb1<sup>flx/flx</sup>* mice (n=4-5); or mice without Notch1 overexpression or Satb1 ablation (*CD11c<sup>Cre</sup>* negative) (n=7). One-way ANOVA using multiple comparisons Tukey's test; \* $p < 0.05$ ; \*\* $p \leq 0.01$ ; \*\*\* $p \leq 0.001$ ; \*\*\*\* $p \leq 0.0001$ . (D) Haematoxylin and Eosin staining of kidneys of *CD11c<sup>Cre</sup>* negative mouse (left) versus *CD11c<sup>Cre</sup>Satb1<sup>flx/flx</sup>Rosa26<sup>N1-ICD</sup>* mice (right).

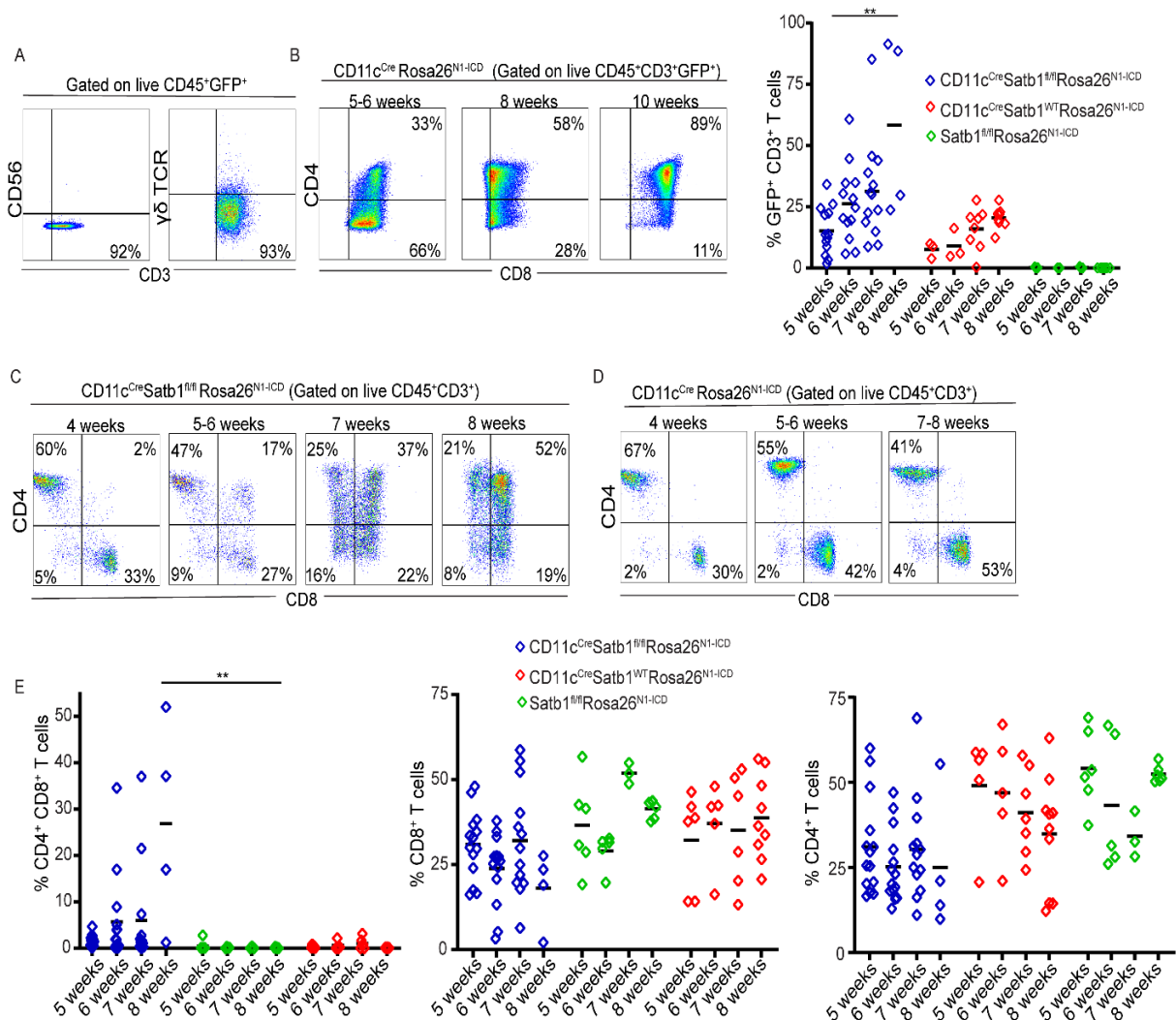


**Figure 6. Satb1 ablation transforms the Notch-dependent expansion of CD8<sup>+</sup> T cells into a full-blown CD4<sup>+</sup>CD8<sup>+</sup> T cell lymphoma.**

(A) Notch-overexpressing (GFP<sup>+</sup>) cells in the peripheral blood of 10-week-old *CD11c<sup>Cre</sup>Satb1<sup>flx/flx</sup>Rosa26<sup>N1-ICD</sup>* mice are CD56<sup>-</sup>γδTCR<sup>+</sup>CD3<sup>+</sup> T cells. (B) An initial population of (GFP<sup>+</sup>) CD8<sup>+</sup> T cells overexpressing Notch1 is progressively transformed into CD4<sup>+</sup>CD8<sup>+</sup> T cells at advanced stages of malignant progression with quantitative representation of CD3<sup>+</sup> GFP<sup>+</sup> T cells from peripheral blood. (C) Progressive accumulation of CD4<sup>+</sup>CD8<sup>+</sup> T cells in the peripheral blood of *CD11c<sup>Cre</sup>Satb1<sup>flx/flx</sup>Rosa26<sup>N1-ICD</sup>* mice. (D) Progressive expansion of CD8<sup>+</sup> T cells, but not CD4<sup>+</sup>CD8<sup>+</sup> malignant lymphocytes, in Notch-overexpressing mice without *Satb1* ablation. (E) Quantitative representation of progressive accumulation of CD4<sup>+</sup>CD8<sup>+</sup>, CD4<sup>+</sup>, and CD8<sup>+</sup> T cells in *CD11c<sup>Cre</sup>Satb1<sup>flx/flx</sup>Rosa26<sup>N1-ICD</sup>* mice (n=4-12), *CD11c<sup>Cre</sup>Rosa26<sup>N1-ICD</sup>* (n=4-6), and *CD11c<sup>Cre</sup>* negative mice (n=6-9). Two-tailed Student's t-tests (b,e); \*\*p≤0.01.

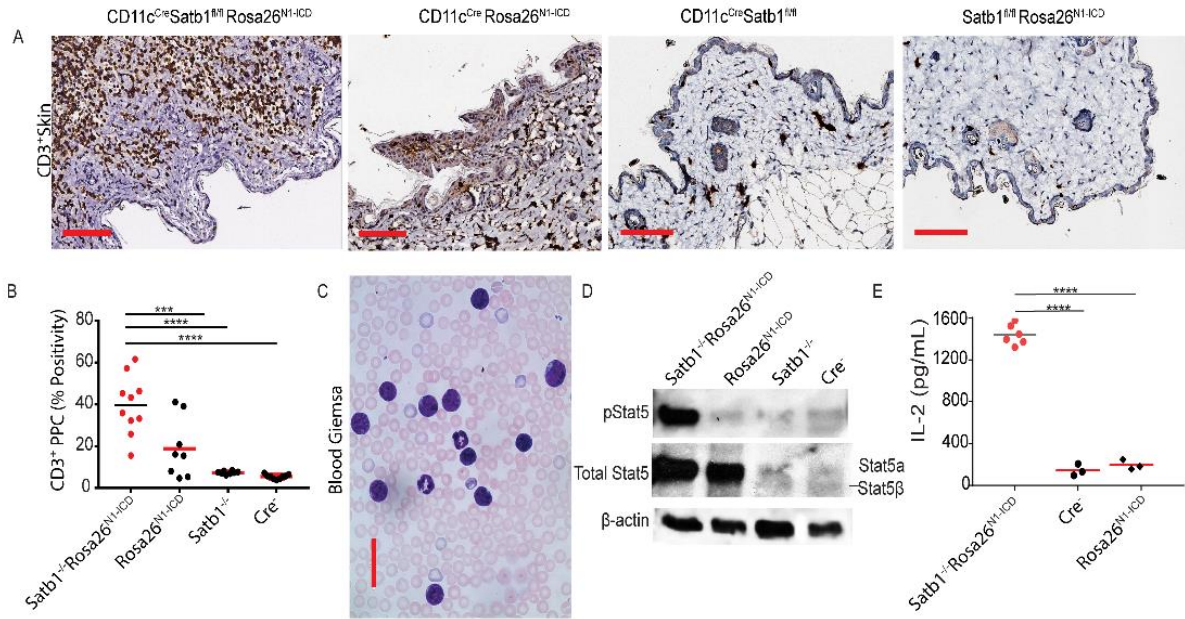


**Figure 7. Satb1 ablation and Notch activation cooperate to transform post-thymic CD8<sup>+</sup> T lymphocytes into skin-homing lymphoma cells with phosphorylated Stat5 and cytokine increase.**

(A) Accumulation of CD3<sup>+</sup> T cells in skin of 10week-old *CD11c<sup>Cre</sup>Satb1<sup>flx</sup>Rosa26<sup>NI-ICD</sup>* mice compared to single genotype littermates. Bar, 100µm. (B) Quantitative Representation of Positive Pixel Count (PPC) of CD3<sup>+</sup> staining of skin from *CD11c<sup>Cre</sup>Satb1<sup>flx</sup>Rosa26<sup>NI-ICD</sup>* (n=10), *CD11c<sup>Cre</sup>Rosa26<sup>NI-ICD</sup>* (n=8), *CD11c<sup>Cre</sup>Satb1<sup>flx</sup>* (n=8), and *CD11c<sup>Cre</sup>* negative mice (n=8). One-way ANOVA using multiple comparisons Tukey's test; \*\*\*p≤0.001; \*\*\*\*p≤0.0001. (C) Representative Giemsa staining of peripheral blood in the *CD11c<sup>Cre</sup>Satb1<sup>flx</sup>Rosa26<sup>NI-ICD</sup>* mice. Bar, 100µm. (D) Western blot analysis of protein extracts from GFP<sup>+</sup> (Notch1-overexpressing) cells sorted from the bone marrow of *CD11c<sup>Cre</sup>Satb1<sup>flx</sup>Rosa26<sup>NI-ICD</sup>* and *CD11c<sup>Cre</sup>Rosa26<sup>NI-ICD</sup>* mice; plus sorted CD8<sup>+</sup> T cell splenocytes from wild-type (*Cre*<sup>-</sup>) and *CD11c<sup>Cre</sup>Satb1<sup>flx</sup>* mice. Representative of 2 independent experiments. (E) 2x10<sup>5</sup> immunopurified CD3<sup>+</sup> T cells were stimulated with 0.5 µg/mL PMA and 1 µg/mL Ionomycin in RMP1 10% FBS for 4 hours at 37°C. Supernatants were diluted 1:40 and IL-2 was quantified by ELISA (Biolegend) for from *CD11c<sup>Cre</sup>Satb1<sup>flx</sup>Rosa26<sup>NI-ICD</sup>* (n=6), *CD11c<sup>Cre</sup>Rosa26<sup>NI-ICD</sup>* (n=3), and *CD11c<sup>Cre</sup>* negative mice (n=3). One-way ANOVA using multiple comparisons Tukey's test; \*\*\*\*p≤0.0001.

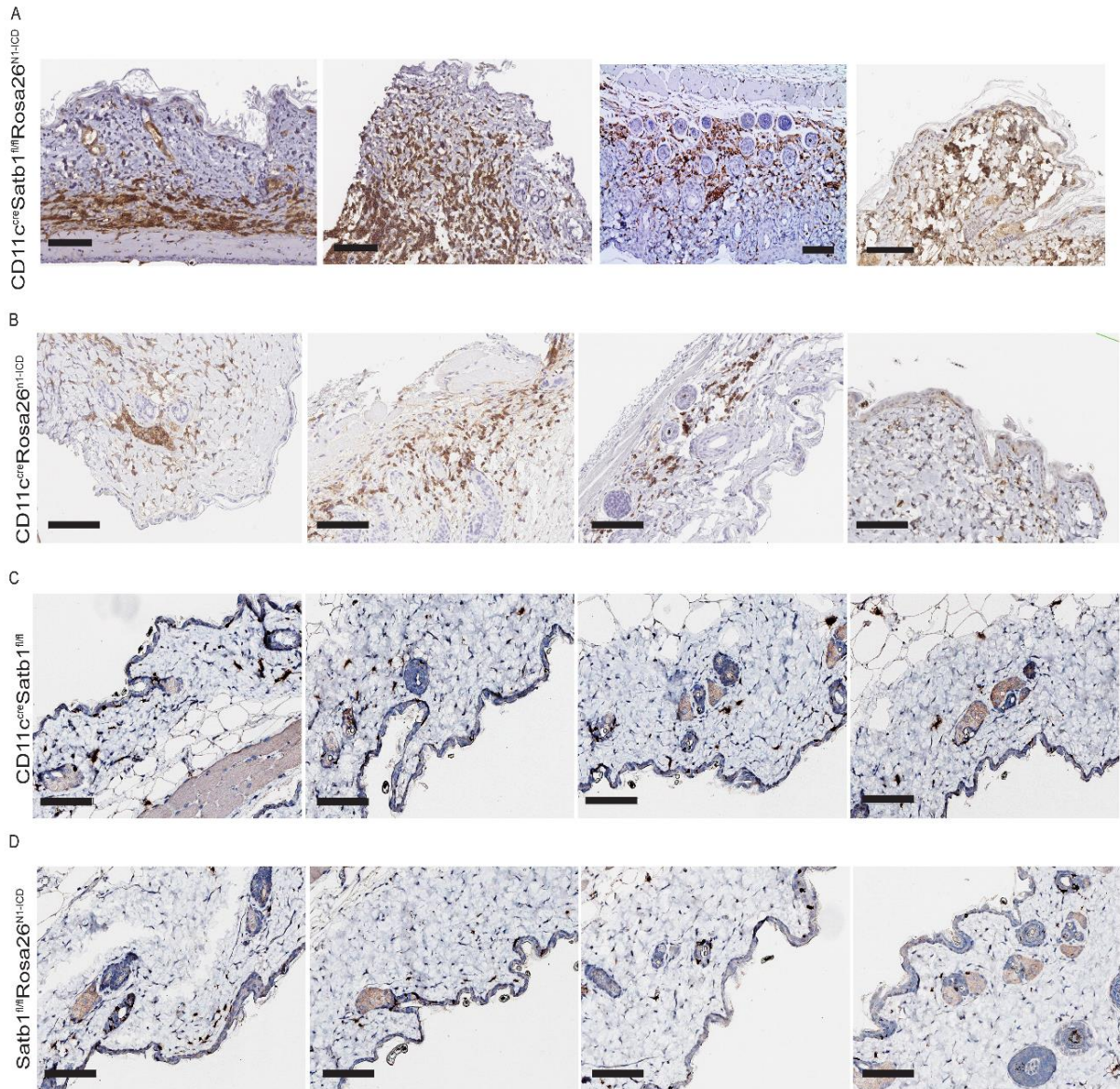


**Figure 8. Immunohistochemistry staining for CD3<sup>+</sup> T cell infiltration in mouse skin for CD11cCre model.** Dermis and epidermis of mice show peripheral staining of CD3 in *CD11c<sup>Cre</sup>Satb1<sup>flx/flx</sup>Rosa26<sup>NI-ICD</sup>* (A), *CD11c<sup>Cre</sup>Rosa26<sup>NI-ICD</sup>* (B), *CD11c<sup>Cre</sup>Satb1<sup>flx/flx</sup>* (C), and *CD11c<sup>Cre</sup>* negative (D) genotypes. Scale, 100um.

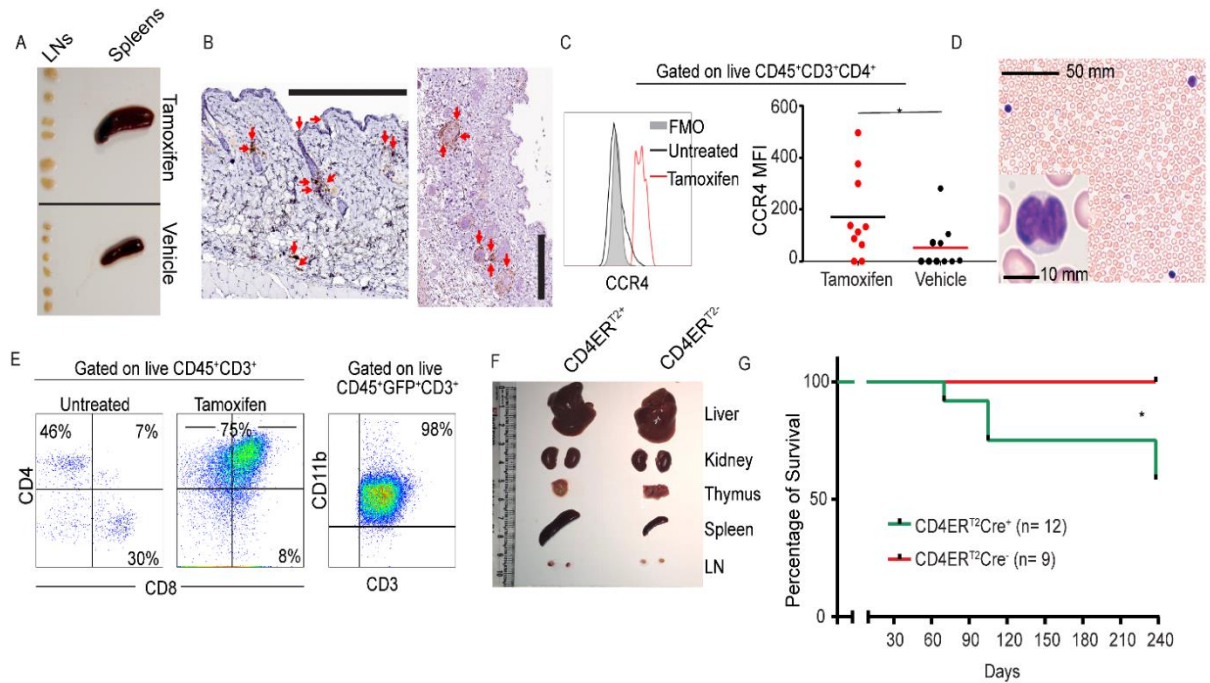


**Figure 9. Satb1 ablation and Notch activation cooperate to transform post-thymic CD4<sup>+</sup> T lymphocytes into skin-homing lymphoma cells.**

(A) Splenomegaly and adenopathy in a *CD4<sup>Cre</sup>ERT2Satb1<sup>flx/flx</sup>Rosa26<sup>NI-ICD</sup>* mouse 2 months after tamoxifen-mediated activation of transgenes. Representative differences in the size of lymph nodes (LNs) and spleens from different *CD4<sup>Cre</sup>ERT2Satb1<sup>flx/flx</sup>Rosa26<sup>NI-ICD</sup>* mice injected with tamoxifen (n=9) versus corn oil (vehicle control) (n=9). (B) Accumulation of CD3<sup>+</sup> T cells in the skin of *CD4<sup>Cre</sup>ERT2Satb1<sup>flx/flx</sup>Rosa26<sup>NI-ICD</sup>* mice, 10 weeks after tamoxifen administration. Bar, 300 $\mu$ m. (C) Representative histogram analysis (left) and median fluorescence intensity (MFI, right) of the expression of CCR4 in CD3<sup>+</sup>CD4<sup>+</sup> T cells in the peripheral blood of *CD4<sup>Cre</sup>ERT2Satb1<sup>flx/flx</sup>Rosa26<sup>NI-ICD</sup>* mice, treated with tamoxifen (n=10) versus corn oil (n=10). Two-tailed Student's t-tests; \*p<0.05. (D) Representative Giemsa staining of peripheral blood in the same mice. Bar, 50 $\mu$ m. A detail of a cerebriform cell is also shown. Bar, 10 $\mu$ m. (E) Expansion of CD4<sup>+</sup>CD8<sup>+</sup>CD11b<sup>+</sup> T cells in the peripheral blood of *CD4<sup>Cre</sup>ERT2Satb1<sup>flx/flx</sup>Rosa26<sup>NI-ICD</sup>* mice 10 weeks after tamoxifen challenge. (F) Splenomegaly and adenopathy in a *CD4<sup>Cre</sup>ERT2Satb1<sup>flx/flx</sup>Rosa26<sup>NI-ICD</sup>* mouse 2 months after tamoxifen-mediated activation of transgenes. Representative differences in the size of lymph nodes (LNs) and spleens from different *CD4<sup>Cre</sup>ERT2Satb1<sup>flx/flx</sup>Rosa26<sup>NI-ICD</sup>* versus *CD4<sup>Cre</sup>ERT2* negative mice. (G) Survival curve of *CD4<sup>Cre</sup>ERT2Satb1<sup>flx/flx</sup>Rosa26<sup>NI-ICD</sup>* mice (n=12) versus mice without *CD4<sup>Cre</sup>ERT2* (n=9). Log-rank (Mantel-Cox) test; p<0.05.

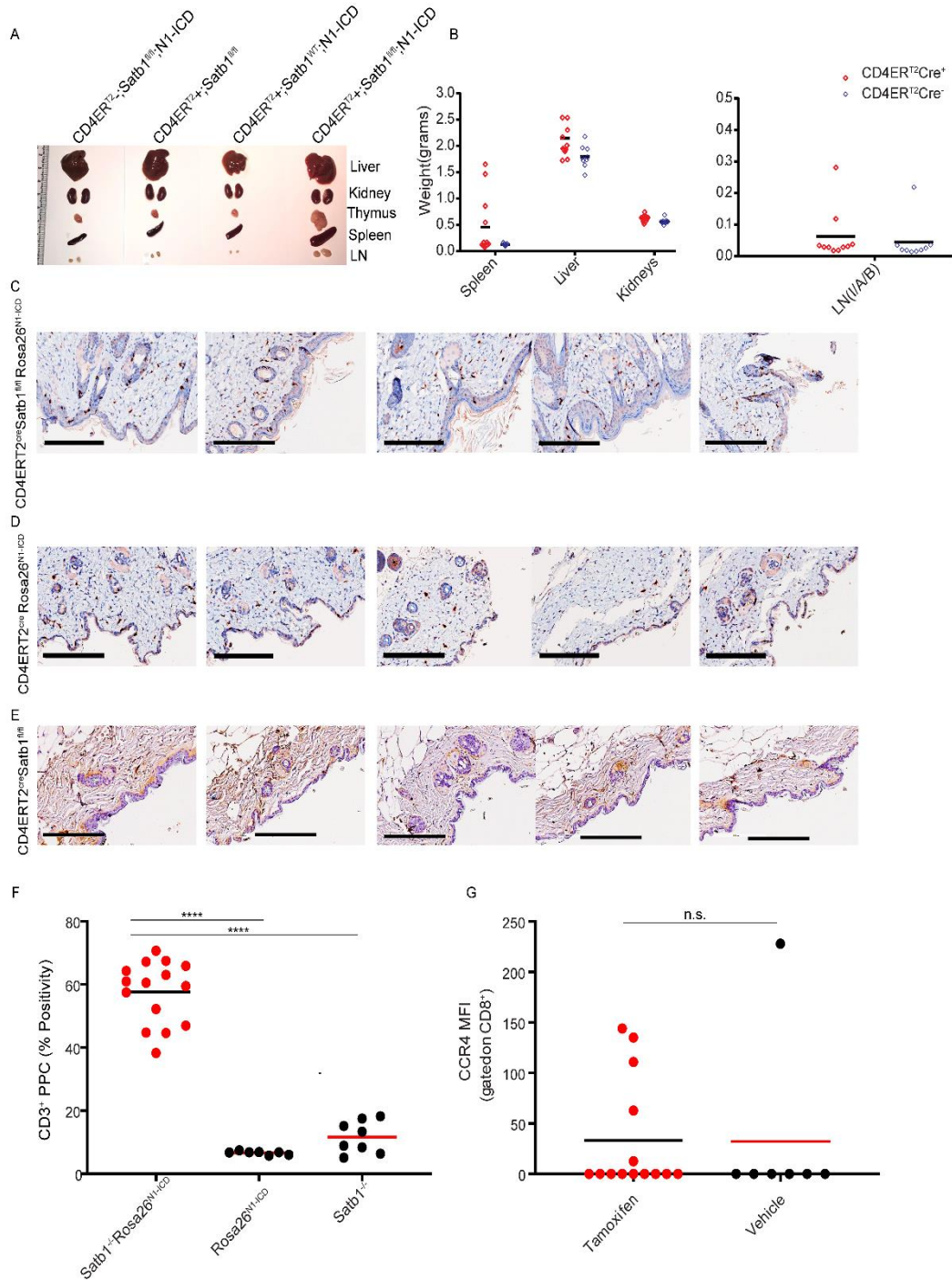


**Figure 10. Organ weight and immunohistochemistry staining for CD3<sup>+</sup> T cell infiltration in mouse skin for *CD4Cre<sup>ERT2</sup>* model.**

(A) Representative photo of liver, kidney, thymus, spleen and inguinal lymph nodes were from *CD4Cre<sup>ERT2</sup>Satb1flx/flxRosa26<sup>N1-ICD</sup>*, *CD4Cre<sup>ERT2</sup>Rosa26<sup>N1-ICD</sup>*, *CD4Cre<sup>ERT2</sup>Satb1flx/flx* and *CD4Cre<sup>ERT2</sup>* negative genotypes (2 replicates). (B) Organ weights of liver, kidney, thymus, spleen and inguinal, axillary, and bilateral lymph nodes. Peripheral staining of CD3 in *CD4<sup>ERT2</sup>Cre<sup>+</sup>Satb1flx/flxRosa26<sup>N1-ICD</sup>* was shown in the dermis and epidermis of the mice (C), *CD4<sup>ERT2</sup>Cre<sup>+</sup>Rosa26<sup>N1-ICD</sup>* (D) *CD4<sup>ERT2</sup>Cre<sup>+</sup>Satb1flx/flx* (E). Scale, 200um. (F) Quantitative Representation of Positive Pixel Count (PPC) of CD3<sup>+</sup> staining of skin from C, D, and E. (G) Median fluorescence intensity (MFI) of the expression of CCR4 in CD3<sup>+</sup>CD8<sup>+</sup> T cells in the peripheral blood of *CD4Cre<sup>ERT2</sup>Satb1flx/flxRosa26<sup>N1-ICD</sup>* mice treated with tamoxifen versus corn oil.

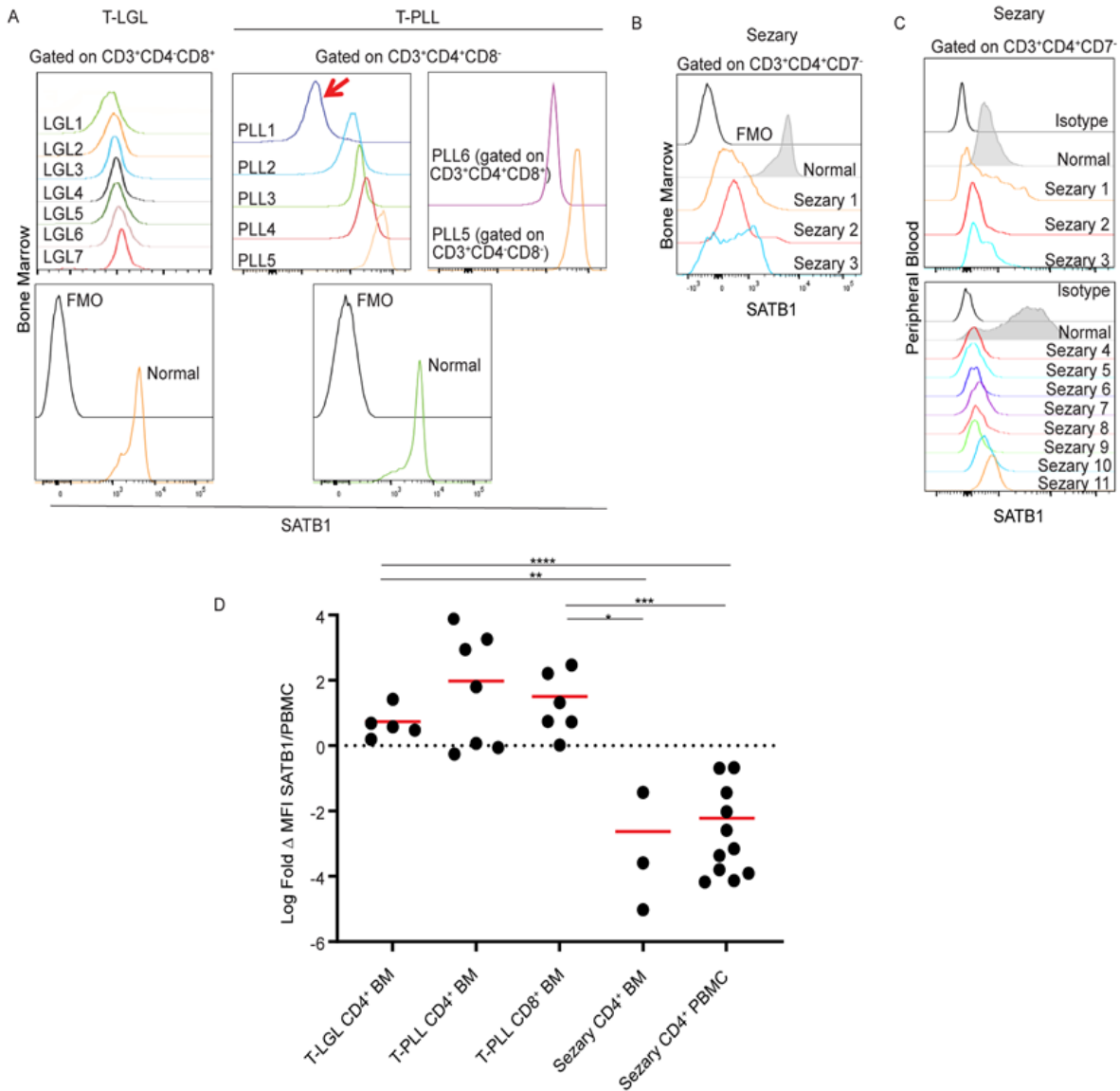


**Figure 11. Sézary cells, but not other malignant lymphocytes, consistently exhibit SATB1 down-regulation.**

(A) Expression of SATB1 in the indicated populations of malignant cells in the bone marrow of patients with T-LGL (n=7) or T-PLL (n=6), compared to SATB1 expression in CD8<sup>+</sup> (T-LGL) or CD4<sup>+</sup> (T-PLL) T cells activated with CD3/CD28 beads for 48 hrs. Gated in live CD45<sup>+</sup>CD3<sup>+</sup> CD4<sup>+</sup> or CD8<sup>+</sup>T cells. FMO refers to “fluorescence minus one” (B) SATB1 down-regulation in bone marrow Sézary cells (n=3). (C) SATB1 down-regulation in non-activated peripheral blood Sézary cells (n=11) compared to normal donor CD4<sup>+</sup> T cells. (D) Log transformed fold change values of SATB1 MFI levels of malignant cells over normal CD4<sup>+</sup> or CD8<sup>+</sup> PBMCs for T-LGL CD4<sup>+</sup> BM (n=5), T-PLL CD4<sup>+</sup> BM (n=7), T-PLL CD8<sup>+</sup> BM (n=6), Sézary CD4<sup>+</sup> BM (n=3), and Sézary CD4<sup>+</sup> PBMC (n=11). Two-tailed Student’s t-tests; \*p<0.05; \*\*p<0.01; \*\*\*p<0.001; \*\*\*\*p<0.0001.

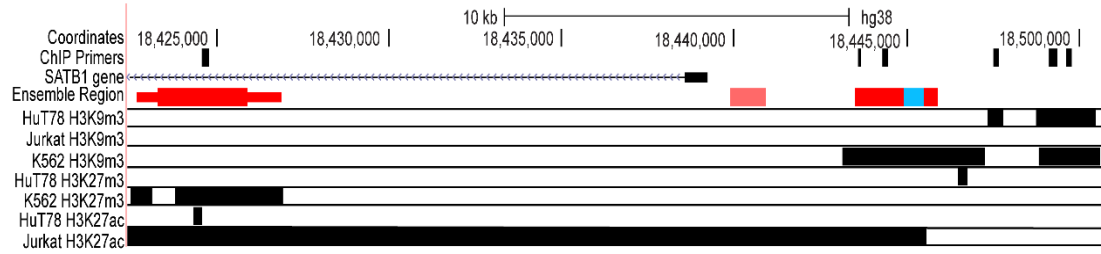


**Figure 12. Peaks adjacent to SATB1 promoter in HuT78, Jurkat, K562 cell lines for ChIP pulled down for H3K27ac, H3K27me3, and H3K9me3 antibodies.**

Peak calling was generated using MACS2 with minimal cut off at  $nq < 0.05$  for narrow peaks and  $nq < 0.05$ ,  $bq < 0.01$  for broad peaks near the TSS of *SATB1* gene. Primers for ChIP-PCR analysis represented by their genomic coordinates on chromosome 3.

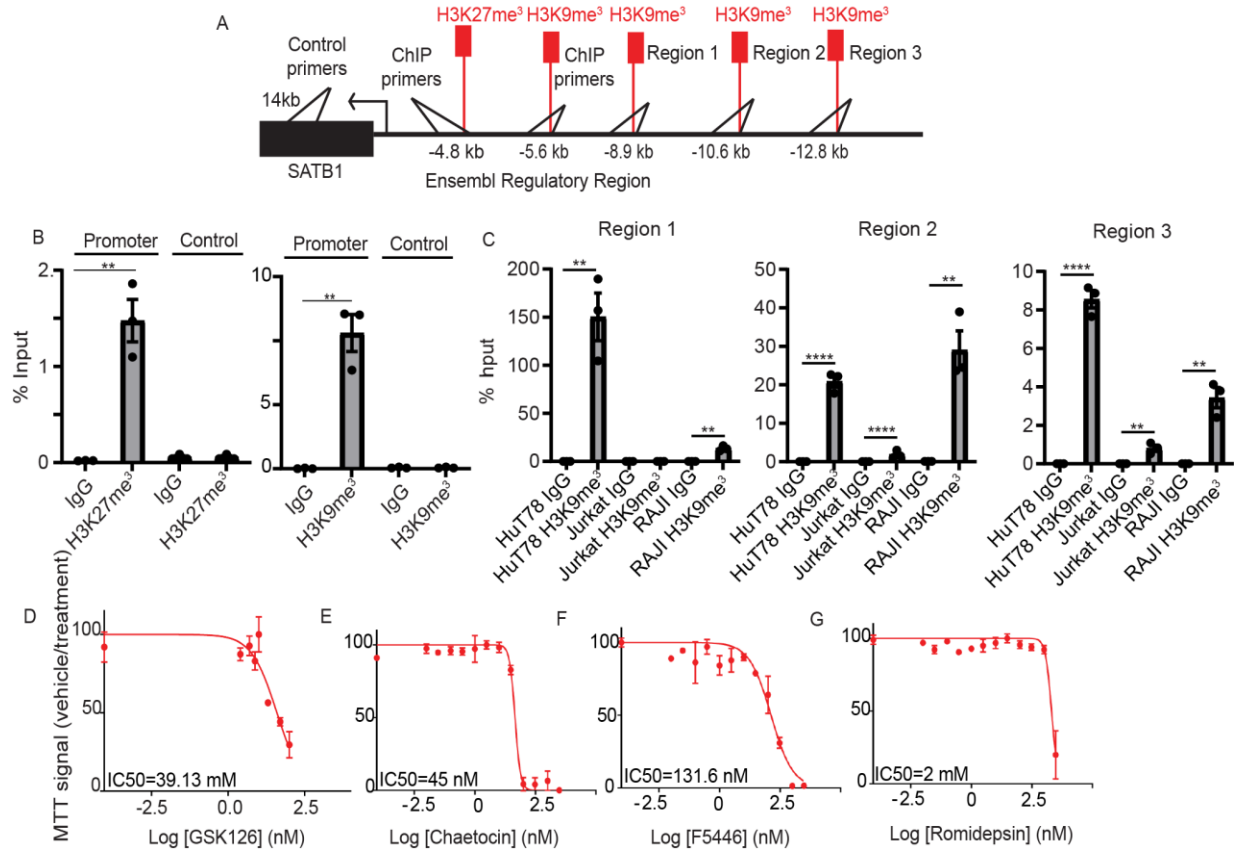


**Figure 13. H3K27me<sup>3</sup> and H3K9me<sup>3</sup> occlude the *SATB1* promoter in a Sézary cell line**

(A) Schematic depiction of primer sites for the regulatory and control regions for ChIP-PCR analysis in B and C. (B) Chromatin Immunoprecipitation quantified by Real-Time Q-PCR with anti-H3K27me<sup>3</sup> (clone#C36B11) (left) or anti-H3K9me<sup>3</sup> (ab8898) (right) versus the control region (~14kb from promoter) and control IgGs pull downs from HuT78 Sézary cells calculated against 2.5% input values. Regions amplified at predicted occupied region ~4.8kb for H3K27me<sup>3</sup> and ~5.6kb for H3K9me<sup>3</sup> from *SATB1* promoter. Representative of 2 independent experiments. (C) Chromatin Immunoprecipitation quantified by Real-Time Q-PCR with anti-H3K9me<sup>3</sup> (ab8898) and control IgGs pull downs from HuT78, Jurkat, and RAJI cells lines calculated against 2.5% input values. Regions amplified based on ChIP-seq data for H3K9me<sup>3</sup> occupied regions near the *SATB1* promoter. (D-G) HuT78 cells were treated with vehicle or growing concentrations of the EZH2 inhibitor GSK126 for 48 hrs in duplicate for MTT assay (D) or SUV39H1 inhibitors Chaetocin (E) and F5446 (F), or the HDAC inhibitor romidepsin (G) in duplicate, and MTT assays were used after 72 hrs. Representative of 2 independent experiments. Two-tailed Student's t-tests (b and c); \*p<0.05; \*\*p≤0.01; \*\*\*p≤0.0001.

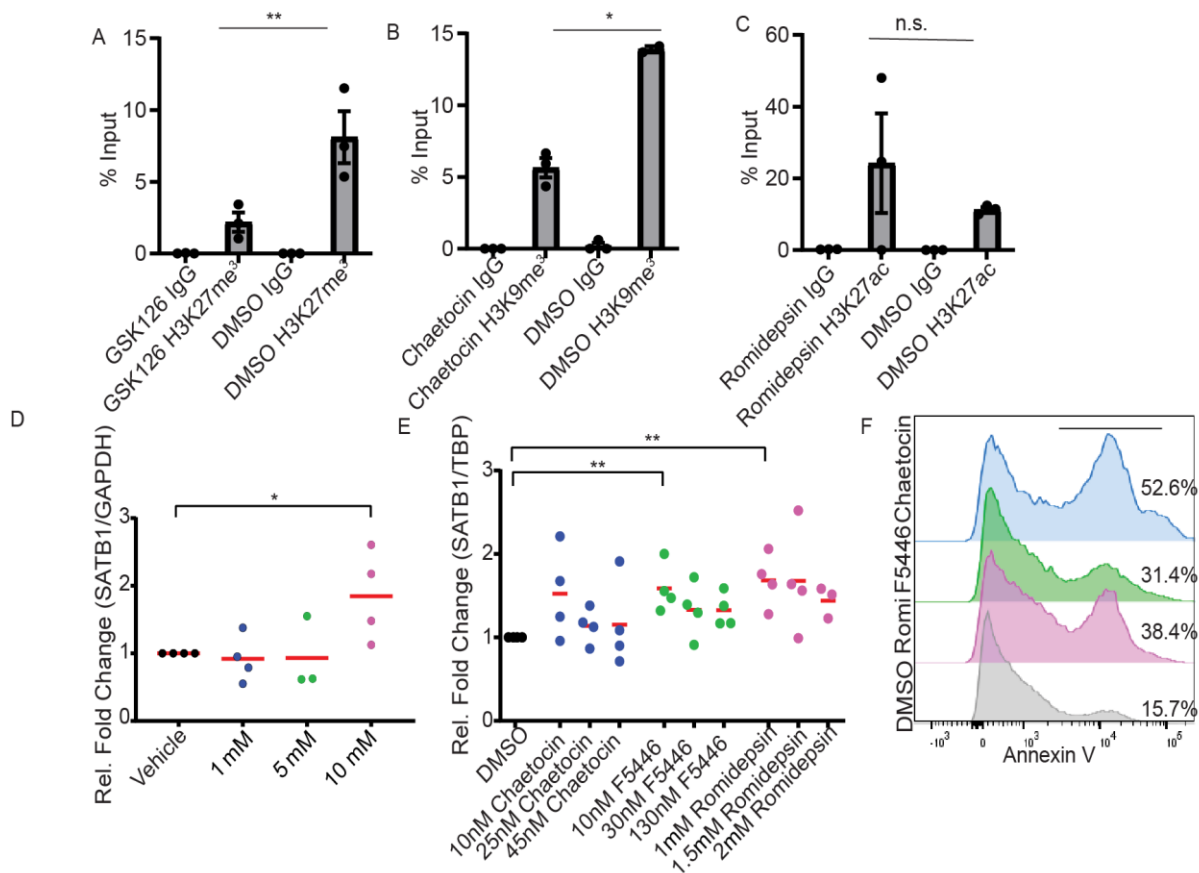
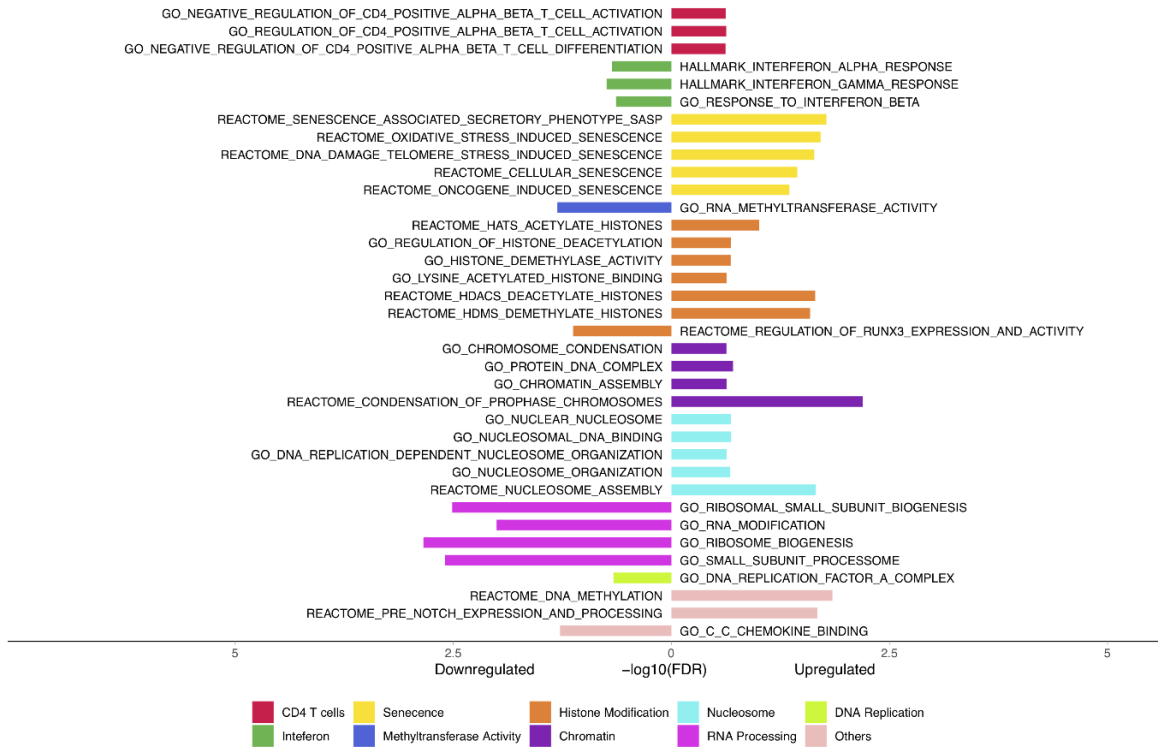


**Figure 14. H3K27me3 and H3K9me3 occlude the *SATB1* promoter in a Sézary cell line**

(A, B, C) ChIP-PCR experiments on HuT78 cells treated with IC50 values of GSK126 (A), Chaetocin (B), and romidepsin (C) pulled down with anti-H3K27me<sup>3</sup> (clone#C36B11), anti-H3K9me<sup>3</sup> (ab8898), or anti-H3K27ac (Abcam; rabbit clone# ab4729), respectively. Representative of 2 independent experiments. (D) RNA was extracted from HuT78 cells identically treated for 48hrs was reverse-transcribed, and *SATB1* mRNA expression was quantified by Q-PCR normalized by human *GAPDH* mRNA. Data pooled from 4 independent experiments are shown. (E) Q-PCR quantification of *SATB1* mRNA expression normalized to *TATA Binding Protein (TBP)* mRNA at 72 hrs after treatment with the indicated doses of Chaetocin, F5446, or romidepsin. Pooled from 4 independent experiments. (F) Histogram staining for Annexin V staining on HuT78 cells treated with the IC50 value of Chaetocin, F5446, or romidepsin. Two-tailed Student's t-tests (a,b,c,d,e); \*p<0.05; \*\*p<0.01; \*\*\*\*p<0.0001.

F5446.vs.DMSO



Chaetocin.vs.DMSO

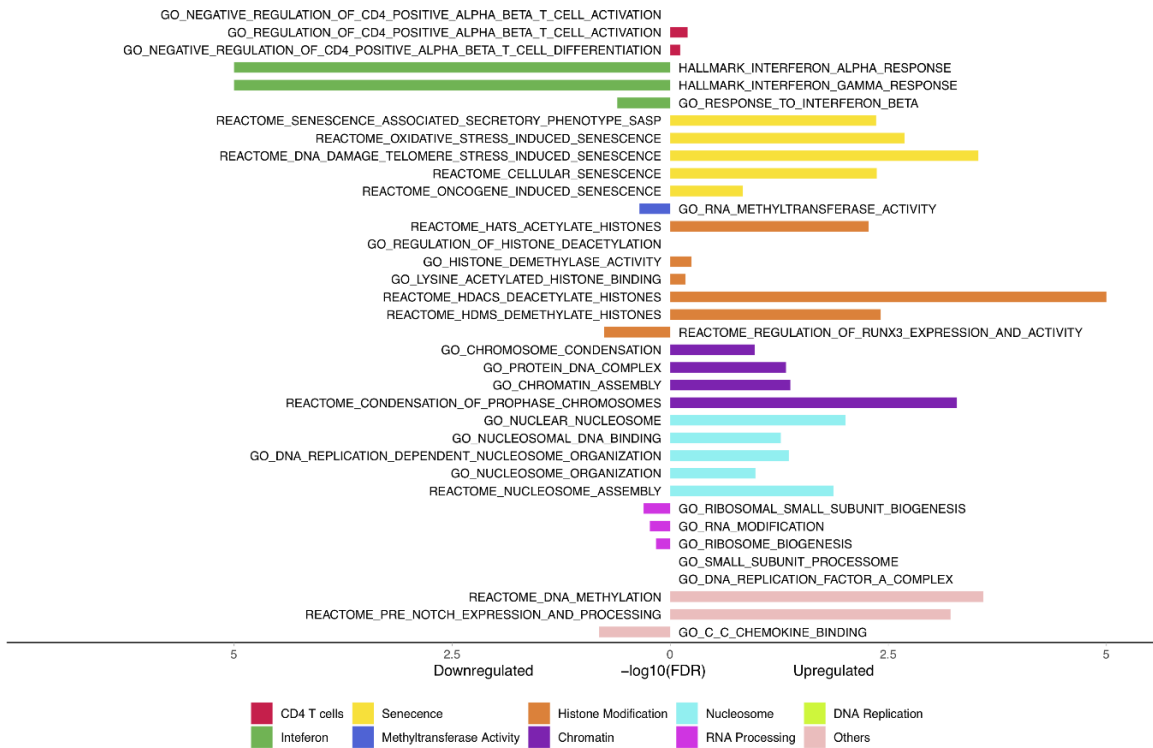


**Figure 15. Categorized Pre-ranked GSEA on HuT78 cell line treated with F5446 and Chaetocin.**

Gene sets with  $FDR \geq 0.05$  were grouped into subcategories based on CD4<sup>+</sup> T cell function, interferon response, proliferation and cellular senescence, methyltransferase activity, histone modification, RNA processing, DNA replication, and nucleosome.

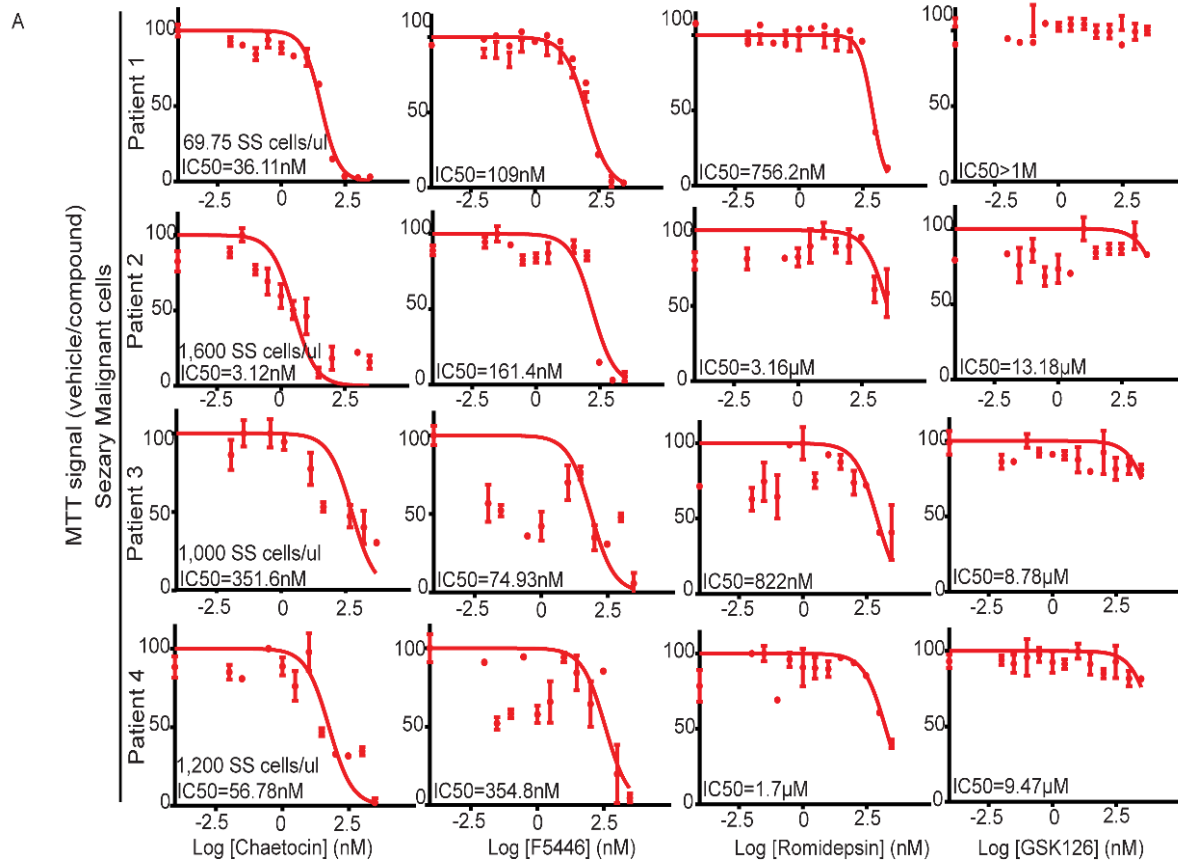


**Figure 16. Screening epigenetic inhibitors in primary Sézary cells**

(A) CD4<sup>+</sup>CD26<sup>-</sup> isolated T cells from peripheral blood apheresis of Sézary patients (n=4) were cultured in R10 media with 100U/ml of human recombinant IL-2 and treated with increasing doses of SUV39H1/2 inhibitors Chaetocin and F5446 (72hrs) as well as romidepsin (72hrs) and GSK126 (48hrs) versus the vehicle control (DMSO) prior to MTT analysis. IC<sub>50</sub> values (nM) were calculated for each patient sample for the respective treatments

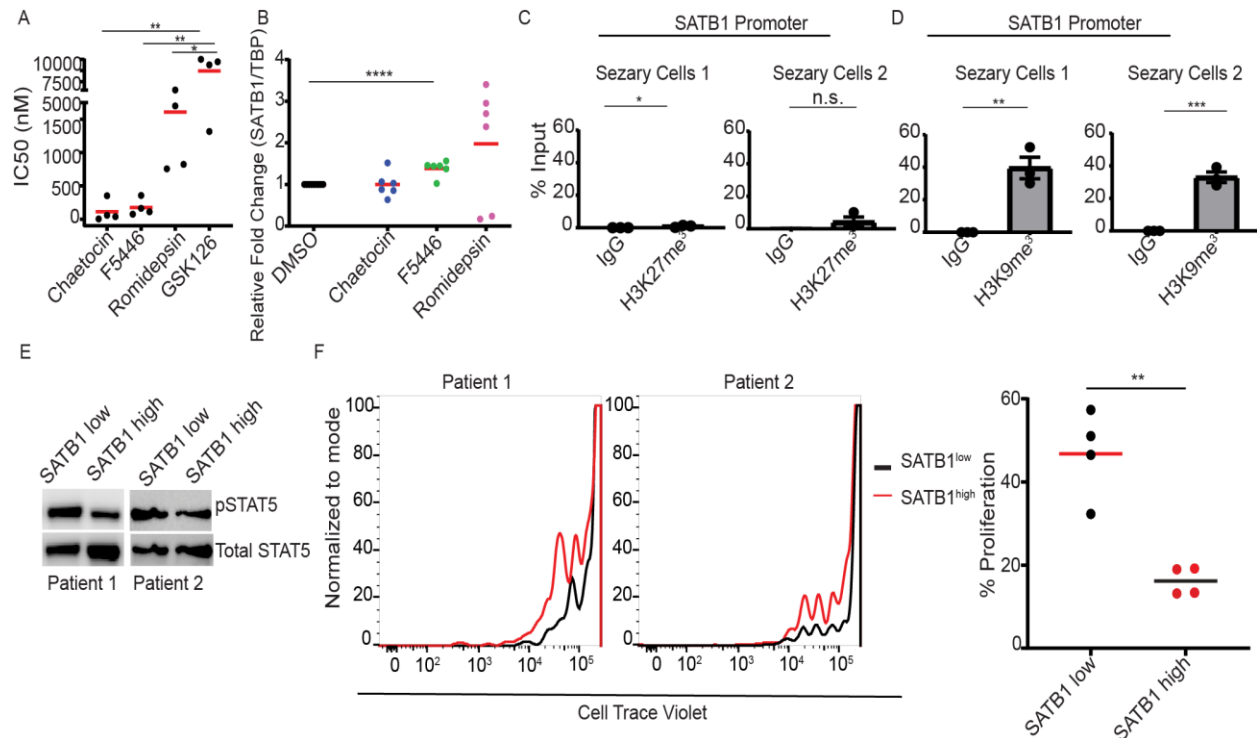


**Figure 17. H3K9me3 repression of SATB1 in malignant Sézary patient cells.**

(A) Summary of IC<sub>50</sub> values for Chaetocin, F5446, romidepsin, and GSK126 for each malignant sample (n=4). One-way ANOVA using multiple comparisons Tukey's test; \*p<0.05; \*\*p<0.01. (B) RNA was extracted from primary CD4<sup>+</sup>CD26<sup>-</sup> cells Sézary patient cells were treated with Chaetocin, F5446, romidepsin or vehicle control (DMSO) for 24-36hrs, and *SATB1* mRNA expression was quantified by Q-PCR normalized by human *TBP* mRNA. Data pooled from 3 patient samples with 2 independent experiments shown (n=6). Two-tailed Student's t-tests; \*\*\*\*p<0.0001. (C) Chromatin Immunoprecipitation quantified by Real-Time Q-PCR with anti-H3K27me<sup>3</sup> (clone#C36B11) or control IgG isotype immunoprecipitation from isolated CD4<sup>+</sup> T cells from peripheral blood of Sézary patients (n=2) calculated against 2.5% input values. Regions amplified at predicted occupied region (~4.8kb) *SATB1* promoter. Representative of 2 independent experiments. Two-tailed Student's t-tests; \*p<0.05; \*\*p<0.01; \*\*\*p<0.001. (D) Similar to (C) except with anti-H3K9me<sup>3</sup> (ab8898) at ~5.6kb region versus the control region (n=2). Representative of 2 independent experiments. Two-tailed Student's t-tests; \*p<0.05; \*\*p<0.01; \*\*\*p<0.001. (E) Primary Sézary CD4<sup>+</sup>CD26<sup>-</sup> cells (n=2) were transduced with retrovirus containing human *SATB1* and sorted for GFP<sup>+</sup> and GFP<sup>-</sup> cells. Western blot was blotted against human pSTAT5 and STAT5 protein in endogenously *SATB1* expressing cells versus ectopically *SATB1* expressing cells (n=2). (F) Primary Sézary cells were labeled with Cell Trace Violet and were serum starved for 24 hours prior to stimulation with anti-CD3/CD28 beads and cultured in complete medium with 100U/mL of rhIL-2 for 5 days. Proliferation was assessed by Cell Trace Violet Dilution using FACS for cells ectopically (n=2) or endogenously (n=2) expressing *SATB1*. Experiment was performed on 2 replicates per patient (n=4). Two-tailed Student's t-tests; \*\*p<0.01.

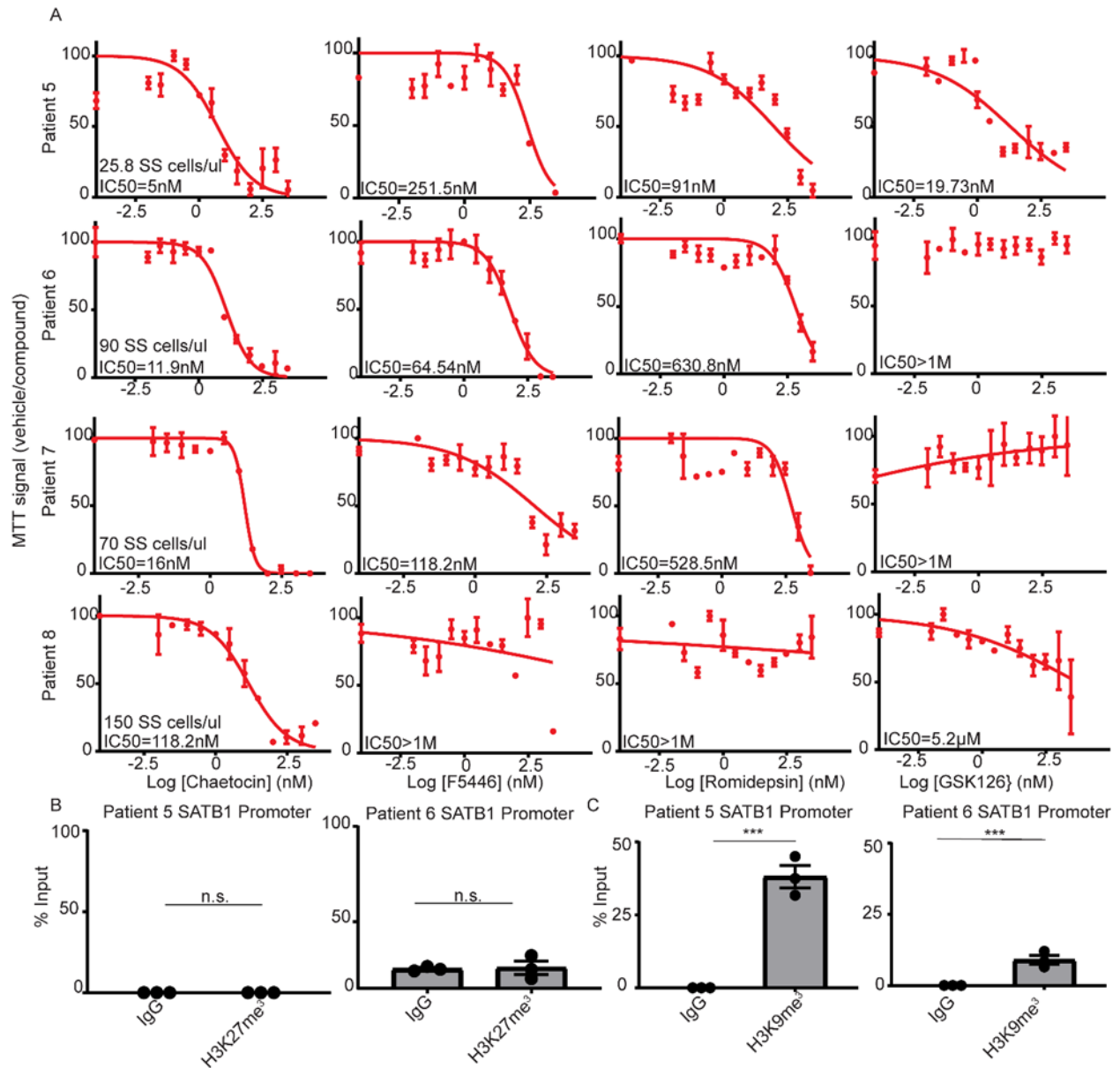


**Figure 18. H3K9me3 repression of SATB1 in CD4<sup>+</sup> T cells of Sézary patients.**

(A) CD4<sup>+</sup> only isolated T cells from peripheral blood apheresis of 4 Sézary patients were cultured in R10 media with 100U/ml of human recombinant IL-2 and treated with increasing doses of SUV39H1/2 inhibitors Chaetocin and F5446 (72hrs) as well as GSK126 (48hrs) and romidepsin (72hrs) versus vehicle control (DMSO) prior to MTT analysis. IC50 values (nM) were calculated for each patient sample for the respective treatments. (B) Chromatin Immunoprecipitation quantified by Real-Time Q-PCR with anti-H3K27me3 (clone#C36B11) or control IgGs pull downs from isolated CD4<sup>+</sup> T cells from peripheral blood of Sézary patients calculated against 2.5% input values. Regions amplified at predicted occupied region (~4.8kb) SATB1 promoter (C) Similar to (B) except with anti-H3K9me3 (ab8898) at ~5.6kb region versus the control region.

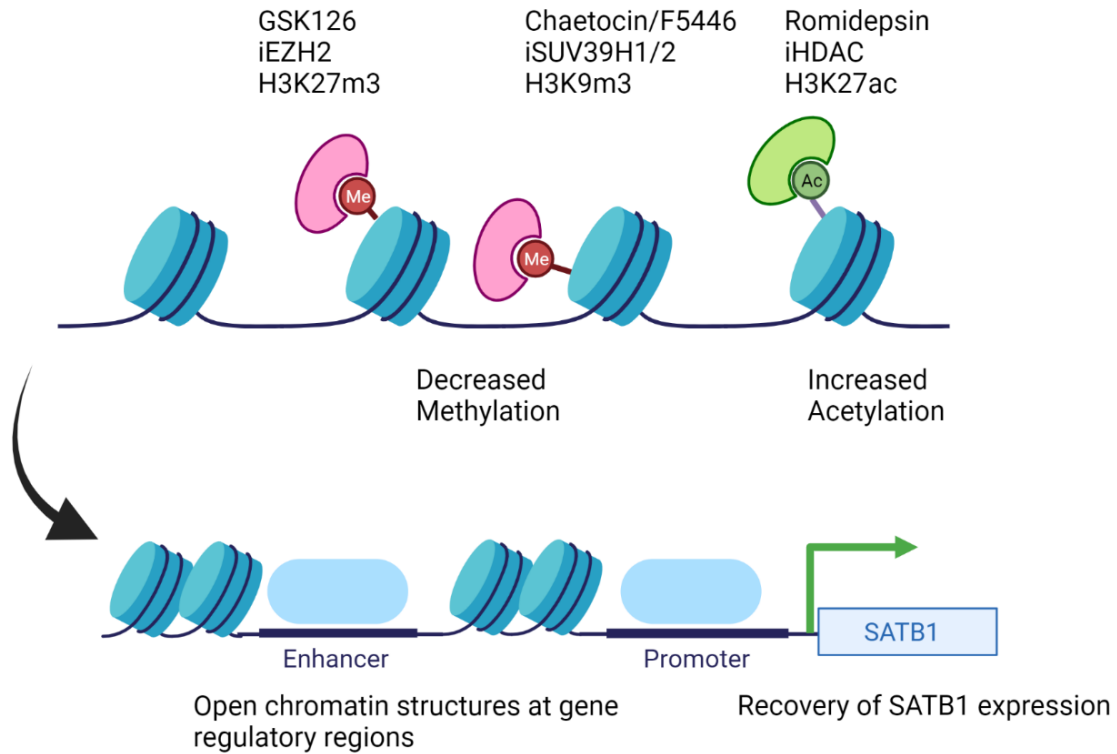


**Figure 19. Summary of epigenetic mechanism silencing *SATB1* expression in Sézary cells**

The region upstream of *SATB1* is populated by regulatory regions which host sites which are deacetylated by HDACs or trimethylated EZH2 or SUV39H1/2 which are inhibited by romidepsin, GSK126, chaetocin, or F5446, respectively. The inhibition of these histone modifications results in the change in chromatin conformation and allows for the restoration of *SATB1* expression in malignant cells.

## CHAPTER THREE: PATHOGENIC MECHANISMS DRIVING CUTANEOUS T CELL LYMPHOMA

### Introduction

Peripheral T cell lymphomas (PTCL) account for about 12% of lymphoid tumors worldwide (111). Among them, Cutaneous T cell Lymphoma (CTCL) CTCL represents a heterogeneous group of diseases characterized by a cutaneous infiltration of malignant T cells. There are no curative therapies available for these diseases, due in part to limited understanding of the origin and pathogenesis of the disease.

The most common forms of CTCL are Mycosis Fungoides (MF) and its leukemic variant, Sézary syndrome, which have an annual incidence of about 0.5 per 100,000 (150). The similarities and differences in the molecular alterations driving these heterogeneous diseases remain poorly understood. Thus, while many mutations in common oncogenes are found in both MF and Sézary syndrome (151), recent studies have also identified differences in structural variants and deletions in tumor suppressor genes, which are much more common in the leukemic variant of the disease (151). For instance, recent studies have suggested a role for mutations in known suppressor genes, oncogenes and epigenetic modifiers in Sézary syndrome, including *TP53*, *ARID1A*, *CDKN2A*, *RBI*, *PTEN*, *PLCG1*, *ZEB1*, *DNMT3A* and the JAK-STAT pathway (114, 129, 151, 152). Some authors have speculated that Sézary syndrome could evolve from mycosis fungoides (153), while other studies have pointed to a different cell of origin for these diseases, based on differential expression of markers of antigen experience. Based on new

evidence on phenotypic heterogeneity among malignant cells in both variants of CTCL, the field has recently evolved to the prevailing view that different functional states and the magnitude of genetic alterations, rather than different cells of origin, determine the manifestation of CTCL in the form of MF vs. Sézary syndrome (154).

T cells egress from the thymus after selection and acquisition of TCRs from migrating lymphoid precursors. Although age-related regression of the thymus is associated with a decline in T cell output, there are T cells with hallmarks of recent thymic egression in individuals in mid-80s (155). The mechanism of initiation of CTCL also remains elusive (156), recent studies found significant heterogeneity in the TCR repertoire of CTCL malignant cells, suggesting that malignant transformation could take place during early T cell development (157). This would help explaining why up to 7% of Sézary syndrome patients show concomitant T cell large granular lymphocytic proliferation in the periphery, which is paradoxically associated with favorable prognosis (158).

To gain insight into the pathogenesis of CTCL, here we aimed to define the origin of CTCL, as well as differences and similarities between MF and Sézary cells. Our results point to heavily altered hematopoiesis in CTCL patients. Malignant T cells sharing mutations in oncogenes with hematopoietic stem cells (HSCs) egress from the thymus with multiple TCRs as premalignant lymphocytes, which complete their malignant transformation in the periphery, expanding into heterogeneous clonotypes and phenotypes. These results have obvious implications for future therapies designed to prevent CTCL recurrence after temporary remission, due to replenishment of peripheral malignant cells from HSCs.

## Results

### *Different stem-like/tumor-initiating cells and differentiation trajectories in Sézary syndrome versus Mycosis fungoides*

To identify CTCL-initiating cells, we first performed single-cell RNA sequencing, coupled to TCR V-D-J sequencing, after enriching CD4<sup>+</sup> T cells followed by either CD7 or CD26 depletion from patient aphaeresis from Sézary syndrome (n=4) and Mycosis fungoides (n=3) (Figure 20A and B). Analysis revealed that multiple clusters (Sézary stem cell, MF stem cell, Transition, MF effector, Proliferation, Mitochondrial Activity, and Treg) emerged from gene expression analysis when comparing the two diseases (Figure 20C). Interestingly, we found phenotypically distinct stem/tumor-initiating cells for both diseases. Compared to the MF cell cluster with hallmarks of stemness, Sézary-initiating (stem-like) cells showed higher expression of AP-1 associated genes *JUN*, *JUNB*, and *FOS* as well as *CXCR4* (Figure 20D). In contrast, Mycosis fungoides patients possessed their own specific stem cell-like/tumor-initiating cluster with differentially expressed genes compared to the Sézary stem cell-like cluster (Figure 20D). Tumor-initiating cells in both diseases differentiate into transitional populations with comparable transcriptional profiles, characterized by decreased co-expression of stem cell-like genes *TCF7*, *IL7R*, *CD27* and acquisition of the activation markers *CD69*, *LAG3*, and *PDCD1* as well as *CXCL13* (Figure 21A). However, only Sézary cells turn into populations sharing the same TCR and attributes of increased mitochondrial activity (*MT-ATP6*, *MT-CO1*, *MT-CYB*, *MT-ND1*), or Treg cells (*FOXP3*). In addition, Sézary cell clonotypes progressively acquired a distinctive proliferative phenotype, characterized by expression of cell cycle genes *MKI67*, *CDK1*, *CCNA2*, *CDCA2*; upregulation of *RUNX3*, *ITGAL*, and *ITGB2*; and downregulation of the stem cell marker *TCF7* and the memory cell marker *CD27* (Figure 21A). In contrast, MF cells

differentiated into a distinctive phenotype with features of effector activity including the expression of *IFNG*, *GZMB*, and *PRFI* (Figure 21B). Therefore, Sézary syndrome and MF originate from phenotypically different cell types, which differentiate into expanded peripheral malignant cells with very distinct molecular attributes.

*Sézary syndrome and Mycosis fungoides are also different in terms of clonality and transcription factors driving malignant phenotypes*

Importantly, single cell ATAC-seq of the 4 Sézary syndrome patients (SS1-SS4) and one mycosis fungoides patient (MF3), confirmed that open or closed chromatin regions match expression patterns identified through single cell RNA-seq (Figure 22A). Furthermore, single cell ATAC-seq revealed highly increased open chromatin peaks for the ZEB1 transcription factor, previously associated with tumor suppressor activity in Sézary syndrome (159), specifically in stem/tumor-initiating cells (Figure 22B). RUNX3 and STAT1::STAT2 binding were high in the MF effector population and low in the differentiated SS proliferative population (Figure 22B). Other transcription factors and genomic organizers previously associated with the pathophysiology of CTCL also showed distinctive (and matching) transcriptional and chromatin structure profiles (Figure 22C).

Most importantly, we observed different clonality between MF and Sézary syndrome. Thus, while malignant cells in both diseases showed a diverse range of clonotypes, MF cells exhibit much broader TCR repertoires, compared to Sézary cells, which correspondingly exhibit larger clones (Figure 23A). Enriched clonotypes in MF samples were contained in the MF effector group (Figure 23B, Figure 24A and D). In contrast, Sézary clonotypes were more equally distributed across stem-like/tumor-initiating populations and more differentiated

populations, including the distinct proliferative subset (Figure 23B, Figure 24B and 3C). The absence of clonal enrichment in Sézary syndrome, compared to MF, suggests that the former disease progresses independently of antigen stimulation, while MF could evolve through the expansion of specific clonotypes that recognize skin antigen. Furthermore, both diseases are driven by the expression of a distinctive pattern of transcription factors, further underscoring differences in the pathophysiology of both diseases.

*Heavily mutated hematopoietic progenitors share mutations in key oncogenes with malignant Sézary cells in all patients analyzed, but not their normal T cell counterparts in some patients*

The presence of malignant cells with multiple TCRs in CTCL, in addition to the maintenance of a relatively uniform repertoire of clonotypes in Sézary syndrome, suggests that at least Sézary cells could arise from hematopoietic progenitors with malignant potential that acquire TCR expression in the thymus.

To test this hypothesis, we conducted whole exome sequencing on CD34<sup>+</sup> hematopoietic stem cells (HSC) extracted from bone marrow biopsies from 5 different patients with Sézary syndrome, as well as autologous (CD4<sup>+</sup>CD26<sup>-</sup>) malignant T cells, normal (CD4<sup>+</sup>CD26<sup>+</sup>) T cells, and CD34<sup>+</sup> HSC cells from the aphaeresis of the same patients. To establish the baseline for calling true mutations without using hematopoietic cells, we cultured bone marrow fibroblasts. Unexpectedly, we found 200 mutations or more in HSCs derived from either the bone marrow or peripheral blood in 4 out of 5 patients (Figure 25A-E). Given that previous studies in patients with chronic myelomonocytic leukemia of similar age identified not more than 10-15 mutations per exome in HSCs (8, 160), these results suggest that patients with Sézary syndrome have an unusually heavy mutational burden in hematopoietic precursors. Most importantly, some of these

mutated genes have been previously identified as key oncdrivers in Sézary syndrome. For instance, different mutations in the coding region of *TP53* (114, 161, 162) were present in autologous HSCs and peripheral Sézary cells in 2 patients, while a third patient showed a shared mutation in the non-coding region of *TP53* (Table 7). In addition, another patient showed different mutations in the known oncdriver *ARID1A* (152, 161) shared between HSCs and peripheral malignant cells, while a shared mutation in the *TNK2* tyrosine kinase gene, previously identified in AML and multiple other malignancies (163), was identified in a fourth patient (Table 7).

Of note, we identified specific mutations present in HSCs and malignant peripheral cells in every patient, ranging from 2 to 183 shared mutations (Appendix A). Interestingly, in 2 out of 5 patients we found multiple mutations only shared between malignant cells and HSCs, which were absent in autologous normal (CD26<sup>+</sup>) T cells (Appendix A), suggesting that malignant and normal lymphocytes in these patients arose from different hematopoietic precursors. Additionally, the variant allele frequency (Figure 25A-E) of these mutations in the HSCs suggests there is a highly heterogenous population of progenitor cells in the bone marrow. Considering the high number of mutations shared between malignant T cells and HSCs (including in oncdrivers), the diversity of TCRs in malignant cells, and the absence of clonal enrichment as tumor-initiating cells differentiate and expand in the periphery, these results indicate that specific pre-thymic clones of mutated T cell precursors with malignant potential acquire multiple TCRs in the thymus, and mature and complete the malignant transformation process independently of antigen recognition post thymic selection.

### *Sézary cells show hallmarks of recent thymic egression, but not response to skin antigens*

Thymic activity greatly decreases with age, while the majority of Sézary patients are older. To gain insight into thymic activity in patients with Sézary syndrome, we first quantified signal joint T cell receptor rearrangement excision circles (sjTRECs) from CD4<sup>+</sup> T cells from peripheral blood of patient samples and compared it to age-matched normal donors. We found that sjTREC signal is retained in Sézary cells as well as in T cells from healthy donors, but not in TCR- hematopoietic cells (n=5) (Figure 26A). To investigate how T cells with malignant potential egressing from the thymus complete their malignant transformation in the periphery, we investigated whether Sézary cells could react to skin antigens. For that purpose, we procured malignant CD26<sup>+</sup> T cells from the blood from three Sézary syndrome patients and allogenic skin biopsies, produced lysates, and used them to pulse autologous antigen presenting cells (APCs). As shown in Figure 26C, we did not observe any increase in proliferation or IL-4 cytokine production in Sézary cells in three independent experiments. Identical results were obtained when autologous APCs were pulsed with lysates from cultured keratinocytes (MHC class II expressing cells from skin) (Figure 26B). Together, these results support that T cells with malignant potential acquire TCRs in the thymus and complete their malignant transformation through different process in Sézary syndrome versus MF.

## **Discussion**

We report that, although Sézary and MF tumor-initiating cells with features of stemness have distinct phenotypes, they differentiate into diverse lymphocytes subsets as they expand, supporting that plasticity and heterogeneity, rather than a fundamentally different cell of origin, explains phenotypic differences between both diseases. Our results support the recent

questioning of the principle of "cell-of-origin" distinction between Sézary syndrome and MF and suggest that different functional states driving phenotypic changes in malignant cells, as previously proposed (154, 164), drive dissimilar evolution in CTCL patients. However, we found that TCR repertoires are maintained in Sézary differentiated cells as they expand from tumor-initiating cells with features of stemness, while MF cells get clonally enriched. Accordingly, MF cells, but not Sézary cells, reacted against skin antigens from CTCL patients, illustrating a new difference in the pathophysiology of these diseases. Overall, despite transcriptional differences between tumor-initiating cells in Sézary syndrome vs. MF, our results support that genomic alterations in the precursors that arrive to the thymus, along with the repertoire of TCRs that these cells acquire, could be the major determinants in the evolution of CTCL into MF or Sézary syndrome.

A major finding of our study is that HSCs in at least Sézary syndrome patients share multiple mutations with malignant cells, including some in the coding region of known oncogenes such as *TP53* and *ARID1A*. These results, together with the presence of multiple TCRs in peripheral malignant cells, plus expression of sjTREC sequences in Sézary cells, can only be interpreted in terms of a mutated lymphocyte progenitor with malignant potential that acquires TCRs in a thymus with residual activity and has the capacity to expand in the periphery without enrichment of a particular clonotype. Since normal T cells in some patients (but not in others) share some of the mutations of HSCs and Sézary cells, these results imply that their malignant transformation could be completed in the periphery through expansion and differentiation, although this clearly does not happen in response to skin antigens in Sézary syndrome, unlike MF. Unexpectedly, we found >200 mutations in HSCs of most patients with Sézary syndrome, which is way above the less than 20 mutations per exome typically found even

in patients with myelodysplasia (165), suggesting major alterations in hematopoiesis in these patients. This could help understanding the propensity of developing other T cell disorders in CTCL patients, and in particular large granular lymphocytic proliferation (T-LGL) in peripheral blood (158, 166). Whether concurrent Sézary syndrome and T-LGL is driven by similar defects in HSCs differentiating into CD4<sup>+</sup> vs. CD8<sup>+</sup> T cells in the thymus needs to be tested in future studies.

A lingering question that remains unanswered is one of the 5 patients analyzed only showed 2 mutations shared between HSCs and Sézary cells; both of them in non-coding areas. A possible explanation is that the pathogenesis of CTCL could be driven in some cases by epigenetic alterations that are independent of mutations (i.e., gene silencing). Future transcriptional and ATAC-seq studies will confirm this proposition.

Overall, our results identify altered hematopoietic progenitors as the likely origin of Sézary syndrome and identify important similarities and differences between the pathophysiology of the different manifestations of CTCL, which has obvious implications for future therapeutic interventions. It is tempting to speculate, for instance, that thymectomy could prevent malignant lymphocytes emerging from the thymus from replenishing the periphery after treatment. Whether lymphocyte progenitors would show their malignant potential through alternative differentiation into malignant B cells, for instance, would need to be clinically addressed, but targeting the bone marrow emerges as a requirement for findings curative interventions for CTCL patients.

## Materials and Methods

### *Human Samples*

De-identified human peripheral blood samples and bone marrow aspirates were procured under a protocol approved by Moffitt's Scientific Review Committee. Cells were thawed in complete RPMI (10% heat-inactivated Fetal Bovine Serum, 0.5 mM Sodium Pyruvate (Gibco, 11360070), 2 mM L-glutamine (Sigma, G7513), 100 I.U/mL Penicillin, 100 ug/mL Streptomycin (Lonza, 17-602E). CD4<sup>+</sup>CD7<sup>+</sup>/CD26<sup>+</sup> and CD4<sup>+</sup>CD7<sup>-</sup>/CD26<sup>-</sup> cells were isolated with EasySep™ Human CD4<sup>+</sup> T cell Isolation Kit (STEM CELL, 17952) and EasySep™ Release Human PE Positive Selection Kit (STEM CELL, 17654) from peripheral blood of Sézary syndrome and mycosis fungoides patients. Human HSC CD34<sup>+</sup> cells from bone marrow aspirates using Human CD34 MicroBead Kit UltraPure kit (Miltenyi, 130-100-453) following manufacturing instructions. Removal for CD45<sup>+</sup> cells for enrichment of human fibroblast from bone marrow aspirates was done using EasySep™ Human CD45 Depletion Kit II (STEM CELL, 17898). Primary bone marrow fibroblasts were grown in Fibroblast Growth Medium 2 (PromoCell, C-23020) according to manufacturing instructions. Human normal primary epidermal keratinocytes (ATCC, PCS-200-011) were grown according to manufacturing instructions using Dermal Cell Basal Medium (ATCC, PCS-200-030) supplemented with the Keratinocyte Growth Kit (ATCC, PCS-200-040).

### *Antibodies and Flow Cytometry*

We used the following anti-human antibodies from Biolegend; CD26 (Clone BA57), CD69 (Clone FN50), and CD4 (Clone OKT4). Human  $\gamma$ -globulin (Sigma, G4386) was used for Fc Receptor blockade. Staining included Zombie NIR (Biolegend, 423105) was used as viability

probe for all samples. For Flow Cytometry, all samples were run on a LSRII (BD) and sorted using a FACS Aria SORP. Data were analyzed using FlowJo v10 software.

#### *Cell Trace Violet Assays*

Cell Trace Assays were performed using CellTrace™ Violet (Invitrogen, C34571) following manufacture's recommendations with 5uM stock concentration resuspended in DMSO starting with  $10^6$  cell/mL cell concentration in sterile PBS. Cells were incubated at 37°C for 20 minutes protected from light. Reaction was quenched using complete cell culture medium 5 times the reaction volume and incubated for 5 minutes, spun for 5 minutes 4°C at 1500rpm, and resuspended at cell concentration of  $10^6$  cells/ml in fresh warm media and cultured for 5-7 days prior to FACs analysis.

#### *Antigen Presentation*

Antigen presenting cells were isolated by depleting T cells from autologous PBMCs from aphaeresis samples using EasySep™ Release Human CD3 Positive Selection Kit (STEM CELL, 17751). T cell-depleted PBMCs were cultured for 4 days with human 160 ng/mL IL-4 (PeproTech, 200-04) and 80 ng/mL GM-CSF (PeproTech, 500-P33) in complete medium added on days 0 and 3. Malignant Sézary/MF (i.e., CD7<sup>-</sup> or CD26<sup>-</sup>) T cells were isolated from PBMCs as previously mentioned. Lysates were generated from skin biopsies or human normal primary epidermal keratinocytes (ATCC, PCS-200-011) using ten successive cycles of freezing and thawing with 10ul of PBS. Lysates were centrifuged at 300g for 10 min at 4°C to remove particulate debris. Supernatant were collected and protein concentration was measuring using Pierce™ BCA protein assay kit (ThermoScientific, 23225). In triplicate, plate T cell-depleted

PBMCs from at ~10,000-50,000/100 uL. Lysates were added to T cell-depleted aphaeresis at a final concentration of 12µg/100 uL. Malignant T cells were mixed with skin/control tissue-pulsed autologous PBMCs (1:10). After approximately 20 hours, supernatant was collected, and ELISA were performed using ELISA MAX™ standard set kits for human IFN-γ (Biolegend, 430101) and IL-4 (Biolegend, 430301) following manufacturer's protocol to assess cytokine concentration.

#### *10x RNA, VDJ, and ATAC sequencing*

Previously described isolated cells using EasySep™ kits were resuspended in recommended 1,000 cells per ul concentration in PBS with 0.04% w/v BSA prior to library prep. The target cell number for encapsulation was 6,000-10,000 cells for single cell RNA sequencing and VDJ sequencing. Libraries were prepared using Chromium Single Cell 5' and V(D)J Enrichment Reagent Kits (v1.1 Chemistry) (10X Genomics, Inc., Pleasanton, CA) following manufacturer's instructions and run on NextSeq 500 150 cycles (26bp x 90bp). Read depth was approximately 40,000 reads for RNA sequencing and 5,000 reads for VDJ sequencing per sample. Cells were prepared as previously described. Target nuclei number for encapsulation was 6,000 to 10,000 cells for single cell ATAC sequencing. Libraries were prepared with Chromium Single Cell ATAC Reagent kit (v1.1 Chemistry) (10X Genomics, Inc., Pleasanton, CA) and run on NextSeq 500 150 cycles (50bp x 50bp). Read depth was approximately 25,000 reads per sample.

### *Single-cell RNA-seq data processing, filtering, batch effect correction, and clustering*

Raw sequencing reads from scRNA-seq were processed using Cell Ranger (v6.1, 10X Genomics) and aligned against GRCh38 human transcriptome. Gene-barcode matrices containing only barcodes with UMI counts passing threshold were imported to Seurat (167) for further analysis. Genes detected in less than 3 cells were excluded; cells with less than 200 genes detected or greater than 10% mitochondrial UMIs were filtered out. Doublets were detected using Scrublet (168), DoubletFinder (169), scDbtFinder (170), and doubletCells implemented in scran (171), assuming 0.08% doublet rate for every 1000 sequenced cells. Cells identified as doublets by at least two algorithms were removed from further analysis. Raw UMI counts were log normalized and the top 5000 variable genes were identified using “vst” method implemented in the *FindVariableFeatures* function in Seurat. T cell receptor and immunoglobulin genes were removed from the variable genes to prevent clustering based on V(D)J transcripts. S and G2/M cell cycle phase scores were assigned to cells using *CellCycleScoring* function.

To further remove batch effects, individual samples were integrated using *FindIntegrationAnchors* and *IntegrateData* functions (172) with 8000 anchor genes and 40 dimensions of canonical correlation analysis (CCA). Integrated data were further scaled using *ScaleData* function by regressing against total reads count, % of mitochondrial UMIs, and cell cycle phase scores. A shared nearest neighbor (SNN) based graph was constructed using top 40 principal components, and clusters were identified using the Louvain algorithm using *FindCluster* function at resolution=1. UMAP projections were generated by *RunUMAP* function and used for all visualization.

### *Differential gene expression analysis, cluster annotation, and trajectory analysis*

Differential expression analysis comparing each cluster versus all others was performed using FindAllMarkers function in Seurat with default settings. Genes with  $\log_2(\text{fold-change}) > 0.25$  and Bonferroni-corrected p-value  $< 0.05$  were considered differentially expressed. Clusters were annotated by comparing differential genes to markers previously associated with T cell stemness/memory, effector activity, proliferation, and exhaustion/dysfunction. Clusters were further merged into major groups based on annotation for further analysis. Marker gene expression was visualized on UMAP project or by violin plot using log-normalized UMI counts. Bubble plot was used to visualize z-score normalized average expression and percentage of expressing cells per cluster or per major group.

### *Trajectory analysis*

Differentiation trajectory was constructed using a partition-based graph abstraction (PAGA) algorithm (173) implemented in R package Scanpy (174). A UMAP dimensionality reduction was performed on batch effects corrected CCA extracted from Seurat and a kNN-like graph at the major group level was constructed using the default settings. All high-connectivity edges with weights higher than 0.1 were drawn on the graph.

### *Single-cell 10X VDJ analysis*

TCR reads sequenced by 10X V(D)J assay were aligned to human GRCh38 reference transcriptome using Cell Ranger VDJ (v6.1, 10X Genomics) to assemble the single TRC chains. Only the assembled chains that were highly confident, of full-length, and productive were kept. Cells with the same amino acid sequences of the CDR3 regions and V(D)J genes for both TRA

and TRB chains were considered originated from the same clone. These cells were further assigned to major groups based on annotation of the paired single-cell RNA assay. Trajectory of the top clonotypes were visualized on UMAP projected generated from paired RNA assay.

#### *Single-cell ATAC-seq data processing, filtering, batch effect correction and clustering*

Raw sequencing reads generated from 10X ATAC assay were processed by cellranger-atac workflow in Cell Ranger (v6.1, 10X Genomics) with default settings to generate mapping and chromatin accessibility. The mapping and chromatin accessibility data were imported to R package Signac v1.3.0 (175) for downstream analysis. Low-quality cells with  $< 3,000$  or  $> 20,000$  fragments in peaks,  $< 15\%$  fraction of fragments in peaks,  $> 4$  ratio of mononucleosomal to nucleosome-free fragments, or  $< 2$  transcriptional start site (TSS) enrichment score were filtered out. A latent semantic indexing (LSI) dimension reduction was performed on the filtered cells. First, peak data were normalized by the frequency-inverse document frequency (TF-IDF) method using *RunTFIDF* function in Signac to correct for different sequencing depth across cells and the different rareness level across peaks. The variable features were selected from peaks present in  $> 20$  cells using *FindTopVariable* function. Next, a singular value decomposition (SVD) dimension reduction was performed on the TF-IDF matrix using the selected peaks followed by Harmony batch correction method implemented in R package harmony (176). A shared nearest neighbor (SNN) based graph was constructed using first 40 reduced dimensions, and clusters were identified using the Louvain algorithm using *FindCluster* function in Seurat at resolution=0.8. UMAP projection was generated using the first 40 reduced dimensions and used for visualization.

### *Gene activity scores and cluster annotation*

It has been shown that gene expression is often correlated with chromatin accessibility at the gene body, promoter, and distal regulatory elements (177, 178). Therefore, we quantify the gene activity by counting reads mapped to gene body and promoter regions (extended 2kb upstream from gene coordinates) using *GeneActivity* function in Signac, and further log-normalized the counts using *NormalizeData* function in Seurat with default settings. Differential expression analysis was performed on the normalized gene activity scores for each cluster identified from variable peaks. Genes with Bonferroni-corrected p-value  $< 0.05$  and an average  $\log_2(\text{fold change}) > 0.25$  were considered differentially expressed and were visualized by R package ComplexHeatmap v2.7.8 (179). Clusters were annotated by comparing the differential genes to the same makers used in single-cell RNA-seq cell annotation. The clusters were further grouped into major groups based on their annotations.

### *Identification of group-specific peaks and TF motifsene activity scores and cluster annotation*

The differential accessible peaks between major groups were identified by logistic regression corrected for differences in sequencing depth across peaks. Peak regions with Bonferroni-corrected p-value  $< 0.05$ ,  $\log_2(\text{fold change}) > 0.25$ , and at least 5% cells accessible at the region were considered differentially accessible and group-specific. These differentially accessible regions were further annotated to their closet genes by *ClosestFeature* function in Signac.

We next investigated the different transcription factor motifs enriched in accessible regions of each major group. Frist, human motif position frequency matrices were retrieved from JASPAR database using R packages JASPAR2020 v0.99 and BSgenome.Hsapiens.UCSC.hg38 v1.4.3, and *getMatrixSet* function in R package TFBSstools v1.31.2. Then a hypergeometric test

for motif enrichment was performed for each group using *FindMotifs* function in Signac by considering GC content in the group-specific peaks. The enrichment scores were calculated as  $-\log_{10}$ (Benjamini–Hochberg corrected *p*-value) and visualized by R package ComplexHeatmap v2.7.8.

### *Whole Exome Sequencing*

Following the collection of patients' cells, genomic DNA was extracted using the QIAgen QIAamp DNA Blood Mini Kit following the manufacturer's protocol (Qiagen, 51104), and the DNA's quality was assessed using the Agilent TapeStation (Agilent Technologies, Inc., Santa Clara, CA). Two hundred ng of DNA was used as input to generate whole-exome sequencing libraries using the Agilent SureSelect XT Clinical Research Exome kit. (Agilent Technologies, Inc., Santa Clara, CA). Briefly, genomic DNA libraries were constructed according to the manufacturer's protocol and the size and quality of the library was evaluated using the Agilent BioAnalyzer (Agilent Technologies, Inc., Santa Clara, CA). Equimolar amounts of library DNA were used for a whole-exome enrichment using the Agilent capture baits, and final libraries were screened on an Agilent TapeStation (Agilent Technologies, Inc., Santa Clara, CA) and quantitated by qPCR with the Kapa Library Quantification Kit (Roche Diagnostics, U.S., Indianapolis, IN). An average of 100 million 75-base paired-end reads per sample were generated using v2 chemistry on an Illumina NextSeq 500 sequencer to achieve an average sequencing depth of 140X.

### *Identification of somatic mutations*

Somatic mutations were identified from whole exome sequencing of matched tumor and normal samples following the strategies described in TCGA's Multi-Center Mutation Calling in

Multiple Cancers project (MC3 project) (180). Short reads were aligned to human reference genome GRCh38 using the Burrows-Wheeler Aligner (*BWA* (181)) and then improved by base quality score recalibration, sequence realignment near indels, and duplicate read removal using the Genome Analysis Tool Kit version 4 (*GATK* (182)) and Picard. SAMSTAT (183) and Picard were used for quality checking of the aligned BAM files. Somatic mutations were further detected from the recalibrated bam using a combination of Mutect2 (183), SomaticSniper (184), MuSe (185), FreeBayes (186), Pindel (187), and Strelka (188) with the default settings. Mutations with reported variant allele frequency  $> 0.01$  in external databases including 1000 Genomes Project (189), NHLBI Exome Sequence Project (ESP) and the Exome Aggregation Consortium (ExAC) (190) were considered germline inherited variations and removed from further analysis. Only point mutations and indels predicted by at least two algorithms were included for subsequent analysis. Additional annotation were added from COSMIC (191), ExAC (190), dbGAP (192), and Ensembl (193) using ANNOVAR (194). The identified somatic mutations were further analyzed and visualized using R packages Maftools (195) and UpSetR (196).

### *Molecular Cloning*

Genomic DNA isolated from CD4<sup>+</sup> T cells from normal donor was used to amplify sjTREC and TRCAC sequencing using primers described in Table 8. Fragments were run on a 1.2% agarose gel and purified using Wizard SV Gel and PCR Clean-Up System (Promega, A9282). Fragments were cloned using Zero Blunt™ TOPO™ PCR Cloning Kit (Invitrogen, K280020) into vector pCR™Blunt II-TOPO® vector. Colonies were grown in LB Broth, Lennox (BD, 240230) with BD Bacto™ Dehydrated Agar (BD, DF0140-15-4) with 50ug/mL

Kanamycin (Gibco, 11815-032) and isolated with QIAGEN Plasmid Maxi kit (QIAGEN, 12163).

### *Q-PCR*

Real Time PCR amplification was carried out using Sybr Green on a 7500 Fast Real-Time PCR system (Applied Biosystem). The average of three independent analyses for gene and sample was calculated using the  $\Delta\Delta$  threshold cycle (Ct) method and TREC was normalized to the endogenous reference control gene TRCAC. Primers used for quantification are described in Table 9. Standard curves were generated from linearized pCR<sup>TM</sup>Blunt II-TOPO<sup>®</sup> vector with restriction enzyme XhoI (New England Biolabs, R0146S) and clean up with QIAquick<sup>®</sup> PCR Purification Kit (QIAGEN, 28106). Serial dilutions were performed in DEPC-treated Water (Thermo Scientific, R0601).

### *Study approval*

Study conformed to approvals granted by Moffitt's research regulatory committees, including IRB approvals MCC 50312, MCC 20403, MCC 19672 and MCC 20032. MCC 50312, MCC 20403, and MCC 20032 for Sézary syndrome and mycosis fungoides peripheral blood samples were acquired with informed written consent protocol MCC 14690. MCC 19672 for peripheral blood and skin biopsies were acquired with informed written consent protocol MCC 14690.

**Table 7. Summary of repeated overlapping mutations across SS patients**

Hugo Symbol	Patient 1		Patient 3		Patient 4		Patient 5	
<b>MAP6</b>			c.C1739T	p.P580L	c.C408A	p.S136R		
<b>PKD2</b>			c.C2384T	p.S795F	c.C2395T	p.P799S		
<b>UNC80*</b>			c.C5415T	p.S1805S			c.T7519A	p.C2507S
<b>TP53*</b>			+		c.G42A	p.W14X	c.262delT	p.Y88fs
<b>GLI2</b>			+				c.C1506T	p.P502P
<b>SCN2A</b>			+				c.G1492A	p.E498K
<b>TNK2*</b>	+						+	
<b>FBN1</b>			+				+	
<b>CATSPERE</b>			+		+			
<b>JPH3</b>			+		+			
<b>WDFY4</b>			+		+			
<b>RP1</b>					+		+	
<b>LAMA1</b>					+		+	
<b>CADPS</b>					+		+	
<b>ARID1A*</b>			c.C6382T	p.Q2128X				
<b>ARID1A*</b>			c.C6381T	p.I2127I				
<b>ARID1B*</b>					c.C2722T	p.P908S		

**Table 8. Primers for cloning of Human sjTREC and TCRA sequences**

Primer ID	Sequence
<b>TREC F</b>	5'-AAAGAGGGCAGCCCTCTCCAAGGC-3'
<b>TREC R</b>	5'-GGCTGATCTTGTCTGACATTTGC-3'
<b>TCRA- SpeI F</b>	5'-GACTAGTATGAGACCGTGACTTGCCAG-3'
<b>TCRA- SpeI R</b>	5'-GACTAGTGCTGTTGTTGAAGGCGTTTGC-3'

**Table 9. RT-qPCR primers for amplification of sjTRAC and TRCAC sequences**

Primer ID	Sequence
<b>TREC qPCR F</b>	5'-CACATCCCTTTCAACCATGCT-3'
<b>TREC qPCR R</b>	5'-TGCAGGTGCCTATGCATCA-3'
<b>TCRAC qPCR F</b>	5'-TGGCCTAACCTGATCCTCTT-3'
<b>TCRAC qPCR R</b>	5'-GGATTTAGAGTCTCTCAGCTGGTACAC-3'

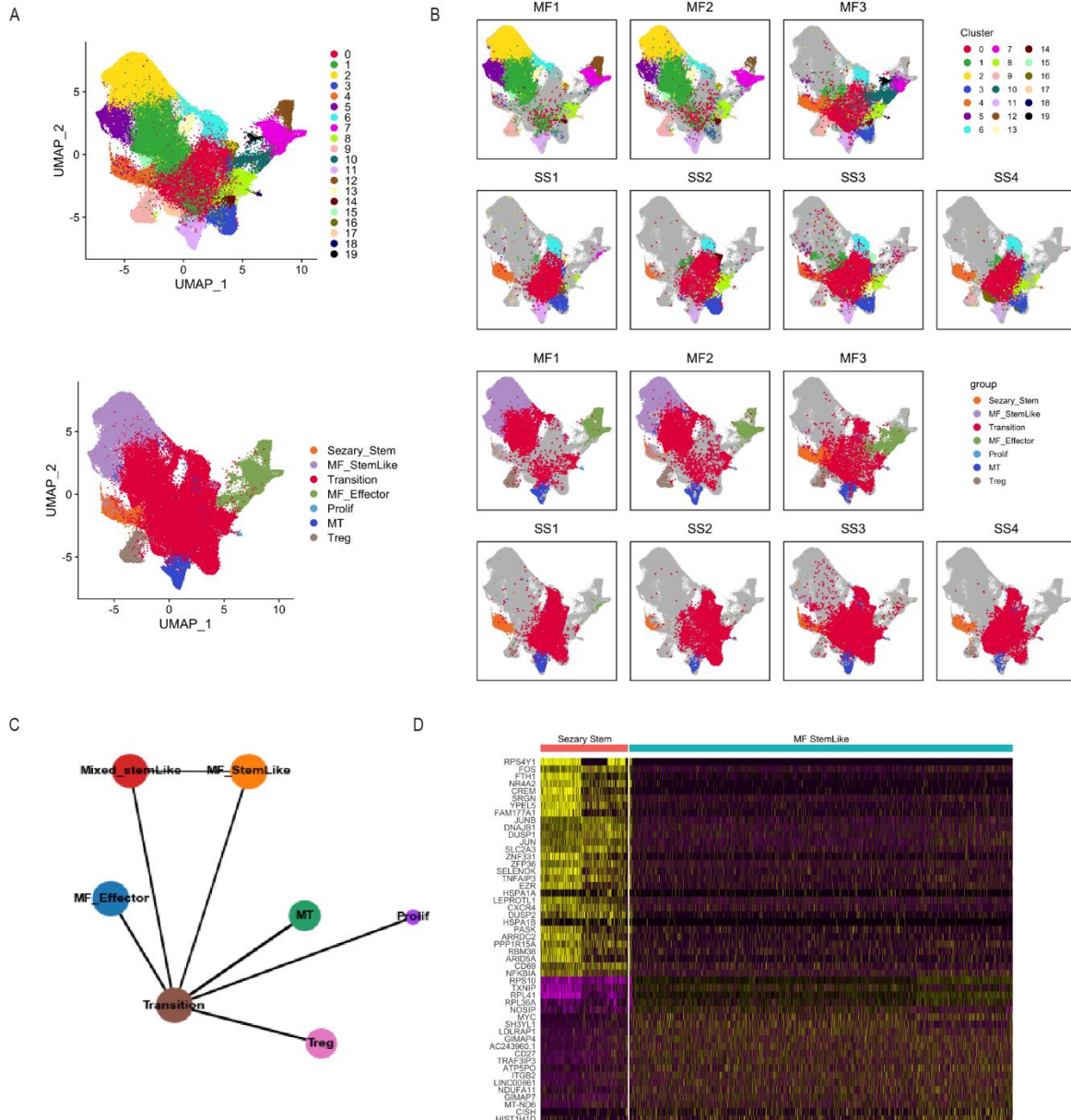
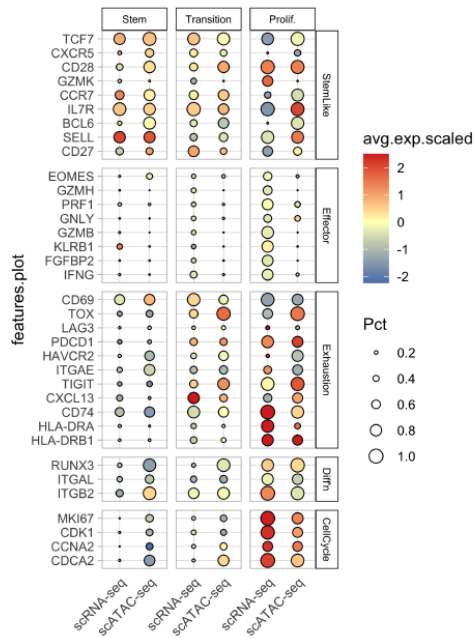


**Figure 20: Gene expression patterns in Sézary syndrome and Mycosis fungoides**

(A) UMAP of combined analysis of single cell RNA-seq from CD4<sup>+</sup>CD26<sup>-</sup> isolated T cells from peripheral blood of Sézary syndrome patients SS1-SS4 (n=4) and mycosis fungoides patients MF1-MF3 (n=3) by cluster (n=20) (above) and by group (n=7) (below). (B) UMAP plots of each individual sample and occupation of cells in each cluster (C) Connection analysis to estimate the relationship between groups with direct connects linked by solid lines. (D) Heat map of most significantly differentially expressed genes in the MF stem cell cluster and the SS stem cell cluster.

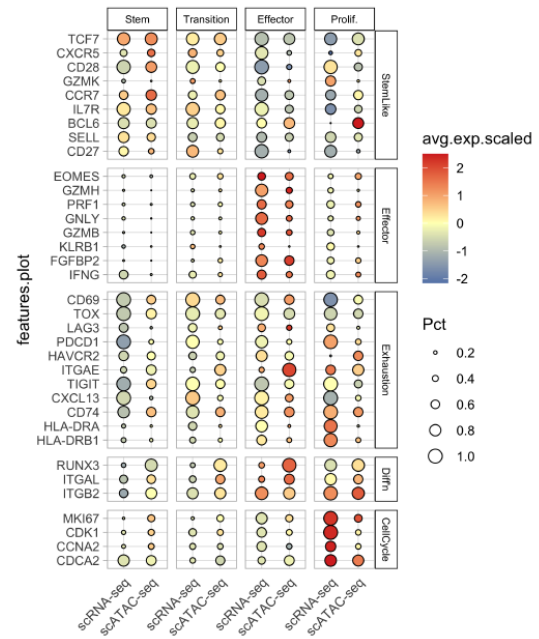
A

# Sezary

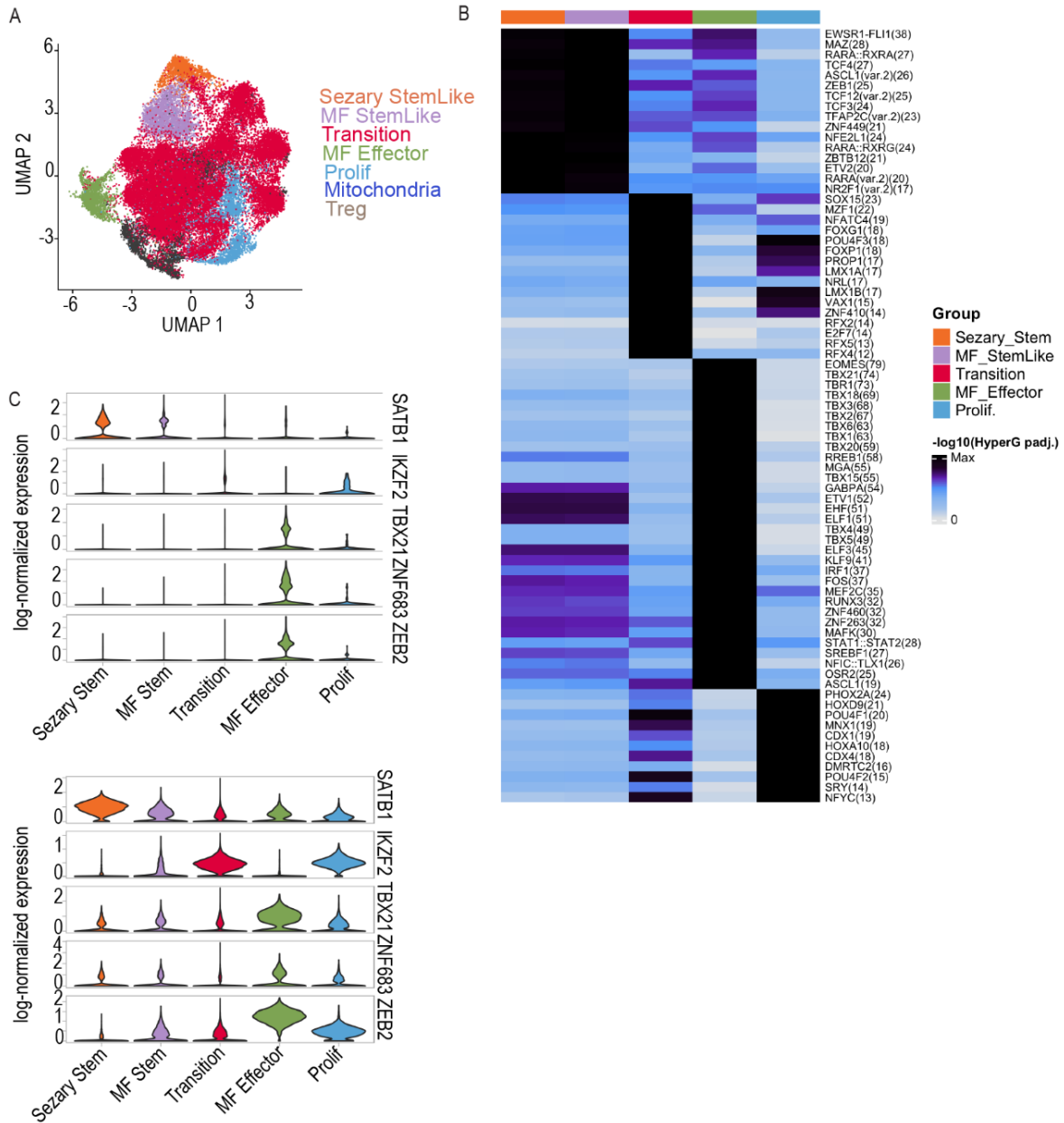


B

# MF

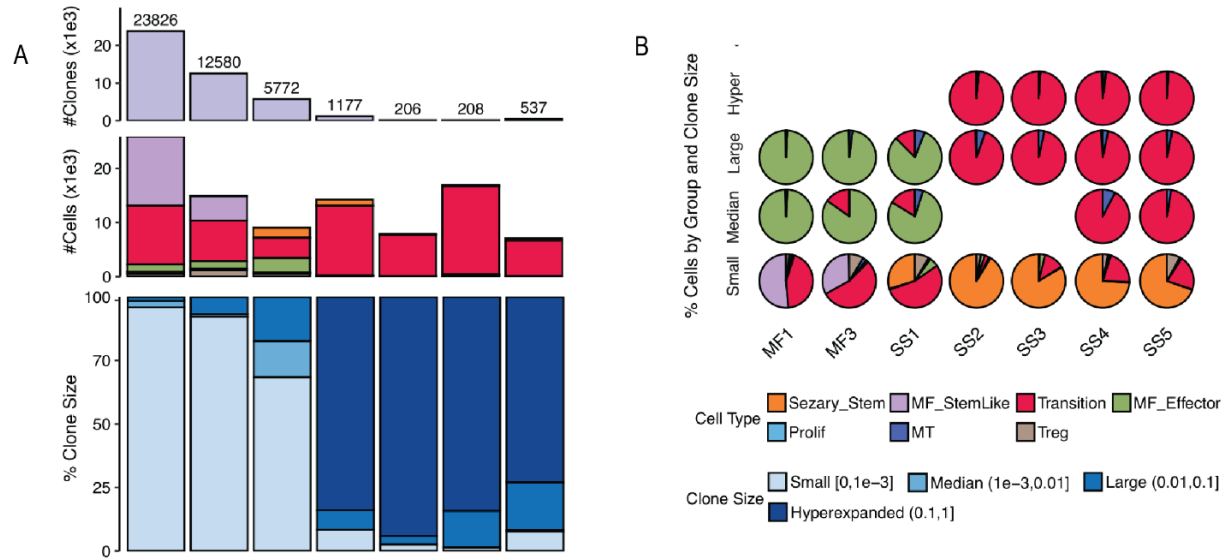


**Figure 21. Gene expression and open chromatin patterns in Sézary syndrome and Mycosis fungoides**  
 Bubble plot of single cell ATAC-seq open chromatin regions and single cell RNA-seq gene expression patterns across phenotypes (Stem-like, Effector, Exhaustion, Proliferation, Mitochondria, Cell Cycle, and Treg) in Sézary syndrome (A) and Mycosis fungoides (B).



**Figure 22: Chromatin conformation patterns in Sézary syndrome and Mycosis fungoides**

(A) UMAP plot of single cell ATAC-seq from CD4<sup>+</sup>CD26<sup>-</sup> isolated T cells from peripheral blood of Sézary syndrome patients SS1-SS4 (n=4) and mycosis fungoides patients MF3 (n=1) by group (n=6). (B) Heat map of predicted transcription factor binding sites based on open chromatin regions from SS1-SS4 and MF3. (C) Violin plots of notable CTCL genes in RNA-seq (above) and ATAC-seq (below) datasets by group.



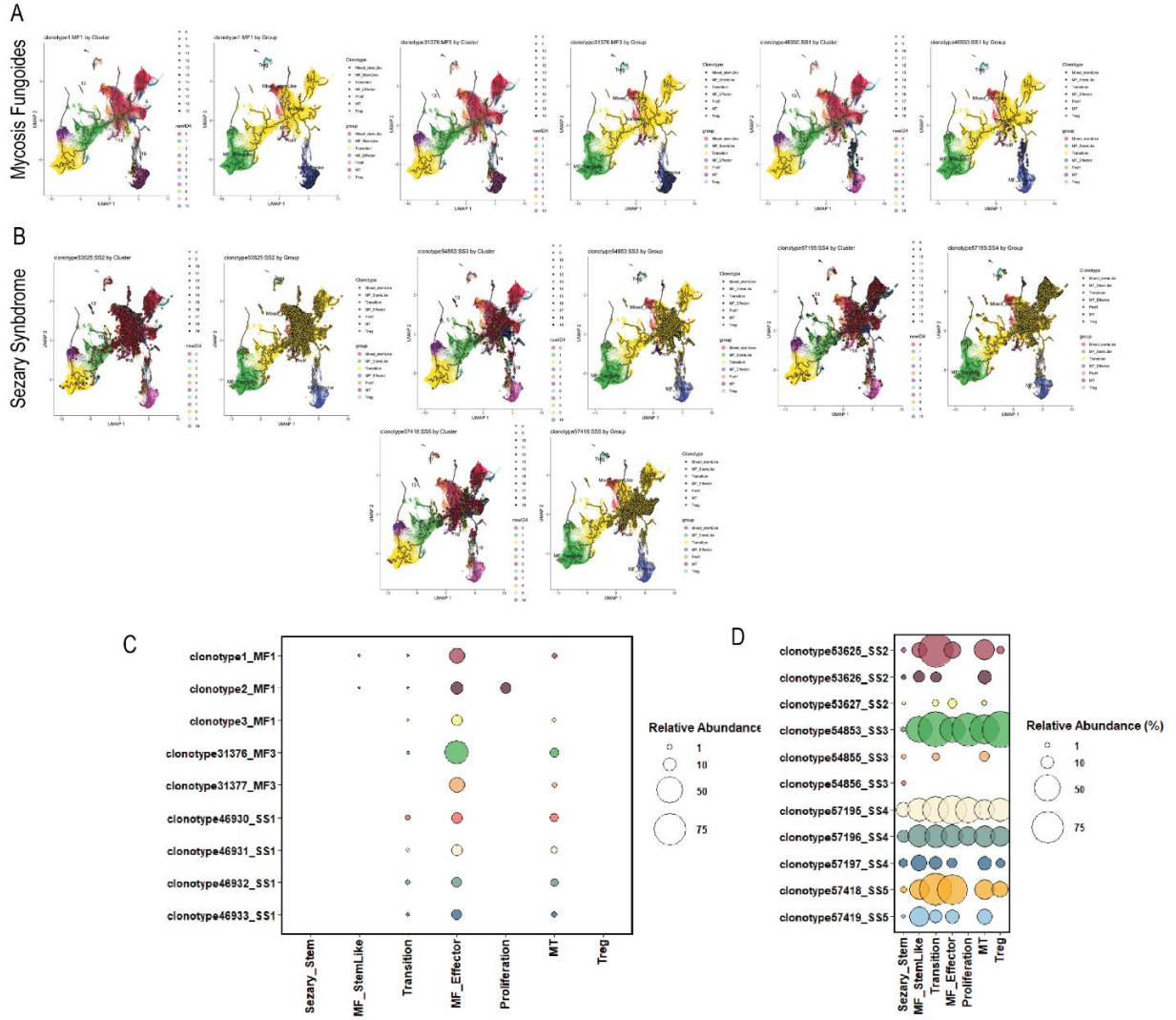


**Figure 24. Clonality distributed across distinct SS and MF groups**

UMAP representing the top clone for each sample and the distribution of the clone in each group in MF samples (A) and Sézary samples (B). Bubble plot of top clones in each sample measuring the abundance of each clonotype per group by adjusting for number of cells per group in MF (C) and SS (D).

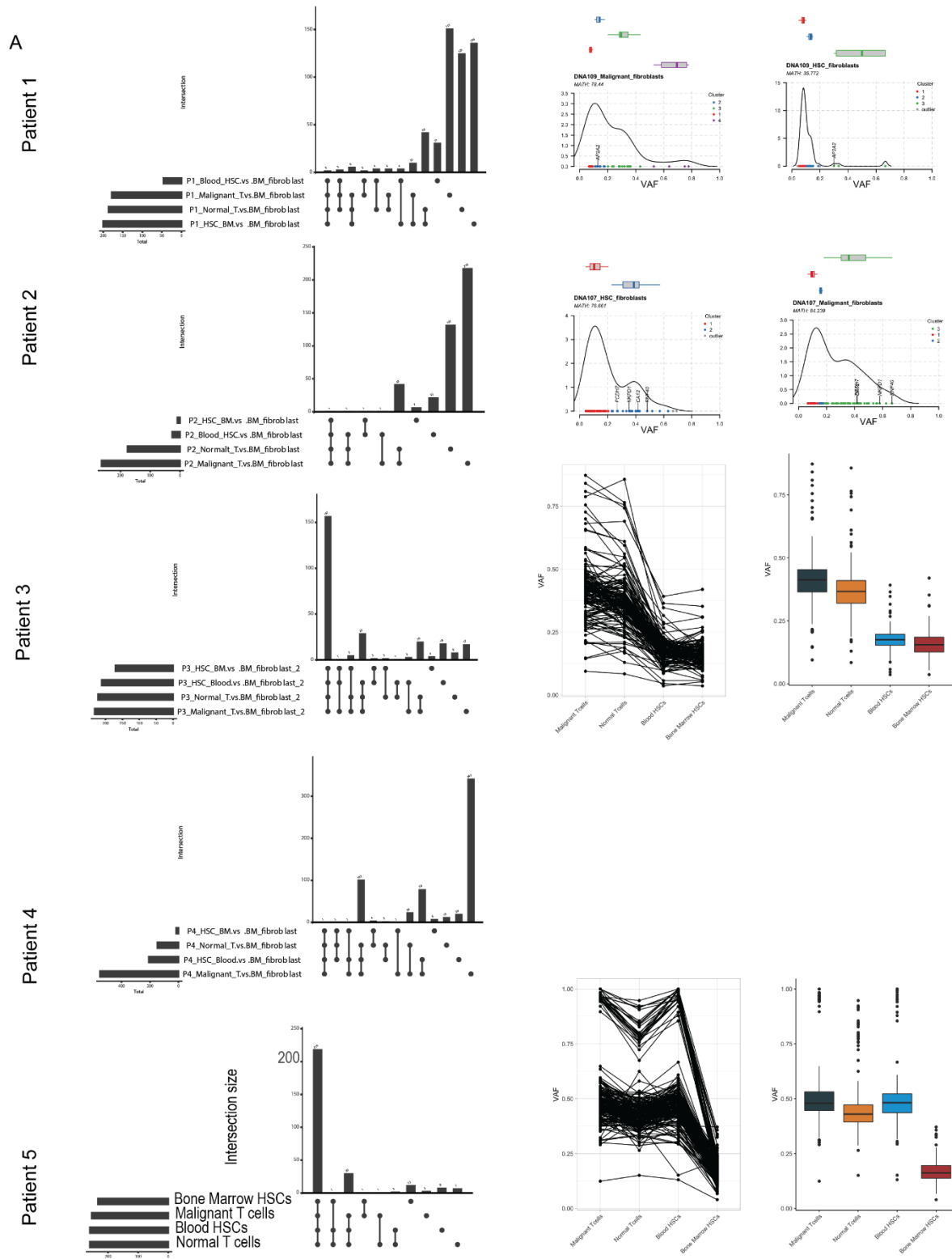


**Figure 25. Somatic mutations overlapping in hematopoietic stem cells and other cell compartments in Sézary syndrome**  
 Upset plot of overlapping mutations across bone marrow HSCs, blood HSCs, Malignant cells, and Normal T cells with corresponding box and whisker plots of VAFs of mutations overlapping between BM HSCs, Blood HSCs, and malignant T cells in patient 1 (A), patient 2 (B), patient 3 (C), patient 4 (D), and patient 5 (E).

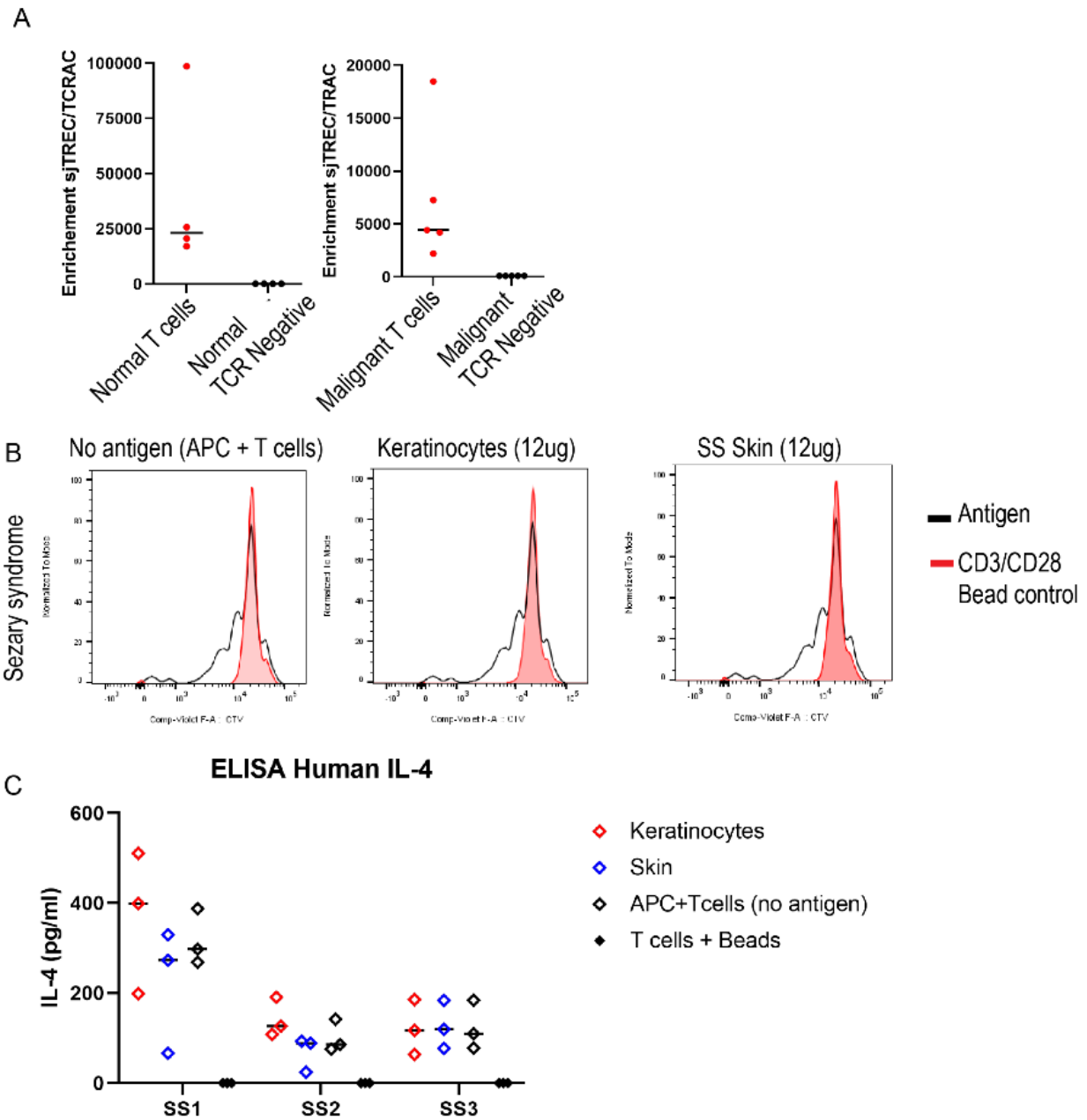


**Figure 26. Thymic egression of Sézary syndrome and Antigen presentation capacity in Sézary syndrome and Mycosis fungoides**

(A) Quantification of TREC via RT qPCR from peripheral blood of either normal donor T cells (n=4) or CD4<sup>+</sup>CD26<sup>-</sup>/CD7<sup>-</sup> malignant T cells (n=4) compared to sample matched TCR negative cells (n=4) using total DNA. (B) Cell Trace Violet quantification at day 7 post antigen pulsing of APCs with autologous Sézary peripheral blood CD4<sup>+</sup>CD26<sup>-</sup>/CD7<sup>-</sup> cells (n=3) against no antigen, keratinocyte lysate (12ug), or allogenic Sézary skin biopsy lysate (12ug). Positive control for proliferation was CD3/CD28 stimulated T cells. Representative of three independent experiments. (C) ELISA of supernatant from antigen presented cells for human IL-4 with a 1:1 dilution. Experiment was done in triplicate.

## CHAPTER FOUR: CONCLUSIONS AND FUTURE PERSPECTIVES

Rare cancers often are incurable with poor outcomes as well as disproportionately impact minority groups. The treatment of these rare and deadly cancers can be challenging; however, as the etiology of these disease are lacking. It is imperative to focus research efforts on the underlying mechanism of these rare cancers, accounting for approximately 20% of total cancer cases (197), to improve outcomes. In the case of CTCL, it is composed of many subgroups with biology which remains largely unknown. This body of work contributes to further understanding the unique biological signatures of two CTCL subtypes, mycosis fungoides and Sézary syndrome.

The initial aim focused on understanding the epigenetic underpinning of Sézary syndrome. It has been previously demonstrated that decreased expression of the molecule *SATB1* is associated with poor prognosis in CTCL, however, it had not been shown to functionally play a role in initiating the disease. The mouse models we developed are unique in CTCL by using conditional transgenic models which knocks out a critical chromatin modifier for T cell development and maturation. This approach is often utilized in other forms of leukemia such as AML, where the mutational drivers are well defined for the disease. However, this is not the case with CTCL where genetic drivers are still being characterized partly due to its heterogenous and rare nature.

The model that was developed simultaneously knocks out *Satb1* as well as activates another important leukemic gene, *Notch1*. The presence of both transgenes was critical to

develop the phenotype which partially recapitulates the clinical presentation of CTCL. *Notch1* activation alone impacted the overall survival of mice but did not exhibit the hallmarks of CTCL such as pSTAT5 increase and CCR4 expression. Considering the effects of Notch1, it would be useful to address whether the order of *Satb1* knock out and *Notch1* activation impacts the progression of the phenotype. Future studies which develop murine models that allow for different permutations of *Satb1* knock out and *Notch1* activation is required. It is vital that potential CTCL driver genes continue to be studied through murine models.

After modeling that *SATBI* plays a pivotal role in CTCL initiation, the next aim was to understand the mechanism behind its downregulation. Considering *SATBI* is not reported to be deleted in previous genomic studies, the next steps were to characterize the repressive epigenetic landscape near the *SATBI* promoter which has not been previously examined. It is possible other forms of gene repression, such as DNA methylation, also play a role in silencing important tumor suppressor; however, the focus of the study was on histone modification. CTCL has been successfully treated with iHDACs in a clinical setting; however, there are still patients who are unresponsive to these class of inhibitors warranting alternative therapeutic options. Here, alternative mechanisms of epigenetic regulation by histone methyltransferases were explored.

Prior to this work, the role of repressive histone methylation was not well examined in the context of Sézary syndrome. The trimethylation of H3K9 showed to play a critical role in the suppression of *SATBI* expression rather than H3K27. This methylation was reversible using a specific SUV39H1/2 inhibitor, F5446. However, F5446 had only been recently developed at the time of the study, which highlights the need for screening additional inhibitors of specific histone modifiers. Restoration of *SATBI* through these class of inhibitors abrogated cell proliferation and phosphorylation of STAT5 showing a potential targetable mechanism against CTCL. Future

studies can address how these histone methyltransferases become more active in Sézary cells and whether this is the result of gain of function mutations or another mechanism controlling chromatin modification. Additionally, more robust drug screening using histone methyltransferase inhibitors in other CTCL and PTCL subtypes might be beneficial in conjunction with iHDACs and other standard therapies.

It is a continually debated topic whether Sézary syndrome and mycosis fungoides are diseases derived from a separate origin. Mycosis fungoides is typically regarded as the earlier stage to Sézary syndrome; however, there are cases of Sézary being *de novo* without prior history of mycosis fungoides. Additionally, mycosis fungoides is characterized as an effector phenotype compared to Sézary syndrome with a central memory phenotype. It was necessary to further investigate the different origins of Sézary syndrome and mycosis fungoides.

The next aim sought to understand the hierarchy of cells by which CTCL develops through single cell analysis of Sézary and mycosis fungoides patients. Previous single cell studies have been conducted in SS and MF but have not explicitly compared the trajectory of differentiation between the two diseases within a single study. It was found that each disease processed its own pattern of differentiation and clonality. Sézary syndrome starts as a stem-like progenitor population which transitions into a proliferative phenotype, whereas mycosis fungoides shares a stem like population with Sézary as well as a process its own unique stem population which transitioned into effector T cells. In terms of TCR patterns, Sézary syndrome demonstrated few dominant clones while mycosis fungoides was very polyclonal. Additionally, the dominant clones in Sézary were present throughout differentiation while mycosis fungoides clones increase in the effector T cell phenotype. This evidence suggests that the origin of Sézary comes from mutated pre-thymic progenitors while mycosis fungoides was derived from antigen

recognition. This study was conducted on cells isolated from only peripheral blood which might exhibit different clonality patterns and TCR repertoire than cells residing in the skin. It has been previously reported that mycosis fungoides cells from skin samples show a more mono or oligo-clonal population that possibility react against skin antigens.

Mutations in pre-thymic progenitor cells from Sézary syndrome have not been previous characterized. CTCL unlike other leukemia or lymphomas does not have well defined genetic drivers apart from what has been described in other leukemia and lymphoma such as *TP53*, *DNMT3A*, and *TET2*. However, it is possible that there are unique genetic drivers which contribute to its heterogeneity which has not been reported. It is important to characterize these pre-thymic mutations to understand the how these cells initiate and subsequently acquire mutations post-thymic selection. This is often done for modeling other leukemia such as AML. Often, the literature claims Sézary and MF as diseases of mature T cells. While it is accurate that these cells display TCR $\alpha\beta$  on the cell surface, this does not exclude the possibility that specific mutated hematopoietic clones drive the disease. It is clear in our study that Sézary maintains stem-like abilities, a common feature in many cancers. Likely, the high mutational burden in the bone marrow of these patients is the consequence of DNA damaging. Future direction would be to perform functional studies *in vitro* and *in vivo* on mutations which are unique to Sézary syndrome which are shared by malignant peripheral lymphocytes and bone marrow progenitors. As previously stated, modeling the order in which mutations are acquired and their impact on disease progression, prognosis, and sensitivity to treatment will be crucial.

## REFERENCES

1. Siegel RL, Miller KD, and Jemal A. Cancer statistics, 2020. *CA: A Cancer Journal for Clinicians*. 2020;70(1):7-30.
2. Shankland KR, Armitage JO, and Hancock BW. Non-Hodgkin lymphoma. *Lancet (London, England)*. 2012;380(9844):848-57.
3. Roshal M, Wood BL, and Fromm JR. Flow cytometric detection of the classical hodgkin lymphoma: clinical and research applications. *Advances in hematology*. 2011;2011:387034.
4. Howlander N, Noone AM, Krapcho M, Garshell J, Miller D, Altekruse SF, et al. SEER cancer statistics review. *National Cancer Institute*. 1975;2008.
5. Surveillance E, and End Results (SEER) Program. 1992-2018.
6. Swerdlow SH, Campo E, Pileri SA, Harris NL, Stein H, Siebert R, et al. The 2016 revision of the World Health Organization classification of lymphoid neoplasms. *Blood*. 2016;127(20):2375-90.
7. Ansell SM. Non-Hodgkin Lymphoma: Diagnosis and Treatment. *Mayo Clinic proceedings*. 2015;90(8):1152-63.
8. Bradford PT, Devesa SS, Anderson WF, and Toro JR. Cutaneous lymphoma incidence patterns in the United States: a population-based study of 3884 cases. *Blood*. 2009;113(21):5064-73.
9. Imam MH, Shenoy PJ, Flowers CR, Phillips A, and Lechowicz MJ. Incidence and survival patterns of cutaneous T-cell lymphomas in the United States. *Leukemia & lymphoma*. 2013;54(4):752-9.
10. Sokolowska-Wojdylo M, Wenzel J, Gaffal E, Lenz J, Speuser P, Erdmann S, et al. Circulating clonal CLA(+) and CD4(+) T cells in Sezary syndrome express the skin-homing chemokine receptors CCR4 and CCR10 as well as the lymph node-homing chemokine receptor CCR7. *The British journal of dermatology*. 2005;152(2):258-64.
11. Campo E, Swerdlow SH, Harris NL, Pileri S, Stein H, and Jaffe ES. The 2008 WHO classification of lymphoid neoplasms and beyond: evolving concepts and practical applications. *Blood*. 2011;117(19):5019-32.
12. Martinez-Escala ME, Kantor RW, Cices A, Zhou XA, Kaplan JB, Pro B, et al. CD8+ mycosis fungoides: A low-grade lymphoproliferative disorder. *Journal of the American Academy of Dermatology*. 2017;77(3):489-96.
13. Ding X, Chen J, Kuai L, Xing M, Ru Y, Luo Y, et al. CD4/CD8 dual-positive mycosis fungoides: A case report and literature review. *Medicine*. 2020;99(42).
14. Miyashiro D, Torrealba MP, Manfrere KC, Pereira J, Sato MN, and Sanches JA. Double-positive CD4 and CD8 Sézary syndrome. *JAAD case reports*. 2017;3(6):485-8.
15. Olsen E, Vonderheid E, Pimpinelli N, Willemze R, Kim Y, Knobler R, et al. Revisions to the staging and classification of mycosis fungoides and Sezary syndrome: a proposal of the International Society for Cutaneous Lymphomas (ISCL) and the cutaneous lymphoma task force of the European Organization of Research and Treatment of Cancer (EORTC). *Blood*. 2007;110(6):1713-22.

16. Whittaker S, Hoppe R, and Prince HM. How I treat mycosis fungoides and Sézary syndrome. *Blood*. 2016;127(25):3142-53.
17. Willemze R, Jaffe ES, Burg G, Cerroni L, Berti E, Swerdlow SH, et al. WHO-EORTC classification for cutaneous lymphomas. *Blood*. 2005;105(10):3768-85.
18. Olsen EA, Whittaker S, Kim YH, Duvic M, Prince HM, Lessin SR, et al. Clinical end points and response criteria in mycosis fungoides and Sézary syndrome: a consensus statement of the International Society for Cutaneous Lymphomas, the United States Cutaneous Lymphoma Consortium, and the Cutaneous Lymphoma Task Force of the European Organisation for Research and Treatment of Cancer. *Journal of clinical oncology : official journal of the American Society of Clinical Oncology*. 2011;29(18):2598-607.
19. Goyal T, and Varshney A. A rare presentation of erythrodermic mycosis fungoides. *Cutis*. 2012;89(5):229-32, 36.
20. Kuo Y-H, and Chang C-H. Erythrodermic mycosis fungoides treated with low-dose methotrexate and 311 nm UV-B: A case report with 3-year follow up and literature review. *Dermatologica Sinica*. 2016;34(1):37-41.
21. Scarisbrick JJ, Hodak E, Bagot M, Stranzenbach R, Stadler R, Ortiz-Romero PL, et al. Blood classification and blood response criteria in mycosis fungoides and Sézary syndrome using flow cytometry: recommendations from the EORTC cutaneous lymphoma task force. *European journal of cancer (Oxford, England : 1990)*. 2018;93:47-56.
22. Morris L, Tran J, and Duvic M. Non-Classic Signs of Sézary Syndrome: A Review. *American Journal of Clinical Dermatology*. 2020;21(3):383-91.
23. Haftcheshmeh SM, Tajbakhsh A, Kazemi M, Esmaeili S-A, Mardani F, Fazeli M, et al. The clinical importance of CD4+CD7- in human diseases. *Journal of Cellular Physiology*. 2019;234(2):1179-89.
24. Rappl G, Abken H, Muche JM, Sterry W, Tilgen W, André S, et al. CD4+CD7- leukemic T cells from patients with Sézary syndrome are protected from galectin-1-triggered T cell death. *Leukemia*. 2002;16(5):840-5.
25. Valk PJ, Verhaak RG, Beijen MA, Erpelinck CA, Barjesteh van Waalwijk van Doorn-Khosrovani S, Boer JM, et al. Prognostically useful gene-expression profiles in acute myeloid leukemia. *The New England journal of medicine*. 2004;350(16):1617-28.
26. Röhrs S, Scherr M, Romani J, Zaborski M, Drexler HG, and Quentmeier H. CD7 in acute myeloid leukemia: correlation with loss of wild-type CEBPA, consequence of epigenetic regulation. *Journal of Hematology & Oncology*. 2010;3(1):15.
27. Lin LI, Chen CY, Lin DT, Tsay W, Tang JL, Yeh YC, et al. Characterization of CEBPA mutations in acute myeloid leukemia: most patients with CEBPA mutations have biallelic mutations and show a distinct immunophenotype of the leukemic cells. *Clinical cancer research : an official journal of the American Association for Cancer Research*. 2005;11(4):1372-9.
28. Kenny AJ, Booth AG, George SG, Ingram J, Kershaw D, Wood EJ, et al. Dipeptidyl peptidase IV, a kidney brush-border serine peptidase. *The Biochemical journal*. 1976;157(1):169-82.
29. Ohnuma K, Uchiyama M, Yamochi T, Nishibashi K, Hosono O, Takahashi N, et al. Caveolin-1 triggers T-cell activation via CD26 in association with CARMA1. *The Journal of biological chemistry*. 2007;282(13):10117-31.

30. Morimoto C, and Schlossman SF. The structure and function of CD26 in the T-cell immune response. *Immunological reviews*. 1998;161:55-70.
31. Cordero OJ, Yang CP, and Bell EB. On the role of CD26 in CD4 memory T cells. *Immunobiology*. 2007;212(2):85-94.
32. Introcaso CE, Hess SD, Kamoun M, Ubriani R, Gelfand JM, and Rook AH. Association of change in clinical status and change in the percentage of the CD4+CD26- lymphocyte population in patients with Sézary syndrome. *Journal of the American Academy of Dermatology*. 2005;53(3):428-34.
33. Lyapichev KA, Bah I, Huen A, Duvic M, Routbort MJ, Wang W, et al. Determination of immunophenotypic aberrancies provides better assessment of peripheral blood involvement by mycosis fungoides/Sézary syndrome than quantification of CD26- or CD7- CD4+ T-cells. *Cytometry Part B: Clinical Cytometry*. 2021;100(2):183-91.
34. Jones D, Dang NH, Duvic M, Washington LT, and Huh YO. Absence of CD26 expression is a useful marker for diagnosis of T-cell lymphoma in peripheral blood. *American journal of clinical pathology*. 2001;115(6):885-92.
35. Ferenczi K, Fuhlbrigge RC, Pinkus J, Pinkus GS, and Kupper TS. Increased CCR4 expression in cutaneous T cell lymphoma. *The Journal of investigative dermatology*. 2002;119(6):1405-10.
36. Shono Y, Suga H, Kamijo H, Fujii H, Oka T, Miyagaki T, et al. Expression of CCR3 and CCR4 Suggests a Poor Prognosis in Mycosis Fungoides and Sézary Syndrome. *Acta dermato-venereologica*. 2019;99(9):809-12.
37. Kallinich T, Muche JM, Qin S, Sterry W, Audring H, and Kroczeck RA. Chemokine receptor expression on neoplastic and reactive T cells in the skin at different stages of mycosis fungoides. *The Journal of investigative dermatology*. 2003;121(5):1045-52.
38. Panina-Bordignon P, Papi A, Mariani M, Di Lucia P, Casoni G, Bellettato C, et al. The C-C chemokine receptors CCR4 and CCR8 identify airway T cells of allergen-challenged atopic asthmatics. *J Clin Invest*. 2001;107(11):1357-64.
39. Matsuo K, Hatanaka S, Kimura Y, Hara Y, Nishiwaki K, Quan YS, et al. A CCR4 antagonist ameliorates atopic dermatitis-like skin lesions induced by dibutyl phthalate and a hydrogel patch containing ovalbumin. *Biomedicine & pharmacotherapy = Biomedecine & pharmacotherapie*. 2019;109:1437-44.
40. Anderson CA, Patel P, Viney JM, Phillips RM, Solari R, and Pease JE. A degradatory fate for CCR4 suggests a primary role in Th2 inflammation. *J Leukoc Biol*. 2020;107(3):455-66.
41. Horna P, Kurant D, Sokol L, Sotomayor EM, Moscinski L, and Glass LF. Flow cytometric identification of immunophenotypically aberrant T-cell clusters on skin shave biopsy specimens from patients with mycosis fungoides. *American journal of clinical pathology*. 2015;143(6):785-96.
42. Watanabe R, Gehad A, Yang C, Scott LL, Teague JE, Schlapbach C, et al. Human skin is protected by four functionally and phenotypically discrete populations of resident and recirculating memory T cells. *Science translational medicine*. 2015;7(279):279ra39.
43. Nicolay JP, Albrecht JD, Alberti-Violetti S, and Berti E. CCR4 in cutaneous T-cell lymphoma: Therapeutic targeting of a pathogenic driver. *European Journal of Immunology*. 2021;51(7):1660-71.

44. Kim EJ, Hess S, Richardson SK, Newton S, Showe LC, Benoit BM, et al. Immunopathogenesis and therapy of cutaneous T cell lymphoma. *J Clin Invest.* 2005;115(4):798-812.
45. Meyer CJ, van Leeuwen AW, van der Loo EM, van de Putte LB, and van Vloten WA. Cerebriform (Sézary like) mononuclear cells in healthy individuals: a morphologically distinct population of T cells. Relationship with mycosis fungoides and Sézary's syndrome. *Virchows Archiv B, Cell pathology.* 1977;25(2):95-104.
46. Carvalho J, Esteves A, Teixeira da Silva F, Couto J, and Ribeiro C. T-cell Prolymphocytic Leukemia, Cerebriform Variant. *Cureus.* 2021;13(2):e13299-e.
47. O'Briain DS, Lawlor E, Sarsfield P, Cooney C, Blaney CH, and Sullivan FJ. Circulating cerebriform lymphoid cells (Sézary-type cells) in a B-cell malignant lymphoma. *Cancer.* 1988;61(8):1587-93.
48. Pulitzer M, Myskowski PL, Horwitz SM, Querfeld C, Connolly B, Li J, et al. Mycosis fungoides with large cell transformation: clinicopathological features and prognostic factors. *Pathology.* 2014;46(7):610-6.
49. Arulogun SO, Prince HM, Ng J, Lade S, Ryan GF, Blewitt O, et al. Long-term outcomes of patients with advanced-stage cutaneous T-cell lymphoma and large cell transformation. *Blood.* 2008;112(8):3082-7.
50. Mehta-Shah N, Horwitz SM, Ansell S, Ai WZ, Barnes J, Barta SK, et al. NCCN Guidelines Insights: Primary Cutaneous Lymphomas, Version 2.2020: Featured Updates to the NCCN Guidelines. *Journal of the National Comprehensive Cancer Network J Natl Compr Canc Netw.* 2020;18(5):522-36.
51. Wright CW, Rumble JM, and Duckett CS. CD30 Activates Both the Canonical and Alternative NF- $\kappa$ B Pathways in Anaplastic Large Cell Lymphoma Cells <sup>\*</sup>. *Journal of Biological Chemistry.* 2007;282(14):10252-62.
52. Smith CA, Gruss HJ, Davis T, Anderson D, Farrar T, Baker E, et al. CD30 antigen, a marker for Hodgkin's lymphoma, is a receptor whose ligand defines an emerging family of cytokines with homology to TNF. *Cell.* 1993;73(7):1349-60.
53. Prince HM, Kim YH, Horwitz SM, Dummer R, Scarisbrick J, Quagliano P, et al. Brentuximab vedotin or physician's choice in CD30-positive cutaneous T-cell lymphoma (ALCANZA): an international, open-label, randomised, phase 3, multicentre trial. *Lancet (London, England).* 2017;390(10094):555-66.
54. Horwitz S, O'Connor OA, Pro B, Trümper L, Iyer S, Advani R, et al. The ECHELON-2 Trial: 5-year results of a randomized, phase III study of brentuximab vedotin with chemotherapy for CD30-positive peripheral T-cell lymphoma. *Annals of oncology : official journal of the European Society for Medical Oncology.* 2021.
55. Advani RH, Moskowitz AJ, Bartlett NL, Vose JM, Ramchandren R, Feldman TA, et al. Brentuximab vedotin in combination with nivolumab in relapsed or refractory Hodgkin lymphoma: 3-year study results. *Blood.* 2021;138(6):427-38.
56. Kuruvilla J, Ramchandren R, Santoro A, Paszkiewicz-Kozik E, Gasiorowski R, Johnson NA, et al. Pembrolizumab versus brentuximab vedotin in relapsed or refractory classical Hodgkin lymphoma (KEYNOTE-204): an interim analysis of a multicentre, randomised, open-label, phase 3 study. *The Lancet Oncology.* 2021;22(4):512-24.
57. Straus DJ, Długosz-Danecka M, Alekseev S, Illés Á, Picardi M, Lech-Maranda E, et al. Brentuximab vedotin with chemotherapy for stage III/IV classical Hodgkin lymphoma: 3-year update of the ECHELON-1 study. *Blood.* 2020;135(10):735-42.

58. Zhang P, and Zhang M. Epigenetics in the Pathogenesis and Treatment of Cutaneous T-Cell Lymphoma. *Frontiers in Oncology*. 2021;11:663961.
59. Chessum N, Jones K, Pasqua E, and Tucker M. In: Lawton G, and Witty DR eds. *Progress in Medicinal Chemistry*. Elsevier; 2015:1-63.
60. El Tawdy A, Amin I, Abdel Hay R, Rashed L, and Gad Z. Assessment of Tissue Level of Histone Deacetylase-2 (HDAC-2) in Patients With Mycosis Fungoides. *Journal of Cutaneous Medicine and Surgery*. 2015;20(1):40-3.
61. Marquard L, Gjerdrum LM, Christensen IJ, Jensen PB, Sehested M, and Ralfkiaer E. Prognostic significance of the therapeutic targets histone deacetylase 1, 2, 6 and acetylated histone H4 in cutaneous T-cell lymphoma. *Histopathology*. 2008;53(3):267-77.
62. Bobrowicz M, Slusarczyk A, Domagala J, Dwojak M, Ignatova D, Chang YT, et al. Selective inhibition of HDAC6 sensitizes cutaneous T-cell lymphoma to PI3K inhibitors. *Oncol Lett*. 2020;20(1):533-40.
63. Tachibana M, Sugimoto K, Fukushima T, and Shinkai Y. Set domain-containing protein, G9a, is a novel lysine-preferring mammalian histone methyltransferase with hyperactivity and specific selectivity to lysines 9 and 27 of histone H3. *The Journal of biological chemistry*. 2001;276(27):25309-17.
64. Rea S, Eisenhaber F, O'Carroll D, Strahl BD, Sun ZW, Schmid M, et al. Regulation of chromatin structure by site-specific histone H3 methyltransferases. *Nature*. 2000;406(6796):593-9.
65. Greiner D, Bonaldi T, Eskeland R, Roemer E, and Imhof A. Identification of a specific inhibitor of the histone methyltransferase SU(VAR)3-9. *Nature chemical biology*. 2005;1(3):143-5.
66. Goyama S, Nitta E, Yoshino T, Kako S, Watanabe-Okochi N, Shimabe M, et al. EVI-1 interacts with histone methyltransferases SUV39H1 and G9a for transcriptional repression and bone marrow immortalization. *Leukemia*. 2010;24(1):81-8.
67. Lai YS, Chen JY, Tsai HJ, Chen TY, and Hung WC. The SUV39H1 inhibitor chaetocin induces differentiation and shows synergistic cytotoxicity with other epigenetic drugs in acute myeloid leukemia cells. *Blood cancer journal*. 2015;5(5):e313.
68. Chaib H, Nebbioso A, Prebet T, Castellano R, Garbit S, Restouin A, et al. Anti-leukemia activity of chaetocin via death receptor-dependent apoptosis and dual modulation of the histone methyl-transferase SUV39H1. *Leukemia*. 2012;26(4):662-74.
69. Paschall AV, Yang D, Lu C, Choi JH, Li X, Liu F, et al. H3K9 Trimethylation Silences Fas Expression To Confer Colon Carcinoma Immune Escape and 5-Fluorouracil Chemoresistance. *Journal of immunology (Baltimore, Md : 1950)*. 2015;195(4):1868-82.
70. Cherblanc FL, Chapman KL, Reid J, Borg AJ, Sundriyal S, Alcazar-Fuoli L, et al. On the histone lysine methyltransferase activity of fungal metabolite chaetocin. *Journal of medicinal chemistry*. 2013;56(21):8616-25.
71. Lu C, Klement JD, Yang D, Albers T, Lebedyeva IO, Waller JL, et al. SUV39H1 regulates human colon carcinoma apoptosis and cell cycle to promote tumor growth. *Cancer letters*. 2020;476:87-96.
72. Lu C, Yang D, Klement JD, Oh IK, Savage NM, Waller JL, et al. SUV39H1 represses the expression of cytotoxic T-lymphocyte effector genes to promote colon tumor immune evasion. *Cancer Immunol Res*. 2019.

73. Trautinger F, Eder J, Assaf C, Bagot M, Cozzio A, Dummer R, et al. European Organisation for Research and Treatment of Cancer consensus recommendations for the treatment of mycosis fungoides/Sézary syndrome - Update 2017. *European journal of cancer (Oxford, England : 1990)*. 2017;77:57-74.
74. Olsen EA, Hodak E, Anderson T, Carter JB, Henderson M, Cooper K, et al. Guidelines for phototherapy of mycosis fungoides and Sézary syndrome: A consensus statement of the United States Cutaneous Lymphoma Consortium. *Journal of the American Academy of Dermatology*. 2016;74(1):27-58.
75. Zackheim HS, Kashani-Sabet M, and Amin S. Topical Corticosteroids for Mycosis Fungoides: Experience in 79 Patients. *Archives of Dermatology*. 1998;134(8):949-54.
76. Abbott RA, Whittaker SJ, Morris SL, Russell-Jones R, Hung T, Bashir SJ, et al. Bexarotene therapy for mycosis fungoides and Sézary syndrome. *The British journal of dermatology*. 2009;160(6):1299-307.
77. Duvic M, Martin AG, Kim Y, Olsen E, Wood GS, Crowley CA, et al. Phase 2 and 3 clinical trial of oral bexarotene (Targretin capsules) for the treatment of refractory or persistent early-stage cutaneous T-cell lymphoma. *Arch Dermatol*. 2001;137(5):581-93.
78. Jumbou O, N'Guyen JM, Tessier MH, Legoux B, and Dréno B. Long-term follow-up in 51 patients with mycosis fungoides and Sézary syndrome treated by interferon-alfa. *The British journal of dermatology*. 1999;140(3):427-31.
79. Bunn PA, Jr., Ihde DC, and Foon KA. The role of recombinant interferon alfa-2a in the therapy of cutaneous T-cell lymphomas. *Cancer*. 1986;57(8 Suppl):1689-95.
80. Kelly WK, O'Connor OA, Krug LM, Chiao JH, Heaney M, Curley T, et al. Phase I study of an oral histone deacetylase inhibitor, suberoylanilide hydroxamic acid, in patients with advanced cancer. *Journal of clinical oncology : official journal of the American Society of Clinical Oncology*. 2005;23(17):3923-31.
81. Mann BS, Johnson JR, Cohen MH, Justice R, and Pazdur R. FDA approval summary: vorinostat for treatment of advanced primary cutaneous T-cell lymphoma. *The oncologist*. 2007;12(10):1247-52.
82. Olsen EA, Kim YH, Kuzel TM, Pacheco TR, Foss FM, Parker S, et al. Phase IIB Multicenter Trial of Vorinostat in Patients With Persistent, Progressive, or Treatment Refractory Cutaneous T-Cell Lymphoma. *Journal of Clinical Oncology*. 2007;25(21):3109-15.
83. Piekarczyk RL, Frye R, Turner M, Wright JJ, Allen SL, Kirschbaum MH, et al. Phase II Multi-Institutional Trial of the Histone Deacetylase Inhibitor Romidepsin As Monotherapy for Patients With Cutaneous T-Cell Lymphoma. *Journal of Clinical Oncology*. 2009;27(32):5410-7.
84. Edelson R, Berger C, Gasparro F, Jegasothy B, Heald P, Wintroub B, et al. Treatment of cutaneous T-cell lymphoma by extracorporeal photochemotherapy. Preliminary results. *The New England journal of medicine*. 1987;316(6):297-303.
85. Legitimo A, Consolini R, Failli A, Fabiano S, Bencivelli W, Scatena F, et al. In vitro treatment of monocytes with 8-methoxypsoralen and ultraviolet A light induces dendritic cells with a tolerogenic phenotype. *Clinical and experimental immunology*. 2007;148(3):564-72.
86. Herrmann JJ, Roenigk HH, Jr., Hurria A, Kuzel TM, Samuelson E, Rademaker AW, et al. Treatment of mycosis fungoides with photochemotherapy (PUVA): long-term follow-up. *Journal of the American Academy of Dermatology*. 1995;33(2 Pt 1):234-42.

87. Geskin L. ECP versus PUVA for the treatment of cutaneous T-cell lymphoma. *Skin therapy letter*. 2007;12(5):1-4.
88. Mann BS, Johnson JR, He K, Sridhara R, Abraham S, Booth BP, et al. Vorinostat for Treatment of Cutaneous Manifestations of Advanced Primary Cutaneous T-Cell Lymphoma. *Clinical Cancer Research*. 2007;13(8):2318.
89. Amengual JE, Lichtenstein R, Lue J, Sawas A, Deng C, Lichtenstein E, et al. A phase 1 study of romidepsin and pralatrexate reveals marked activity in relapsed and refractory T-cell lymphoma. *Blood*. 2018;131(4):397-407.
90. Kim YH, Bagot M, Pinter-Brown L, Rook AH, Porcu P, Horwitz SM, et al. Mogamulizumab versus vorinostat in previously treated cutaneous T-cell lymphoma (MAVORIC): an international, open-label, randomised, controlled phase 3 trial. *Lancet Oncol*. 2018;19(9):1192-204.
91. Ishida T, Ito A, Sato F, Kusumoto S, Iida S, Inagaki H, et al. Stevens-Johnson Syndrome associated with mogamulizumab treatment of adult T-cell leukemia / lymphoma. *Cancer Sci*. 2013;104(5):647-50.
92. Fuji S, Inoue Y, Utsunomiya A, Moriuchi Y, Uchimaru K, Choi I, et al. Pretransplantation Anti-CCR4 Antibody Mogamulizumab Against Adult T-Cell Leukemia/Lymphoma Is Associated With Significantly Increased Risks of Severe and Corticosteroid-Refractory Graft-Versus-Host Disease, Nonrelapse Mortality, and Overall Mortality. *Journal of clinical oncology : official journal of the American Society of Clinical Oncology*. 2016;34(28):3426-33.
93. Dai J, Almazan TH, Hong EK, Khodadoust MS, Arai S, Weng W-K, et al. Potential Association of Anti-CCR4 Antibody Mogamulizumab and Graft-vs-Host Disease in Patients With Mycosis Fungoides and Sézary Syndrome. *JAMA Dermatology*. 2018;154(6):728-30.
94. Netchiporouk E, Gantchev J, Tsang M, Thibault P, Watters AK, Hughes JM, et al. Analysis of CTCL cell lines reveals important differences between mycosis fungoides/Sézary syndrome vs. HTLV-1(+) leukemic cell lines. *Oncotarget*. 2017;8(56):95981-98.
95. Woetmann A, Lovato P, Eriksen KW, Krejsgaard T, Labuda T, Zhang Q, et al. Nonmalignant T cells stimulate growth of T-cell lymphoma cells in the presence of bacterial toxins. *Blood*. 2007;109(8):3325-32.
96. Starkebaum G, Loughran TP, Jr., Waters CA, and Ruscetti FW. Establishment of an IL-2 independent, human T-cell line possessing only the p70 IL-2 receptor. *International journal of cancer*. 1991;49(2):246-53.
97. O'Connell MA, Cleere R, Long A, O'Neill LA, and Kelleher D. Cellular proliferation and activation of NF kappa B are induced by autocrine production of tumor necrosis factor alpha in the human T lymphoma line HuT 78. *The Journal of biological chemistry*. 1995;270(13):7399-404.
98. Mann DL, O'Brien SJ, Gilbert DA, Reid Y, Popovic M, Read-Connole E, et al. Origin of the HIV-susceptible human CD4+ cell line H9. *AIDS research and human retroviruses*. 1989;5(3):253-5.
99. Abrams JT, Lessin S, Ghosh SK, Ju W, Vonderheid EC, Nowell P, et al. A clonal CD4-positive T-cell line established from the blood of a patient with Sézary syndrome. *The Journal of investigative dermatology*. 1991;96(1):31-7.

100. Kaltoft K, Bisballe S, Rasmussen HF, Thestrup-Pedersen K, Thomsen K, and Sterry W. A continuous T-cell line from a patient with Sézary syndrome. *Archives of dermatological research*. 1987;279(5):293-8.
101. Doeing DC, Borowicz JL, and Crockett ET. Gender dimorphism in differential peripheral blood leukocyte counts in mice using cardiac, tail, foot, and saphenous vein puncture methods. *BMC clinical pathology*. 2003;3(1):3.
102. Kohnken R, Porcu P, and Mishra A. Overview of the Use of Murine Models in Leukemia and Lymphoma Research. *Frontiers in Oncology*. 2017;7:22.
103. Charley MR, Tharp M, Locker J, Deng JS, Goslen JB, Mauro T, et al. Establishment of a human cutaneous T-cell lymphoma in C.B-17 SCID mice. *The Journal of investigative dermatology*. 1990;94(3):381-4.
104. Thaler S, Burger AM, Schulz T, Brill B, Bittner A, Oberholzer PA, et al. Establishment of a mouse xenograft model for mycosis fungoides. *Experimental dermatology*. 2004;13(7):406-12.
105. van der Fits L, Rebel HG, Out-Luiting JJ, Pouw SM, Smit F, Vermeer KG, et al. A novel mouse model for Sézary syndrome using xenotransplantation of Sézary cells into immunodeficient RAG2(-/-)  $\gamma$ c(-/-) mice. *Experimental dermatology*. 2012;21(9):706-9.
106. Krejsgaard T, Kopp K, Ralfkiaer E, Willumsgaard AE, Eriksen KW, Labuda T, et al. A novel xenograft model of cutaneous T-cell lymphoma. *Experimental dermatology*. 2010;19(12):1096-102.
107. Andrique L, Poglio S, Prochazkova-Carlotti M, Kadin ME, Giese A, Idrissi Y, et al. Intrahepatic Xenograft of Cutaneous T-Cell Lymphoma Cell Lines: A Useful Model for Rapid Biological and Therapeutic Evaluation. *The American journal of pathology*. 2016;186(7):1775-85.
108. Mishra A, La Perle K, Kwiatkowski S, Sullivan LA, Sams GH, Johns J, et al. Mechanism, Consequences, and Therapeutic Targeting of Abnormal IL15 Signaling in Cutaneous T-cell Lymphoma. *Cancer Discov*. 2016;6(9):986-1005.
109. Marks-Konczalik J, Dubois S, Losi JM, Sabzevari H, Yamada N, Feigenbaum L, et al. IL-2-induced activation-induced cell death is inhibited in IL-15 transgenic mice. *Proceedings of the National Academy of Sciences of the United States of America*. 2000;97(21):11445-50.
110. Cornejo MG, Kharas MG, Werneck MB, Le Bras S, Moore SA, Ball B, et al. Constitutive JAK3 activation induces lymphoproliferative syndromes in murine bone marrow transplantation models. *Blood*. 2009;113(12):2746-54.
111. Beltran BE, Castro D, De La Cruz-Vargas JA, Cotrina E, Gallo A, Sotomayor EM, et al. The neutrophil-lymphocyte ratio is prognostic in patients with early stage aggressive peripheral T cell lymphoma. *British journal of haematology*. 2019;184(4):650-3.
112. Rodd AL, Ververis K, and Karagiannis TC. Current and Emerging Therapeutics for Cutaneous T-Cell Lymphoma: Histone Deacetylase Inhibitors. *Lymphoma*. 2012;2012:10.
113. Kamstrup MR, Gjerdrum LM, Biskup E, Lauenborg BT, Ralfkiaer E, Woetmann A, et al. Notch1 as a potential therapeutic target in cutaneous T-cell lymphoma. *Blood*. 2010;116(14):2504-12.
114. da Silva Almeida AC, Abate F, Khiabani H, Martinez-Escala E, Guitart J, Tensen CP, et al. The mutational landscape of cutaneous T cell lymphoma and Sézary syndrome. *Nature genetics*. 2015;47(12):1465-70.

115. Naik R, and Galande S. SATB family chromatin organizers as master regulators of tumor progression. *Oncogene*. 2018.
116. Tesone AJ, Rutkowski MR, Brencicova E, Svoronos N, Perales-Puchalt A, Stephen TL, et al. Satb1 Overexpression Drives Tumor-Promoting Activities in Cancer-Associated Dendritic Cells. *Cell Rep*. 2016;14(7):1774-86.
117. Ma Y, Walsh MJ, Bernhardt K, Ashbaugh CW, Trudeau SJ, Ashbaugh IY, et al. CRISPR/Cas9 Screens Reveal Epstein-Barr Virus-Transformed B Cell Host Dependency Factors. *Cell Host & Microbe*. 2017;21(5):580-91.e7.
118. Kitagawa Y, Ohkura N, Kidani Y, Vandenbon A, Hirota K, Kawakami R, et al. Guidance of regulatory T cell development by Satb1-dependent super-enhancer establishment. *Nat Immunol*. 2017;18(2):173-83.
119. Borghesi L. Hematopoiesis in steady-state versus stress: self-renewal, lineage fate choice, and the conversion of danger signals into cytokine signals in hematopoietic stem cells. *J Immunol*. 2014;193(5):2053-8.
120. Fredholm S, Willerslev-Olsen A, Met O, Kubat L, Glud M, Mathiasen SL, et al. Special AT rich-binding1 protein (SATB1) in malignant T cells. *J Invest Dermatol*. 2018.
121. Murtaugh LC, Stanger BZ, Kwan KM, and Melton DA. Notch signaling controls multiple steps of pancreatic differentiation. *Proc Natl Acad Sci U S A*. 2003;100(25):14920-5.
122. Vinay DS, and Kwon BS. CD11c+CD8+ T cells: two-faced adaptive immune regulators. *Cell Immunol*. 2010;264(1):18-22.
123. Seo SK, Choi JH, Kim YH, Kang WJ, Park HY, Suh JH, et al. 4-1BB-mediated immunotherapy of rheumatoid arthritis. *Nat Med*. 2004;10(10):1088-94.
124. Payne KK, Mine JA, Biswas S, Chaurio RA, Perales-Puchalt A, Anadon CM, et al. BTN3A1 governs antitumor responses by coordinating  $\alpha\beta$  and  $\gamma\delta$  T cells. *Science*. 2020;369(6506):942-9.
125. Aghajani K, Keerthivasan S, Yu Y, and Gounari F. Generation of CD4CreER(T(2)) transgenic mice to study development of peripheral CD4-T-cells. *Genesis*. 2012;50(12):908-13.
126. Campbell JJ, Clark RA, Watanabe R, and Kupper TS. Sezary syndrome and mycosis fungoides arise from distinct T-cell subsets: a biologic rationale for their distinct clinical behaviors. *Blood*. 2010;116(5):767-71.
127. Duvic M, Pinter-Brown LC, Foss FM, Sokol L, Jorgensen JL, Challagundla P, et al. Phase 1/2 study of mogamulizumab, a defucosylated anti-CCR4 antibody, in previously treated patients with cutaneous T-cell lymphoma. *Blood*. 2015;125(12):1883-9.
128. Mindur JE, Ito N, Dhib-Jalbut S, and Ito K. Early treatment with anti-VLA-4 mAb can prevent the infiltration and/or development of pathogenic CD11b+CD4+ T cells in the CNS during progressive EAE. *PLoS One*. 2014;9(6):e99068.
129. Wang Y, Su M, Zhou LL, Tu P, Zhang X, Jiang X, et al. Deficiency of SATB1 expression in Sezary cells causes apoptosis resistance by regulating FasL/CD95L transcription. *Blood*. 2011;117(14):3826-35.
130. Jones PA, and Baylin SB. The epigenomics of cancer. *Cell*. 2007;128(4):683-92.
131. Becker JS, Nicetto D, and Zaret KS. H3K9me3-Dependent Heterochromatin: Barrier to Cell Fate Changes. *Trends Genet*. 2016;32(1):29-41.
132. Bennett RL, and Licht JD. Targeting Epigenetics in Cancer. *Annu Rev Pharmacol Toxicol*. 2018;58:187-207.

133. Collins PL, Kyle KE, Egawa T, Shinkai Y, and Oltz EM. The histone methyltransferase SETDB1 represses endogenous and exogenous retroviruses in B lymphocytes. *Proc Natl Acad Sci U S A*. 2015;112(27):8367-72.
134. Kim YH, Bagot M, Pinter-Brown L, Rook AH, Porcu P, Horwitz SM, et al. Mogamulizumab versus vorinostat in previously treated cutaneous T-cell lymphoma (MAVORIC): an international, open-label, randomised, controlled phase 3 trial. *Lancet Oncol*. 2018;19(9):1192-204.
135. Cai S, Lee CC, and Kohwi-Shigematsu T. SATB1 packages densely looped, transcriptionally active chromatin for coordinated expression of cytokine genes. *Nat Genet*. 2006;38(11):1278-88.
136. Yasui D, Miyano M, Cai S, Varga-Weisz P, and Kohwi-Shigematsu T. SATB1 targets chromatin remodelling to regulate genes over long distances. *Nature*. 2002;419(6907):641-5.
137. Zhang Q, Nowak I, Vonderheid EC, Rook AH, Kadin ME, Nowell PC, et al. Activation of Jak/STAT proteins involved in signal transduction pathway mediated by receptor for interleukin 2 in malignant T lymphocytes derived from cutaneous anaplastic large T-cell lymphoma and Sezary syndrome. *Proc Natl Acad Sci U S A*. 1996;93(17):9148-53.
138. Grzanka D, Gagat M, Izdebska M, and Marszalek A. Expression of special AT-rich sequence-binding protein 1 is an independent prognostic factor in cutaneous T-cell lymphoma. *Oncol Rep*. 2015;33(1):250-66.
139. Dobin A, Davis CA, Schlesinger F, Drenkow J, Zaleski C, Jha S, et al. STAR: ultrafast universal RNA-seq aligner. *Bioinformatics (Oxford, England)*. 2013;29(1):15-21.
140. Anders S, Pyl PT, and Huber W. HTSeq--a Python framework to work with high-throughput sequencing data. *Bioinformatics (Oxford, England)*. 2015;31(2):166-9.
141. Love MI, Huber W, and Anders S. Moderated estimation of fold change and dispersion for RNA-seq data with DESeq2. *Genome biology*. 2014;15(12):550.
142. Subramanian A, Tamayo P, Mootha VK, Mukherjee S, Ebert BL, Gillette MA, et al. Gene set enrichment analysis: a knowledge-based approach for interpreting genome-wide expression profiles. *Proceedings of the National Academy of Sciences of the United States of America*. 2005;102(43):15545-50.
143. Ashburner M, Ball CA, Blake JA, Botstein D, Butler H, Cherry JM, et al. Gene ontology: tool for the unification of biology. The Gene Ontology Consortium. *Nature genetics*. 2000;25(1):25-9.
144. Langmead B, and Salzberg SL. Fast gapped-read alignment with Bowtie 2. *Nature methods*. 2012;9(4):357-9.
145. Martin M. Cutadapt removes adapter sequences from high-throughput sequencing reads. *2011*. 2011;17(1):3.
146. Zhang Y, Liu T, Meyer CA, Eeckhoute J, Johnson DS, Bernstein BE, et al. Model-based analysis of ChIP-Seq (MACS). *Genome biology*. 2008;9(9):R137.
147. Yu G, Wang LG, and He QY. CHIPseeker: an R/Bioconductor package for ChIP peak annotation, comparison and visualization. *Bioinformatics (Oxford, England)*. 2015;31(14):2382-3.
148. Ramírez F, Ryan DP, Grüning B, Bhardwaj V, Kilpert F, Richter AS, et al. deepTools2: a next generation web server for deep-sequencing data analysis. *Nucleic acids research*. 2016;44(W1):W160-5.

149. Shen L, Shao N, Liu X, and Nestler E. ngs.plot: Quick mining and visualization of next-generation sequencing data by integrating genomic databases. *BMC genomics*. 2014;15:284.
150. Rodd AL, Ververis K, and Karagiannis TC. Current and Emerging Therapeutics for Cutaneous T-Cell Lymphoma: Histone Deacetylase Inhibitors. *Lymphoma*. 2012;2012:290685.
151. Park J, Daniels J, Wartewig T, Ringbloom KG, Martinez-Escala ME, Choi S, et al. Integrated genomic analyses of cutaneous T-cell lymphomas reveal the molecular bases for disease heterogeneity. *Blood*. 2021;138(14):1225-36.
152. Kiel MJ, Sahasrabudde AA, Rolland DCM, Velusamy T, Chung F, Schaller M, et al. Genomic analyses reveal recurrent mutations in epigenetic modifiers and the JAK-STAT pathway in Sézary syndrome. *Nature communications*. 2015;6:8470.
153. Vakiti A, Padala SA, and Singh D. *StatPearls*. Treasure Island (FL): StatPearls Publishing Copyright © 2021, StatPearls Publishing LLC.; 2021.
154. Horna P, Moscinski LC, Sokol L, and Shao H. Naïve/memory T-cell phenotypes in leukemic cutaneous T-cell lymphoma: Putative cell of origin overlaps disease classification. *Cytometry Part B, Clinical cytometry*. 2019;96(3):234-41.
155. Mitchell WA, Lang PO, and Aspinall R. Tracing thymic output in older individuals. *Clinical and experimental immunology*. 2010;161(3):497-503.
156. Bagherani N, and Smoller BR. An overview of cutaneous T cell lymphomas. *F1000Research*. 2016;5.
157. Hamrouni A, Fogh H, Zak Z, Ødum N, and Gniadecki R. Clonotypic Diversity of the T-cell Receptor Corroborates the Immature Precursor Origin of Cutaneous T-cell Lymphoma. *Clinical cancer research : an official journal of the American Association for Cancer Research*. 2019;25(10):3104-14.
158. Zhang Y, Seminario-Vidal L, Varnadoe C, Lu Y, Dong N, Salamanca C, et al. Clinical characteristics and prognostic factors of 70 patients with Sézary syndrome: a single-institutional experience at Moffitt cancer center. *Leukemia & lymphoma*. 2021:1-8.
159. Caprini E, Bresin A, Cristofolletti C, Helmer Citterich M, Tocco V, Scala E, et al. Loss of the candidate tumor suppressor ZEB1 (TCF8, ZFHX1A) in Sézary syndrome. *Cell death & disease*. 2018;9(12):1178.
160. Hunter A, and Padron E. Genomic Landscape and Risk Stratification in Chronic Myelomonocytic Leukemia. *Current hematologic malignancy reports*. 2021;16(3):247-55.
161. Choi J, Goh G, Walradt T, Hong BS, Bunick CG, Chen K, et al. Genomic landscape of cutaneous T cell lymphoma. *Nature genetics*. 2015;47(9):1011-9.
162. Mirza AS, Horna P, Teer JK, Song J, Akabari R, Hussaini M, et al. New Insights Into the Complex Mutational Landscape of Sézary Syndrome. *Frontiers in oncology*. 2020;10:514.
163. Maxson JE, Abel ML, Wang J, Deng X, Reckel S, Luty SB, et al. Identification and Characterization of Tyrosine Kinase Nonreceptor 2 Mutations in Leukemia through Integration of Kinase Inhibitor Screening and Genomic Analysis. *Cancer research*. 2016;76(1):127-38.
164. Phyto ZH, Shanbhag S, and Rozati S. Update on Biology of Cutaneous T-Cell Lymphoma. *Frontiers in oncology*. 2020;10:765.

165. Ball M, List AF, and Padron E. When clinical heterogeneity exceeds genetic heterogeneity: thinking outside the genomic box in chronic myelomonocytic leukemia. *Blood*. 2016;128(20):2381-7.
166. Saggini A, Saraceno R, Anemona L, Chimenti S, and Di Stefani A. Mycosis fungoides in the setting of T-cell large granular lymphocyte proliferative disorder. *Acta dermatovenereologica*. 2012;92(3):288-9.
167. Satija R, Farrell JA, Gennert D, Schier AF, and Regev A. Spatial reconstruction of single-cell gene expression data. *Nat Biotechnol*. 2015;33(5):495-502.
168. Wolock SL, Lopez R, and Klein AM. Scrublet: Computational Identification of Cell Doublets in Single-Cell Transcriptomic Data. *Cell Syst*. 2019;8(4):281-91 e9.
169. McGinnis CS, Murrow LM, and Gartner ZJ. DoubletFinder: Doublet Detection in Single-Cell RNA Sequencing Data Using Artificial Nearest Neighbors. *Cell Syst*. 2019;8(4):329-37 e4.
170. Germain P, Lun A, Macnair W, and Robinson M. Doublet identification in single-cell sequencing data using scDblFinder [version 1; peer review: 1 approved, 1 approved with reservations]. *F1000Research*. 2021;10(979).
171. Lun AT, McCarthy DJ, and Marioni JC. A step-by-step workflow for low-level analysis of single-cell RNA-seq data with Bioconductor. *F1000Res*. 2016;5:2122.
172. Hao Y, Hao S, Andersen-Nissen E, Mauck WM, 3rd, Zheng S, Butler A, et al. Integrated analysis of multimodal single-cell data. *Cell*. 2021;184(13):3573-87 e29.
173. Wolf FA, Hamey FK, Plass M, Solana J, Dahlin JS, Gottgens B, et al. PAGA: graph abstraction reconciles clustering with trajectory inference through a topology preserving map of single cells. *Genome Biol*. 2019;20(1):59.
174. Wolf FA, Angerer P, and Theis FJ. SCANPY: large-scale single-cell gene expression data analysis. *Genome Biol*. 2018;19(1):15.
175. Stuart T, Srivastava A, Lareau C, and Satija R. bioRxiv; 2020.
176. Korsunsky I, Millard N, Fan J, Slowikowski K, Zhang F, Wei K, et al. Fast, sensitive and accurate integration of single-cell data with Harmony. *Nature Methods*. 2019;16(12):1289-96.
177. Pliner HA, Packer JS, McFaline-Figueroa JL, Cusanovich DA, Daza RM, Aghamirzaie D, et al. Cicero Predicts cis-Regulatory DNA Interactions from Single-Cell Chromatin Accessibility Data. *Mol Cell*. 2018;71(5):858-71.e8.
178. Granja JM, Klemm S, McGinnis LM, Kathiria AS, Mezger A, Corces MR, et al. Single-cell multiomic analysis identifies regulatory programs in mixed-phenotype acute leukemia. *Nat Biotechnol*. 2019;37(12):1458-65.
179. Gu Z, Eils R, and Schlesner M. Complex heatmaps reveal patterns and correlations in multidimensional genomic data. *Bioinformatics*. 2016;32(18):2847-9.
180. Ellrott K, Bailey MH, Saksena G, Covington KR, Kandath C, Stewart C, et al. Scalable Open Science Approach for Mutation Calling of Tumor Exomes Using Multiple Genomic Pipelines. *Cell Syst*. 2018;6(3):271-81 e7.
181. Li H, and Durbin R. Fast and accurate short read alignment with Burrows-Wheeler transform. *Bioinformatics*. 2009;25(14):1754-60.
182. McKenna A, Hanna M, Banks E, Sivachenko A, Cibulskis K, Kernytsky A, et al. The Genome Analysis Toolkit: a MapReduce framework for analyzing next-generation DNA sequencing data. *Genome research*. 2010;20(9):1297-303.

183. Cibulskis K, Lawrence MS, Carter SL, Sivachenko A, Jaffe D, Sougnez C, et al. Sensitive detection of somatic point mutations in impure and heterogeneous cancer samples. *Nat Biotechnol.* 2013;31(3):213-9.
184. Larson DE, Harris CC, Chen K, Koboldt DC, Abbott TE, Dooling DJ, et al. SomaticSniper: identification of somatic point mutations in whole genome sequencing data. *Bioinformatics (Oxford, England).* 2012;28(3):311-7.
185. Fan Y, Xi L, Hughes DST, Zhang J, Zhang J, Futreal PA, et al. MuSE: accounting for tumor heterogeneity using a sample-specific error model improves sensitivity and specificity in mutation calling from sequencing data. *Genome Biology.* 2016;17(1):178.
186. Garrison EP, and Marth GJaG. Haplotype-based variant detection from short-read sequencing. 2012.
187. Ye K, Schulz MH, Long Q, Apweiler R, and Ning Z. Pindel: a pattern growth approach to detect break points of large deletions and medium sized insertions from paired-end short reads. *Bioinformatics.* 2009;25(21):2865-71.
188. Saunders CT, Wong WS, Swamy S, Becq J, Murray LJ, and Cheetham RK. Strelka: accurate somatic small-variant calling from sequenced tumor-normal sample pairs. *Bioinformatics.* 2012;28(14):1811-7.
189. Tate JG, Bamford S, Jubb HC, Sondka Z, Beare DM, Bindal N, et al. COSMIC: the Catalogue Of Somatic Mutations In Cancer. *Nucleic Acids Res.* 2019;47(D1):D941-d7.
190. Lek M, Karczewski KJ, Minikel EV, Samocha KE, Banks E, Fennell T, et al. Analysis of protein-coding genetic variation in 60,706 humans. *Nature.* 2016;536(7616):285-91.
191. Forbes SA, Beare D, Gunasekaran P, Leung K, Bindal N, Boutselakis H, et al. COSMIC: exploring the world's knowledge of somatic mutations in human cancer. *Nucleic acids research.* 2015;43(Database issue):D805-D11.
192. Sherry ST, Ward MH, Kholodov M, Baker J, Phan L, Smigielski EM, et al. dbSNP: the NCBI database of genetic variation. *Nucleic acids research.* 2001;29(1):308-11.
193. Aken BL, Ayling S, Barrell D, Clarke L, Curwen V, Fairley S, et al. The Ensembl gene annotation system. *Database (Oxford).* 2016;2016:baw093.
194. Wang K, Li M, and Hakonarson H. ANNOVAR: functional annotation of genetic variants from high-throughput sequencing data. *Nucleic Acids Res.* 2010;38(16):e164.
195. Mayakonda A, Lin D-C, Assenov Y, Plass C, and Koeffler HP. Maftools: efficient and comprehensive analysis of somatic variants in cancer. *Genome Res.* 2018;28(11):1747-56.
196. Conway JR, Lex A, and Gehlenborg N. UpSetR: an R package for the visualization of intersecting sets and their properties. *Bioinformatics.* 2017;33(18):2938-40.
197. DeSantis CE, Kramer JL, and Jemal A. The burden of rare cancers in the United States. *CA: a cancer journal for clinicians.* 2017;67(4):261-72.

**APPENDIX A:  
TABLE OF MUTATIONS IN CTCL PATIENTS**

**Table A1. Summary of overlapping mutations in samples of SS patients**

Hugo Symbol	txChange	aaChange	HSC BM	HSC PB	Malignant T cell	Normal T cell
<b>Patient 1 (200 mutations in BM HSCs and 46 mutations in Blood HSCs)</b>						
<b>SHOX2</b>	c.G145C	p.D49H	+	-	+	-
<b>PCDH7</b>	c.A1166C	p.D389A	+	-	+	-
<b>GATA4</b>	c.G65C	p.G22A	+	-	+	-
<b>ADAMDEC1</b>	c.T668C	p.I223T	+	-	+	-
<b>CA12</b>	c.T150G	p.C50W	+	-	+	-
<b>CMTM1</b>	c.T525G	p.V175V	+	-	+	-
<b>CC2D1A</b>			+	-	+	-
<b>NCAPH</b>			+	-	+	-
<b>APOC4</b>			+	-	+	-
<b>DCAF8L2</b>	c.424_435del	p.142_145del	-	+	+	-
<b>GRIN2C</b>			-	+	+	-
<b>LINC02324</b>			-	+	+	-
<b>CELSR1</b>			-	+	+	-
<b>GRIN3B</b>			+	+	+	+
<b>WDFY1</b>			+	-	+	+
<b>TNK2</b>			+	-	+	+

**Table A1 (Continued)**

Hugo Symbol	txChange	aaChange	HSC BM	HSC PB	Malignant T cell	Normal T cell
<b>LOC101927859</b>			+	-	+	+
<b>SGK2</b>			+	-	+	+
<b>RNF40</b>	c.C36G	p.D12E	+	-	+	+
<b>TYMSOS</b>	c.A58G	p.S20G	+	-	+	+
<b>PCDH10</b>	c.A663G	p.G221G	+	-	+	+
<b>Patient 4 (15 mutations in BM HSCs and 206 mutations in Blood HSCs)</b>						
<b>MEF2C-AS1</b>			+	-	+	-
<b>OR6B2</b>			+	+	+	-
<b>RHCE</b>	c.G133C	p.V45L	-	+	+	-
<b>ARHGEF11</b>	c.C3320T	p.P1107L	-	+	+	-
<b>LRRC52</b>	c.C419T	p.S140L	-	+	+	-
<b>TATDN3</b>	c.A480C	p.E160D	-	+	+	-
<b>ANO3</b>	c.G760A	p.G254R	-	+	+	-
<b>FIBIN</b>	c.T215C	p.V72A	-	+	+	-
<b>ATG2A</b>	c.C2140T	p.P714S	-	+	+	-
<b>PIK3C2G</b>	c.G2914A	p.D972N	-	+	+	-
<b>ARID1B</b>	c.C2722T	p.P908S	-	+	+	-
<b>GPR37</b>	c.G1219A	p.D407N	-	+	+	-
<b>RPUSD2</b>	c.G508A	p.D170N	-	+	+	-
<b>TPTE</b>	c.G97A	p.E33K	-	+	+	-
<b>MYO7B</b>	c.G3862A	p.E1288K	-	+	+	-
<b>ZKSCAN7</b>	c.G508A	p.E170K	-	+	+	-
<b>CACNA1D</b>	c.G6367A	p.D2123N	-	+	+	-
<b>ATP13A4</b>	c.T2536C	p.C846R	-	+	+	-
<b>INTU</b>	c.C2296T	p.P766S	-	+	+	-
<b>CLGN</b>	c.G1086A	p.M362I	-	+	+	-

**Table A1 (Continued)**

<b>Hugo Symbol</b>	<b>txChange</b>	<b>aaChange</b>	<b>HSC BM</b>	<b>HSC PB</b>	<b>Malignant T cell</b>	<b>Normal T cell</b>
<b>NIPBL</b>	c.C2206T	p.P736S	-	+	+	-
<b>APBA1</b>	c.G307A	p.G103S	-	+	+	-
<b>MTMR6</b>	c.C559T	p.P187S	-	+	+	-
<b>HEATR5A</b>	c.C1093T	p.L365F	-	+	+	-
<b>MGAT2</b>	c.1233_1240del	p.L411fs	-	+	+	-
<b>HHIPL1</b>	c.G2296A	p.E766K	-	+	+	-
<b>SHC2</b>	c.G474A	p.M158I	-	+	+	-
<b>PLVAP</b>	c.G985A	p.A329T	-	+	+	-
<b>PHLDB3</b>	c.G29A	p.G10E	-	+	+	-
<b>KLHL4</b>	c.C198A	p.N66K	-	+	+	-
<b>COL4A6</b>	c.C3910T	p.L1304F	-	+	+	-
<b>DNASE1L1</b>	c.A722G	p.H241R	-	+	+	-
<b>TNN</b>	c.G3204A	p.S1068S	-	+	+	-
<b>CDH3</b>	c.C2226T	p.S742S	-	+	+	-
<b>GSDMB</b>	c.C843T	p.S281S	-	+	+	-
<b>HLF</b>	c.G534A	p.E178E	-	+	+	-
<b>NOTCH4</b>	c.G3636A	p.K1212K	-	+	+	-
<b>SRSF3</b>	c.T147G	p.A49A	-	+	+	-
<b>RBP3</b>	c.G1920A	p.V640V	-	+	+	-
<b>KNSTRN</b>	c.C12T	p.P4P	-	+	+	-
<b>FER</b>	c.C276T	p.H92H	-	+	+	-
<b>SEC14L6</b>	c.G843A	p.T281T	-	+	+	-
<b>H6PD</b>			-	+	+	-
<b>MYSM1</b>			-	+	+	-
<b>NMNAT2</b>			-	+	+	-

**Table A1 (Continued)**

<b>Hugo Symbol</b>	<b>txChange</b>	<b>aaChange</b>	<b>HSC BM</b>	<b>HSC PB</b>	<b>Malignant T cell</b>	<b>Normal T cell</b>
<b>HMCN1</b>			-	+	+	-
<b>REXO2</b>			-	+	+	-
<b>KIRREL3</b>			-	+	+	-
<b>ERN2</b>			-	+	+	-
<b>CMIP</b>			-	+	+	-
<b>LOC339059</b>			-	+	+	-
<b>CPNE7</b>			-	+	+	-
<b>MYO15A</b>			-	+	+	-
<b>SCRN2</b>			-	+	+	-
<b>SPATA20</b>			-	+	+	-
<b>LAMA1</b>			-	+	+	-
<b>ADGRF2</b>			-	+	+	-
<b>DDX31</b>	c.C255T	p.V85V	-	+	+	-
<b>ARHGAP22</b>			-	+	+	-
<b>WDFY4</b>			-	+	+	-
<b>COL13A1</b>			-	+	+	-
<b>RYR3</b>			-	+	+	-
<b>MIR3156-3</b>			-	+	+	-
<b>CADPS</b>			-	+	+	-
<b>MYLK</b>			-	+	+	-
<b>EPHA5</b>			-	+	+	-
<b>PRSS12</b>			-	+	+	-
<b>PRDM9</b>			-	+	+	-
<b>ARL14EPL</b>			-	+	+	-
<b>TEX26</b>			-	+	+	-
<b>PIN1</b>			-	+	+	-
<b>SHANK3</b>			-	+	+	-

**Table A1 (Continued)**

<b>Hugo Symbol</b>	<b>txChange</b>	<b>aaChange</b>	<b>HSC BM</b>	<b>HSC PB</b>	<b>Malignant T cell</b>	<b>Normal T cell</b>
<b>DMD</b>			-	+	+	-
<b>MAP6</b>	c.C1739T	p.P580L	-	+	+	+
<b>C1QTNF12</b>	c.C817T	p.Q273X	-	+	+	+
<b>DOCK7</b>	c.C3869T	p.S1290L	-	+	+	+
<b>LRRIQ3</b>	c.G1196A	p.R399Q	-	+	+	+
<b>S1PR1</b>	c.C1073T	p.S358F	-	+	+	+
<b>HRNR</b>	c.G1574A	p.R525H	-	+	+	+
<b>IQGAP3</b>	c.G194A	p.G65E	-	+	+	+
<b>CATSPERE</b>	c.C1591T	p.R531X	-	+	+	+
<b>ZNF215</b>	c.G611A	p.R204H	-	+	+	+
<b>ABCC8</b>	c.286delG	p.D96fs	-	+	+	+
<b>GPR83</b>	c.T871A	p.F291I	-	+	+	+
<b>CBL</b>	c.C2573T	p.S858F	-	+	+	+
<b>MYLK3</b>	c.G640A	p.E214K	-	+	+	+
<b>DRC7</b>	c.G1642A	p.E548K	-	+	+	+
<b>JPH3</b>	c.G313A	p.A105T	-	+	+	+
<b>USP43</b>	c.G1219A	p.G407R	-	+	+	+
<b>GAS7</b>	c.C143T	p.P48L	-	+	+	+
<b>DSEL</b>	c.G657T	p.E219D	-	+	+	+
<b>CFB</b>	c.G760A	p.G254R	-	+	+	+
<b>DGKI</b>	c.T1971A	p.H657Q	-	+	+	+
<b>MGAM</b>	c.G3949A	p.D1317N	-	+	+	+
<b>ADARB2</b>	c.G1623A	p.W541X	-	+	+	+
<b>BEND7</b>	c.G521A	p.R174Q	-	+	+	+
<b>FRMPD2</b>	c.C2362T	p.P788S	-	+	+	+
<b>FAM170B</b>	c.C805T	p.R269W	-	+	+	+
<b>CAMKMT</b>	c.T494C	p.V165A	-	+	+	+

**Table A1 (Continued)**

<b>Hugo Symbol</b>	<b>txChange</b>	<b>aaChange</b>	<b>HSC BM</b>	<b>HSC PB</b>	<b>Malignant T cell</b>	<b>Normal T cell</b>
<b>LRP1B</b>	c.G1069A	p.D357N	-	+	+	+
<b>FAM47E</b>	c.G685C	p.D229H	-	+	+	+
<b>PKD2</b>	c.C2384T	p.S795F	-	+	+	+
<b>ADGRV1</b>	c.G15262A	p.E5088K	-	+	+	+
<b>APBB3</b>	c.G1210A	p.G404R	-	+	+	+
<b>PCDHB8</b>	c.G29A	p.R10K	-	+	+	+
<b>SLITRK1</b>	c.G595A	p.E199K	-	+	+	+
<b>SLC7A10</b>	c.G577A	p.G193R	-	+	+	+
<b>PRX</b>	c.C1747T	p.P583S	-	+	+	+
<b>VRK3</b>	c.T842C	p.F281S	-	+	+	+
<b>NR0B1</b>	c.T529A	p.F177I	-	+	+	+
<b>CHST7</b>	c.C913A	p.R305S	-	+	+	+
<b>PRICKLE3</b>	c.G1247A	p.G416E	-	+	+	+
<b>PJA1</b>	c.G1510T	p.A504S	-	+	+	+
<b>GPR101</b>	c.G1120A	p.E374K	-	+	+	+
<b>MYLK3</b>			-	+	+	+
<b>TP53</b>			-	+	+	+
<b>UBE4B</b>	c.C1039T	p.L347L	-	+	+	+
<b>HSPG2</b>	c.G10365A	p.Q3455Q	-	+	+	+
<b>PSRC1</b>	c.G585A	p.S195S	-	+	+	+
<b>ADAM2</b>	c.T1788C	p.D596D	-	+	+	+
<b>OR4A16</b>	c.G858A	p.S286S	-	+	+	+
<b>RBM14</b>	c.C1752T	p.P584P	-	+	+	+
<b>ADCY7</b>	c.C672T	p.I224I	-	+	+	+
<b>SLC12A4</b>	c.C285T	p.T95T	-	+	+	+
<b>PTCHD4</b>	c.G2037A	p.V679V	-	+	+	+
<b>SPATA8</b>	c.G99A	p.S33S	-	+	+	+

**Table A1 (Continued)**

<b>Hugo Symbol</b>	<b>txChange</b>	<b>aaChange</b>	<b>HSC BM</b>	<b>HSC PB</b>	<b>Malignant T cell</b>	<b>Normal T cell</b>
<b>KCNJ15</b>	c.C504T	p.I168I	-	+	+	+
<b>RANBP2</b>	c.C4155T	p.L1385L	-	+	+	+
<b>SH3D19</b>	c.C609T	p.I203I	-	+	+	+
<b>GABRB2</b>	c.C942T	p.V314V	-	+	+	+
<b>SLITRK1</b>	c.G594A	p.L198L	-	+	+	+
<b>ZNF568</b>	c.G1254A	p.R418R	-	+	+	+
<b>TTC28</b>	c.G603A	p.V201V	-	+	+	+
<b>WDR13</b>	c.C393T	p.F131F	-	+	+	+
<b>GNB1</b>			-	+	+	+
<b>DEPDC1-AS1</b>			-	+	+	+
<b>LAMC1</b>			-	+	+	+
<b>CHRM3</b>			-	+	+	+
<b>RP1</b>			-	+	+	+
<b>PRMT8</b>			-	+	+	+
<b>RBM19</b>			-	+	+	+
<b>CDH13</b>			-	+	+	+
<b>KLHDC4</b>			-	+	+	+
<b>P2RX1</b>			-	+	+	+
<b>ABCA9</b>			-	+	+	+
<b>CASKIN2</b>			-	+	+	+
<b>TUBB2A</b>			-	+	+	+
<b>SNRNP48</b>			-	+	+	+
<b>ELOVL2</b>			-	+	+	+
<b>DCDC2</b>			-	+	+	+
<b>MUC21</b>			-	+	+	+
<b>LAMA2</b>			-	+	+	+
<b>EGFR</b>			-	+	+	+

**Table A1 (Continued)**

<b>Hugo Symbol</b>	<b>txChange</b>	<b>aaChange</b>	<b>HSC BM</b>	<b>HSC PB</b>	<b>Malignant T cell</b>	<b>Normal T cell</b>
<b>ABCB1</b>			-	+	+	+
<b>ABCB8</b>			-	+	+	+
<b>ABRAXAS2</b>			-	+	+	+
<b>ERMN</b>			-	+	+	+
<b>KCNH7</b>			-	+	+	+
<b>PTPRN</b>			-	+	+	+
<b>PLCD1</b>			-	+	+	+
<b>OR5H14</b>			-	+	+	+
<b>KALRN</b>			-	+	+	+
<b>PCOLCE2</b>			-	+	+	+
<b>ZBBX</b>			-	+	+	+
<b>MECOM</b>			-	+	+	+
<b>UBE2K</b>			-	+	+	+
<b>UBE2K</b>			-	+	+	+
<b>ASIC5</b>			-	+	+	+
<b>SLC45A2</b>			-	+	+	+
<b>SLC45A2</b>			-	+	+	+
<b>ANKRD55</b>			-	+	+	+
<b>NKX2-5</b>			-	+	+	+
<b>SLC24A2</b>			-	+	+	+
<b>TEK</b>			-	+	+	+
<b>SUPT16H</b>			-	+	+	+
<b>TTL5</b>			-	+	+	+
<b>C3P1</b>			-	+	+	+
<b>MYO9B</b>			-	+	+	+
<b>NCCRP1</b>			-	+	+	+
<b>POLR3H</b>			-	+	+	+

**Table A1 (Continued)**

Hugo Symbol	txChange	aaChange	HSC BM	HSC PB	Malignant T cell	Normal T cell
<b>POLR3H</b>			-	+	+	+
<b>TBC1D22A</b>			-	+	+	+
<b>CXorf56</b>			-	+	+	+
<b>Patient 3 (170 mutations in BM HSCs and 210 mutations in Blood HSCs)</b>						
<b>ATP13A2</b>	c.G2425A	p.V809M	+	+	+	+
<b>VWA5B1</b>	c.G2963A	p.R988H	+	+	+	+
<b>ARID1A</b>	c.C6382T	p.Q2128X	+	+	+	+
<b>SLC1A7</b>	c.G263A	p.R88H	+	+	+	+
<b>ARMC1</b>	c.G184T	p.A62S	+	+	+	+
<b>PKHD1L1</b>	c.G4307A	p.G1436E	+	+	+	+
<b>CSMD3</b>	c.G3161A	p.R1054H	+	+	+	+
<b>COL22A1</b>	c.G145A	p.V49M	+	+	+	+
<b>OR5P3</b>	c.G260A	p.R87K	+	+	+	+
<b>ACCSL</b>	c.G256A	p.A86T	+	+	+	+
<b>C2CD3</b>	c.C2296T	p.P766S	+	+	+	+
<b>MAP6</b>	c.C408A	p.S136R	+	+	+	+
<b>ADAMTS20</b>	c.3862delA	p.T1288fs	+	+	+	+
<b>ACTR6</b>	c.C1012T	p.R338X	+	+	+	+
<b>ACACB</b>	c.G3923A	p.S1308N	+	+	+	+
<b>SSTR5</b>	c.G112A	p.A38T	+	+	+	+
<b>VWA3A</b>	c.T398C	p.I133T	+	+	+	+
<b>CHP2</b>	c.G505A	p.D169N	+	+	+	+
<b>TAOK2</b>	c.C2254T	p.P752S	+	+	+	+
<b>SRCAP</b>	c.A1235G	p.D412G	+	+	+	+
<b>TP53</b>	c.G42A	p.W14X	+	+	+	+
<b>KRTAP16-1</b>	c.G1349A	p.R450H	+	+	+	+
<b>DSC3</b>	c.G163A	p.E55K	+	+	+	+

**Table A1 (Continued)**

<b>Hugo Symbol</b>	<b>txChange</b>	<b>aaChange</b>	<b>HSC BM</b>	<b>HSC PB</b>	<b>Malignant T cell</b>	<b>Normal T cell</b>
<b>GCLC</b>	c.C415T	p.Q139X	+	+	+	+
<b>PLEKHG1</b>	c.C640T	p.L214F	+	+	+	+
<b>SCIN</b>	c.C374T	p.P125L	+	+	+	+
<b>TSPAN13</b>	c.T134G	p.V45G	+	+	+	+
<b>MUC17</b>	c.G5642T	p.S188I	+	+	+	+
<b>PLXNA4</b>	c.G1109A	p.R370Q	+	+	+	+
<b>TACC2</b>	c.C1822T	p.P608S	+	+	+	+
<b>ITGA11</b>	c.G1189A	p.E397K	+	+	+	+
<b>SIM2</b>	c.C1158A	p.Y386X	+	+	+	+
<b>HECW2</b>	c.G1027A	p.E343K	+	+	+	+
<b>IQCA1</b>	c.C2198T	p.T733M	+	+	+	+
<b>SLC6A11</b>	c.G731A	p.W244X	+	+	+	+
<b>TMEM40</b>	c.G170A	p.R57Q	+	+	+	+
<b>PRR23A</b>	c.G451A	p.A151T	+	+	+	+
<b>SI</b>	c.C1643A	p.A548D	+	+	+	+
<b>TBCCD1</b>	c.T1025G	p.V342G	+	+	+	+
<b>UGT2B4</b>	c.G687A	p.M229I	+	+	+	+
<b>PKD2</b>	c.C2395T	p.P799S	+	+	+	+
<b>CLCN3</b>	c.A2362G	p.I788V	+	+	+	+
<b>ZNF608</b>	c.A2170G	p.K724E	+	+	+	+
<b>HTR4</b>	c.G124A	p.V42M	+	+	+	+
<b>FLT4</b>	c.G1960A	p.E654K	+	+	+	+
<b>CA9</b>	c.G838A	p.E280K	+	+	+	+
<b>C9orf84</b>	c.A199G	p.T67A	+	+	+	+
<b>OR1N2</b>	c.C701T	p.S234F	+	+	+	+
<b>AKAP6</b>	c.C1520T	p.P507L	+	+	+	+
<b>TRIM9</b>	c.T1400A	p.L467Q	+	+	+	+

**Table A1 (Continued)**

<b>Hugo Symbol</b>	<b>txChange</b>	<b>aaChange</b>	<b>HSC BM</b>	<b>HSC PB</b>	<b>Malignant T cell</b>	<b>Normal T cell</b>
<b>COL5A3</b>	c.G3959A	p.R1320Q	+	+	+	+
<b>ACTN4</b>	c.C776T	p.T259I	+	+	+	+
<b>RINL</b>	c.G262A	p.G88R	+	+	+	+
<b>ZNF579</b>	c.C1559T	p.S520F	+	+	+	+
<b>TNRC6B</b>	c.C766A	p.L256I	+	+	+	+
<b>CHKB</b>	c.C902G	p.T301R	+	+	+	+
<b>SHROOM4</b>	c.C2563T	p.P855S	+	+	+	+
<b>ELN</b>			+	+	+	+
<b>CAD</b>			+	+	+	+
<b>NSD3</b>	c.C2598T	p.F866F	+	+	+	+
<b>MTSS1L</b>	c.C1059T	p.S353S	+	+	+	+
<b>ARID1A</b>	c.C6381T	p.I2127I	+	+	+	+
<b>DIO1</b>			+	+	+	+
<b>NOTCH2</b>	c.A5358T	p.R1786R	+	+	+	+
<b>IVL</b>	c.G1383A	p.K461K	+	+	+	+
<b>SLAMF1</b>	c.C66T	p.S22S	+	+	+	+
<b>C4BPB</b>	c.C336T	p.I112I	+	+	+	+
<b>LOXL2</b>	c.C2211T	p.D737D	+	+	+	+
<b>DGKZ</b>	c.C261T	p.I87I	+	+	+	+
<b>CAND1</b>	c.C1242T	p.D414D	+	+	+	+
<b>MAP1LC3B2</b>	c.C345T	p.S115S	+	+	+	+
<b>PDK2</b>	c.C438T	p.L146L	+	+	+	+
<b>KIF13A</b>	c.C1089T	p.N363N	+	+	+	+
<b>LAMA4</b>	c.G1116A	p.K372K	+	+	+	+
<b>PRDM15</b>	c.C1623T	p.D541D	+	+	+	+
<b>CNTNAP5</b>	c.G1227T	p.L409L	+	+	+	+
<b>UNC80</b>	c.C5415T	p.S1805S	+	+	+	+

**Table A1 (Continued)**

<b>Hugo Symbol</b>	<b>txChange</b>	<b>aaChange</b>	<b>HSC BM</b>	<b>HSC PB</b>	<b>Malignant T cell</b>	<b>Normal T cell</b>
<b>UBA7</b>	c.C2565T	p.T855T	+	+	+	+
<b>ALAS1</b>	c.G633A	p.K211K	+	+	+	+
<b>FAM160A1</b>	c.C201T	p.Y67Y	+	+	+	+
<b>GRIA2</b>	c.C2367T	p.Y789Y	+	+	+	+
<b>LVRN</b>	c.A2056C	p.R686R	+	+	+	+
<b>NRG2</b>	c.A1779G	p.G593G	+	+	+	-
<b>HAVCR1</b>	c.C876T	p.T292T	+	+	+	+
<b>PTPN21</b>	c.C2169T	p.S723S	+	+	+	+
<b>FSD1</b>	c.C1116T	p.G372G	+	+	+	+
<b>ACTN4</b>	c.C777T	p.T259T	+	+	+	+
<b>LILRB4</b>	c.G996A	p.G332G	+	+	+	+
<b>ZNF579</b>	c.C1560T	p.S520S	+	+	+	+
<b>TXNRD2</b>			+	+	+	+
<b>SELENOO</b>			+	+	+	+
<b>PHEX</b>	c.C609T	p.F203F	+	+	+	+
<b>CPXCR1</b>	c.G900A	p.G300G	+	+	+	+
<b>CACNA1C</b>			+	+	+	+
<b>COL21A1</b>			+	+	+	+
<b>ST6GALNAC3</b>			+	+	+	+
<b>DPYD</b>			+	+	+	+
<b>PKP1</b>			+	+	+	+
<b>PPFIA4</b>			+	+	+	+
<b>LBR</b>			+	+	+	+
<b>LBR</b>			+	+	+	+
<b>DCTN6</b>			+	+	+	+
<b>NRBP2</b>			+	+	+	+
<b>NRBP2</b>			+	+	+	+

**Table A1 (Continued)**

<b>Hugo Symbol</b>	<b>txChange</b>	<b>aaChange</b>	<b>HSC BM</b>	<b>HSC PB</b>	<b>Malignant T cell</b>	<b>Normal T cell</b>
<b>PLCZ1</b>			+	+	+	+
<b>ITPR2</b>			+	+	+	+
<b>LRRK2</b>			+	+	+	+
<b>TNS2</b>			+	+	+	+
<b>LOC100506869</b>			+	+	+	+
<b>TTC41P</b>			+	+	+	+
<b>HYDIN</b>			+	+	+	+
<b>CHST5</b>			+	+	+	+
<b>JPH3</b>			+	+	+	+
<b>MLX</b>			+	+	+	+
<b>LINC00470</b>			+	+	+	+
<b>ARHGAP28</b>			+	+	+	+
<b>LDLRAD4</b>			+	+	+	+
<b>GABRR1</b>			+	+	+	+
<b>AFG1L</b>			+	+	+	+
<b>PTPRK</b>			+	+	+	+
<b>ADGB</b>			+	+	+	+
<b>SYNE1</b>			+	+	+	+
<b>AKR1C8P</b>			+	+	+	+
<b>C10orf67</b>			+	+	+	+
<b>LINC00999</b>			+	+	+	+
<b>WDFY4</b>			+	+	+	+
<b>KNL1</b>			+	+	+	+
<b>FBN1</b>			+	+	+	+
<b>TRIM54</b>			+	+	+	+
<b>TRIM54</b>			+	+	+	+
<b>DYSF</b>			+	+	+	+

**Table A1 (Continued)**

<b>Hugo Symbol</b>	<b>txChange</b>	<b>aaChange</b>	<b>HSC BM</b>	<b>HSC PB</b>	<b>Malignant T cell</b>	<b>Normal T cell</b>
<b>GLI2</b>			+	+	+	+
<b>DAPL1</b>			+	+	+	+
<b>ROBO1</b>			+	+	+	+
<b>ROBO1</b>			+	+	+	+
<b>CFAP44-AS1</b>			+	+	+	+
<b>PLOD2</b>			+	+	+	+
<b>AADA2L2</b>			+	+	+	+
<b>KDR</b>			+	+	+	+
<b>UGT2B15</b>			+	+	+	+
<b>LNCPRESS2</b>			+	+	+	+
<b>GYPE</b>			+	+	+	+
<b>GPM6A</b>			+	+	+	+
<b>PANK3</b>			+	+	+	+
<b>FNBP1</b>			+	+	+	+
<b>COL5A1</b>			+	+	+	+
<b>LCN9</b>			+	+	+	+
<b>IFT88</b>			+	+	+	+
<b>FRY</b>			+	+	+	+
<b>OR4E1</b>			+	+	+	+
<b>MIR5195</b>			+	+	+	+
<b>THOP1</b>			+	+	+	+
<b>LINC00661</b>			+	+	+	+
<b>LINC00661</b>			+	+	+	+
<b>NCAN</b>			+	+	+	+
<b>ATP13A1</b>			+	+	+	+
<b>ATP13A1</b>			+	+	+	+
<b>STX16-NPEPL1</b>			+	+	+	+

**Table A1 (Continued)**

Hugo Symbol	txChange	aaChange	HSC BM	HSC PB	Malignant T cell	Normal T cell
<b>MID1</b>			+	+	+	+
<b>KMT5B</b>	c.G323T	p.R108M	+	-	+	+
<b>HCN1</b>	c.G1679A	p.R560H	+	-	+	+
<b>DNAH14</b>			+	-	+	+
<b>FLOT1</b>			+	-	+	+
<b>LOC105373394</b>			+	-	+	+
<b>ABCA10</b>			+	-	-	+
<b>YWHAB</b>			+	-	-	+
<b>PANK3</b>			+	+	-	-
<b>CACYBP</b>			-	+	+	+
<b>CATSPERE</b>			-	+	+	+
<b>CCKBR</b>			-	+	+	+
<b>LTBP3</b>			-	+	+	-
<b>C16orf70</b>			-	+	+	+
<b>CCL23</b>			-	+	+	+
<b>COL19A1</b>			-	+	+	+
<b>SCN2A</b>			-	+	+	+
<b>PTH1R</b>			-	+	+	+
<b>SLC34A2</b>			-	+	+	+
<b>FBN2</b>			-	+	+	+
<b>MIR4537</b>			-	+	+	+
<b>CBARP</b>			-	+	+	+
<b>COL1A2</b>			-	+	+	+
<b>Patient 5 (232 mutations in BM HSCs and 259 mutations in Blood HSCs)</b>						
<b>LOC100133091</b>			+	-	+	-
<b>SERINC2</b>	c.G296A	p.R99H	+	+	+	+
<b>NFIA</b>	c.C1118T	p.S373L	+	+	+	+

**Table A1 (Continued)**

<b>Hugo Symbol</b>	<b>txChange</b>	<b>aaChange</b>	<b>HSC BM</b>	<b>HSC PB</b>	<b>Malignant T cell</b>	<b>Normal T cell</b>
<b>ERICH3</b>	c.C1220T	p.P407L	+	+	+	+
<b>CLCA2</b>	c.G73A	p.E25K	+	+	+	+
<b>CDC7</b>	c.G1294A	p.G432R	+	+	+	+
<b>AMPD1</b>	c.C563T	p.P188L	+	+	+	+
<b>MAN1A2</b>	c.G853A	p.E285K	+	+	+	+
<b>INSRR</b>	c.C322T	p.R108C	+	+	+	+
<b>OLFML2B</b>	c.G571A	p.E191K	+	+	+	+
<b>BRINP2</b>	c.C1352T	p.S451F	+	+	+	+
<b>KCNH1</b>	c.G2030A	p.R677K	+	+	+	+
<b>USH2A</b>	c.G7999A	p.E2667K	+	+	+	+
<b>PCM1</b>	c.T3181A	p.C1061S	+	+	+	+
<b>UNC5D</b>	c.C1952G	p.S651C	+	+	+	+
<b>COLEC10</b>	c.G194A	p.G65D	+	+	+	+
<b>SLC1A2</b>	c.A679C	p.K227Q	+	+	+	+
<b>OR5B17</b>	c.T401C	p.M134T	+	+	+	+
<b>NRXN2</b>	c.G3058A	p.D1020N	+	+	+	+
<b>MMP3</b>	c.G139A	p.D47N	+	+	+	+
<b>DYNC2H1</b>	c.G10550A	p.R3517H	+	+	+	+
<b>PDZRN4</b>	c.A2192G	p.E731G	+	+	+	+
<b>KRT83</b>	c.G310A	p.A104T	+	+	+	+
<b>KIF5A</b>	c.A842G	p.D281G	+	+	+	+
<b>PHLDA1</b>	c.G783C	p.E261D	+	+	+	+
<b>TMEM132D</b>	c.C2273T	p.A758V	+	+	+	+
<b>C16orf89</b>	c.C920T	p.S307L	+	+	+	+
<b>DNAH3</b>	c.G5365A	p.A1789T	+	+	+	+
<b>LAT</b>	c.C193G	p.P65A	+	+	+	+
<b>TUBB3</b>	c.C853T	p.P285S	+	+	+	+

**Table A1 (Continued)**

<b>Hugo Symbol</b>	<b>txChange</b>	<b>aaChange</b>	<b>HSC BM</b>	<b>HSC PB</b>	<b>Malignant T cell</b>	<b>Normal T cell</b>
<b>TUBB3</b>	c.C854T	p.P285L	+	+	+	+
<b>TP53</b>	c.262delT	p.Y88fs	+	+	+	+
<b>ACACA</b>	c.G5191A	p.E1731K	+	+	+	+
<b>C17orf64</b>	c.G191A	p.R64Q	+	+	+	+
<b>GPRC5C</b>	c.C1184T	p.S395F	+	+	+	+
<b>SEC14L1</b>	c.C44T	p.P15L	+	+	+	+
<b>ASXL3</b>	c.T107A	p.V36D	+	+	+	+
<b>F13A1</b>	c.G1504A	p.G502R	+	+	+	+
<b>RREB1</b>	c.C478T	p.P160S	+	+	+	+
<b>DST</b>	c.G109A	p.G37S	+	+	+	+
<b>SNAP91</b>	c.A92C	p.K31T	+	+	+	+
<b>NT5E</b>	c.C1220T	p.T407I	+	+	+	+
<b>AFDN</b>	c.C1150A	p.L384M	+	+	+	+
<b>PHF14</b>	c.C1627T	p.Q543X	+	+	+	+
<b>PCLO</b>	c.C2644T	p.R882X	+	+	+	+
<b>SEMA3E</b>	c.C689T	p.A230V	+	+	+	+
<b>RUNDC3B</b>	c.G305A	p.R102Q	+	+	+	+
<b>TRRAP</b>	c.C2165T	p.S722F	+	+	+	+
<b>FLNC</b>	c.T5930C	p.V1977A	+	+	+	+
<b>PDZD8</b>	c.G949A	p.A317T	+	+	+	+
<b>SPESP1</b>	c.G775A	p.D259N	+	+	+	+
<b>EPC2</b>	c.C1196T	p.A399V	+	+	+	+
<b>NEB</b>	c.G7407T	p.K2469N	+	+	+	+
<b>SCN3A</b>	c.G5788A	p.E1930K	+	+	+	+
<b>SCN2A</b>	c.G1492A	p.E498K	+	+	+	+
<b>SCN1A</b>	c.C5656T	p.R1886X	+	+	+	+
<b>PDE1A</b>	c.A210T	p.K70N	+	+	+	+

**Table A1 (Continued)**

<b>Hugo Symbol</b>	<b>txChange</b>	<b>aaChange</b>	<b>HSC BM</b>	<b>HSC PB</b>	<b>Malignant T cell</b>	<b>Normal T cell</b>
<b>DNAH7</b>	c.T5055G	p.D1685E	+	+	+	+
<b>KLF7</b>	c.C753A	p.C251X	+	+	+	+
<b>UNC80</b>	c.T7519A	p.C2507S	+	+	+	+
<b>SPEG</b>	c.G7625A	p.R2542Q	+	+	+	+
<b>ARL4C</b>	c.G583A	p.D195N	+	+	+	+
<b>ESPNL</b>	c.C1387T	p.R463C	+	+	+	+
<b>DNAH12</b>	c.T10333A	p.F3445I	+	+	+	+
<b>PDZRN3</b>	c.C515T	p.A172V	+	+	+	+
<b>CRYBG3</b>	c.C2722T	p.Q908X	+	+	+	+
<b>IGSF10</b>	c.C149T	p.S50F	+	+	+	+
<b>DGKG</b>	c.C1088T	p.A363V	+	+	+	+
<b>PROM1</b>	c.G691A	p.G231R	+	+	+	+
<b>PPARGC1A</b>	c.G995A	p.R332Q	+	+	+	+
<b>ERVMER34-1</b>	c.C1297T	p.R433X	+	+	+	+
<b>ADAD1</b>	c.G253A	p.E85K	+	+	+	+
<b>TLR3</b>	c.G1780C	p.G594R	+	+	+	+
<b>FAT2</b>	c.G8738A	p.G2913E	+	+	+	+
<b>SH3PXD2B</b>	c.G1601A	p.G534E	+	+	+	+
<b>GOLGA2</b>	c.C1376G	p.S459C	+	+	+	+
<b>SETX</b>	c.C7330T	p.P2444S	+	+	+	+
<b>SERTM1</b>	c.G121A	p.V41I	+	+	+	+
<b>FOXO1</b>	c.A925C	p.N309H	+	+	+	+
<b>CCDC168</b>	c.G9837T	p.Q3279H	+	+	+	+
<b>JPH4</b>	c.C249A	p.Y83X	+	+	+	+
<b>CERS4</b>	c.G890A	p.G297D	+	+	+	+
<b>OR7E24</b>	c.G419A	p.R140Q	+	+	+	+
<b>JUNB</b>	c.C845T	p.A282V	+	+	+	+

**Table A1 (Continued)**

<b>Hugo Symbol</b>	<b>txChange</b>	<b>aaChange</b>	<b>HSC BM</b>	<b>HSC PB</b>	<b>Malignant T cell</b>	<b>Normal T cell</b>
<b>KIAA1683</b>	c.A1702C	p.K568Q	+	+	+	+
<b>KLK5</b>	c.G752T	p.C251F	+	+	+	+
<b>KLK12</b>	c.T274A	p.S92T	+	+	+	+
<b>CYP24A1</b>	c.T914C	p.I305T	+	+	+	+
<b>MTMR3</b>	c.G3103T	p.E1035X	+	+	+	+
<b>MAP7D2</b>	c.G1993A	p.D665N	+	+	+	+
<b>TAZ</b>	c.T334A	p.F112I	+	+	+	+
<b>DNAH12</b>			+	+	+	+
<b>MYH15</b>			+	+	+	+
<b>COL16A1</b>	c.G348A	p.T116T	+	+	+	+
<b>HFE2</b>	c.T183C	p.I61I	+	+	+	+
<b>ADAM7</b>	c.C408T	p.N136N	+	+	+	+
<b>ZNF16</b>	c.C762T	p.N254N	+	+	+	+
<b>ARHGEF12</b>	c.C1962G	p.A654A	+	+	+	+
<b>KCNA5</b>	c.G942A	p.P314P	+	+	+	+
<b>R3HDM2</b>	c.C2178T	p.D726D	+	+	+	+
<b>SVOP</b>	c.C204T	p.F68F	+	+	+	+
<b>RANBP10</b>	c.C543T	p.I181I	+	+	+	+
<b>ABR</b>	c.C174T	p.N58N	+	+	+	+
<b>GPRC5C</b>	c.C1185T	p.S395S	+	+	+	+
<b>DCC</b>	c.C2589T	p.S863S	+	+	+	+
<b>NT5E</b>	c.C1221T	p.T407T	+	+	+	+
<b>TRDN</b>	c.G441A	p.K147K	+	+	+	+
<b>TRRAP</b>	c.C2166T	p.S722S	+	+	+	+
<b>FBXO24</b>	c.C909T	p.Y303Y	+	+	+	+
<b>TAS2R38</b>	c.C198T	p.F66F	+	+	+	+
<b>SSPO</b>	c.C7989T	p.L2663L	+	+	+	+

**Table A1 (Continued)**

<b>Hugo Symbol</b>	<b>txChange</b>	<b>aaChange</b>	<b>HSC BM</b>	<b>HSC PB</b>	<b>Malignant T cell</b>	<b>Normal T cell</b>
<b>GLI2</b>	c.C1506T	p.P502P	+	+	+	+
<b>KLHL41</b>	c.C1311T	p.V437V	+	+	+	+
<b>FSIP2</b>	c.C9222T	p.F3074F	+	+	+	+
<b>LRRN1</b>	c.G1761A	p.Q587Q	+	+	+	+
<b>CAND2</b>	c.C654T	p.D218D	+	+	+	+
<b>SCN5A</b>	c.C3855T	p.L1285L	+	+	+	+
<b>SLC6A20</b>	c.G366A	p.P122P	+	+	+	+
<b>SLC38A3</b>	c.C1407T	p.I469I	+	+	+	+
<b>CRYBG3</b>	c.C2721T	p.C907C	+	+	+	+
<b>CLSTN2</b>	c.C1317T	p.P439P	+	+	+	+
<b>MASP1</b>	c.G1692A	p.L564L	+	+	+	+
<b>KCNIP4</b>	c.C33T	p.T11T	+	+	+	+
<b>ATP10D</b>	c.C4012T	p.L1338L	+	+	+	+
<b>DCHS2</b>	c.C3576T	p.D1192D	+	+	+	+
<b>HAPLN1</b>	c.C267G	p.L89L	+	+	+	+
<b>GOLGA2</b>	c.C1377T	p.S459S	+	+	+	+
<b>PCDH9</b>	c.G3471A	p.K1157K	+	+	+	+
<b>PTPRS</b>	c.C2583T	p.F861F	+	+	+	+
<b>TNPO2</b>	c.G2064A	p.L688L	+	+	+	+
<b>JUNB</b>	c.C846T	p.A282A	+	+	+	+
<b>KIAA1683</b>	c.G1701A	p.V567V	+	+	+	+
<b>CEACAM20</b>	c.C447T	p.S149S	+	+	+	+
<b>TMEM150B</b>	c.C480T	p.S160S	+	+	+	+
<b>HSPG2</b>			+	+	+	+
<b>CSF3R</b>			+	+	+	+
<b>FHL3</b>			+	+	+	+
<b>CSMD1</b>			+	+	+	+

**Table A1 (Continued)**

<b>Hugo Symbol</b>	<b>txChange</b>	<b>aaChange</b>	<b>HSC BM</b>	<b>HSC PB</b>	<b>Malignant T cell</b>	<b>Normal T cell</b>
<b>BMP1</b>			+	+	+	+
<b>RP1</b>			+	+	+	+
<b>RALYL</b>			+	+	+	+
<b>C11orf96</b>			+	+	+	+
<b>CASP4</b>			+	+	+	+
<b>NCAM1</b>			+	+	+	+
<b>TMEM218</b>			+	+	+	+
<b>GOLT1B</b>			+	+	+	+
<b>NXPH4</b>			+	+	+	+
<b>PPFIA2</b>			+	+	+	+
<b>TBX5</b>			+	+	+	+
<b>LUC7L</b>			+	+	+	+
<b>TPSG1</b>			+	+	+	+
<b>SMIM22</b>			+	+	+	+
<b>EEF2KMT</b>			+	+	+	+
<b>RMI2</b>			+	+	+	+
<b>SERPINF1</b>			+	+	+	+
<b>KANSL1</b>			+	+	+	+
<b>TLL6</b>			+	+	+	+
<b>SMCHD1</b>			+	+	+	+
<b>LAMA1</b>			+	+	+	+
<b>LOXHD1</b>			+	+	+	+
<b>MDGA1</b>			+	+	+	+
<b>POLH</b>			+	+	+	+
<b>HACE1</b>			+	+	+	+
<b>ROS1</b>			+	+	+	+
<b>EZR</b>			+	+	+	+

**Table A1 (Continued)**

<b>Hugo Symbol</b>	<b>txChange</b>	<b>aaChange</b>	<b>HSC BM</b>	<b>HSC PB</b>	<b>Malignant T cell</b>	<b>Normal T cell</b>
<b>CHST12</b>			+	+	+	+
<b>TSC22D4</b>			+	+	+	+
<b>CTTNBP2</b>			+	+	+	+
<b>FLNC</b>			+	+	+	+
<b>FLNC</b>			+	+	+	+
<b>ZNF212</b>			+	+	+	+
<b>BLACE</b>			+	+	+	+
<b>BLACE</b>			+	+	+	+
<b>USP6NL</b>			+	+	+	+
<b>SEC61A2</b>			+	+	+	+
<b>PLEKHS1</b>			+	+	+	+
<b>PDCD6IPP2</b>			+	+	+	+
<b>TMCO5A</b>			+	+	+	+
<b>PLA2G4D</b>			+	+	+	+
<b>FBN1</b>			+	+	+	+
<b>CSNK1G1</b>			+	+	+	+
<b>SH3GL3</b>			+	+	+	+
<b>EML6</b>			+	+	+	+
<b>TTN</b>			+	+	+	+
<b>CPS1</b>			+	+	+	+
<b>CAV3</b>			+	+	+	+
<b>METTL6</b>			+	+	+	+
<b>GADL1</b>			+	+	+	+
<b>CCDC36</b>			+	+	+	+
<b>CADPS</b>			+	+	+	+
<b>ABI3BP</b>			+	+	+	+
<b>TM4SF1</b>			+	+	+	+

**Table A1 (Continued)**

<b>Hugo Symbol</b>	<b>txChange</b>	<b>aaChange</b>	<b>HSC BM</b>	<b>HSC PB</b>	<b>Malignant T cell</b>	<b>Normal T cell</b>
<b>TNK2</b>			+	+	+	+
<b>TBC1D1</b>			+	+	+	+
<b>TBC1D1</b>			+	+	+	+
<b>PDCL2</b>			+	+	+	+
<b>TECRL</b>			+	+	+	+
<b>FRAS1</b>			+	+	+	+
<b>PCDH18</b>			+	+	+	+
<b>PCDH18</b>			+	+	+	+
<b>FAT1</b>			+	+	+	+
<b>FAT1</b>			+	+	+	+
<b>LECT2</b>			+	+	+	+
<b>DCTN4</b>			+	+	+	+
<b>MYH6</b>			+	+	+	+
<b>MYH6</b>			+	+	+	+
<b>NRXN3</b>			+	+	+	+
<b>SBNO2</b>			+	+	+	+
<b>FAM129C</b>			+	+	+	+
<b>THEG5</b>			+	+	+	+
<b>IZUMO2</b>			+	+	+	+
<b>EPB41L1</b>			+	+	+	+
<b>KCNQ2</b>			+	+	+	+
<b>SGSM1</b>			+	+	+	+
<b>LINC01640</b>			+	+	+	+
<b>PLXNB2</b>			+	+	+	+
<b>MAP3K15</b>			+	+	+	+
<b>CLCN5</b>			+	+	+	+
<b>L1CAM</b>			+	+	+	+

**Table A1 (Continued)**

Hugo Symbol	txChange	aaChange	HSC BM	HSC PB	Malignant T cell	Normal T cell
PIK3C2A			-	+	+	+
ZFHX3			-	+	+	+
FAM84A			-	+	+	+
PNMA8A			-	+	+	+
FOXL1			-	+	+	+
HOOK1			-	+	+	+
HYDIN2			-	+	+	+
TUSC3			-	+	+	+
KAT6A			-	+	+	+
MSC-AS1			-	+	+	+
PUF60			-	+	+	+
MTNR1B			-	+	+	+
LGALS9C			-	+	+	+
CCT6B			-	+	+	+
SMURF1			-	+	+	+
ARPP21			-	+	+	+
KY			-	+	+	+
MAP3K13			-	+	+	+
OLFM1			-	+	+	+
GOLGA2P9			-	+	+	+
BCR			-	+	+	+
DRICH1			-	+	+	+
SLC5A4			-	+	+	+
<b>Patient 2 (9 mutations in BM HSCs and 26 mutations in Blood HSCs)</b>						
NOS3			-	+	+	+
RFX1			-	+	+	+

## APPENDIX B: COPYRIGHT PERMISSION

### Payment Information

Carly Harro  
carly.harro@moffitt.org  
Payment method: Invoice

**Billing Address:**  
Mrs. Carly Harro  
Moffitt Cancer Center  
12902 USF Magnolia Drive  
33612  
Tampa, FL 33612  
United States  
  
+1 (813) 763-4374  
carly.harro@moffitt.org

**Customer Location:**  
Mrs. Carly Harro  
Moffitt Cancer Center  
12902 USF Magnolia Drive  
33612  
Tampa, FL 33612  
United States

### Order Details

1. Blood : journal of the American Society of Hematology

**Billing Status:**  
Open

Order License ID 1184902-1  
Order detail status Completed  
ISSN 1528-0020

Type of use  
Publisher  
Portion

[Print License](#)  
Republish in a thesis/dissert...  
AMERICAN SOCIETY OF HEM...  
Chart/graph/table/figure

**0.00 USD**  
Republishing Permission  
[Publisher Terms and Conditions](#)

[View Details](#)

### Payment Information

Carly Harro  
carly.harro@moffitt.org  
Payment method: Invoice

**Billing Address:**  
Mrs. Carly Harro  
Moffitt Cancer Center  
12902 USF Magnolia Drive  
33612  
Tampa, FL 33612  
United States  
  
+1 (813) 763-4374  
carly.harro@moffitt.org

**Customer Location:**  
Mrs. Carly Harro  
Moffitt Cancer Center  
12902 USF Magnolia Drive  
33612  
Tampa, FL 33612  
United States

### Order Details

1. The journal of clinical investigation

**Billing Status:**  
Open

Order License ID 1184910-1  
Order detail status Completed  
ISSN 0021-9738

Type of use  
Publisher  
Portion

[Print License](#)  
Republish in a thesis/dissert...  
AMERICAN SOCIETY FOR CLI...  
Chapter/article

**0.00 USD**  
Republishing Permission

[View Details](#)

**APPENDIX C:  
INSTITUTIONAL ANIMAL CARE AND USE COMMITTEE APPROVAL**



RESEARCH INTEGRITY AND COMPLIANCE  
INSTITUTIONAL ANIMAL CARE & USE COMMITTEE

---

**MEMORANDUM**

**TO:** Jose Conejo-Garcia,

**FROM:**   
Farah Moulvi, MSPH, IACUC Coordinator  
Institutional Animal Care & Use Committee  
Research Integrity & Compliance

**DATE:** 6/3/2019

**PROJECT TITLE:** Targetable epigenetic mechanism driving Cutaneous T cell Lymphoma  
Epigenetic mechanisms governing Sezary Syndrome

**FUNDING SOURCE:** National Cancer Institute

**IACUC PROTOCOL #:** R IS00006598

**PROTOCOL STATUS:** Amendment APPROVED

---

The Institutional Animal Care and Use Committee (IACUC) received your Modification concerning the above referenced IACUC protocol.

On 6/3/2019 the IACUC reviewed and approved your Modification for the following:

**Modification: Amendment Request for IACUC Study 2.1.1**

**Added: New or Additional Protocol Title**

**Modification: Amendment - Update Title 2.2.1**

**Main Study Title:**

**Targetable epigenetic mechanism driving Cutaneous T cell Lymphoma**

**Old Value: Epigenetic mechanisms governing Sezary Syndrome**

**Additional Study Titles:**

**Epigenetic mechanisms governing Sezary Syndrome**

---

RESEARCH & INNOVATION • RESEARCH INTEGRITY AND COMPLIANCE  
INSTITUTIONAL ANIMAL CARE AND USE COMMITTEE  
PHS No. A4100-01, AAALAC No. 000434, USDA No. 58-R-0015  
University of South Florida • 12901 Bruce B. Downs Blvd., MDC35 • Tampa, FL 33612-4799  
(813) 974-7106 • FAX (813) 974-7091

**APPENDIX D:  
IRB APPROVAL**



**APPROVAL NOTICE**

MOD00442604

**DATE:** 17 Jun 2019  
**TO:** Jose Conejo-Garcia, MD, PhD  
**PROTOCOL:** NIH - MCC 20032, Targetable epigenetic mechanism driving Cutaneous T cell Lymphoma (Pro00033657)  
**APPROVAL DATE:** 17 Jun 2019 - Via Expedited Review, IRB# 00000971

---

**IRB APPROVED:**

**Documentation:**

- Protocol (Version 3, Dated 06/10/2019)
- Summary of Changes (Dated June 10, 2019) for Protocol (Version 3, Dated 06/10/2019)

The IRB has reviewed and approved the above referenced documentation.

Waiver of Consent and Waiver of Authorization remain in effect.

Please review the IRB Handbook located in the "Reference Materials" section of Advarra CIRBITM Platform ([www.cirbi.net](http://www.cirbi.net)). A copy of the most recent IRB roster is also available.

Thank you for continuing to use Advarra IRB to provide oversight for your research project.



## PROTOCOL APPROVAL

**DATE:** 10 Sep 2020

**TO:** Jose Conejo-Garcia, MD, PhD

**PROTOCOL:** Moffitt Cancer Center - MCC 50370, Molecular Characterization and Cell of Origin of Erythrodermic Mycosis Fungoides and Sézary Syndrome (MF/SS) Cells (Pro00046535)

**APPROVAL DATE:** 10 Sep 2020 - Via Expedited Review, IRB# 00000971

**EXPIRATION DATE:** 10 Sep 2021

---

### IRB APPROVED DOCUMENTATION:

**Protocol Version:** • Protocol (Version Date: 08/12/2020)

The IRB approved the above referenced protocol and your site on 10 Sep 2020.

The IRB determined above referenced study met the criteria for a Waiver of Consent per 45 CFR 46.116(d) and a Waiver of HIPAA Authorization per 45 CFR 164.512(i)(2ii). The IRB granted the Waiver of Consent and Waiver of HIPAA Authorization.

If you wish to have the IRB reconsider the imposed modifications, you may follow the procedures outlined below:

1. Submit supporting documentation that addresses the IRB's concerns.
2. Provide a written justification for relief of any IRB imposed condition.

Please note the following COVID-19 considerations:

1. Please ensure that you have adequate study staff and resources before you begin conducting the study.
2. Please consider delaying enrollment if your study procedures may be impacted by the pandemic; or please submit a modification to change the procedures.
3. Please note that screening questions relating to COVID-19 are not considered research questions unless you will be collecting data on COVID-19.

If the study is expected to last beyond the approval period, you must request and receive re-approval prior to the expiration date noted above. A report to the Board on the status of this study is due prior to the expiration date or at the time the study closes, whichever is earlier. It is recommended that you submit status reports at least 4 weeks prior to your expiration date to avoid any additional fees or lapses in approval.